DESIGN, FABRICATION AND TEST OF GRAPHITE/EPOXY METERING TRUSS STRUCTURE COMPONENTS

Phase III Final Report

June 1972 to September 1974

September 1974

Prepared Under Contract No. NAS8-26675

By

Advanced Composite Group
GRUMMAN AEROSPACE CORPORATION
Bethpage, New York 11714

For

Marshall Space Flight Center
NATIONAL AERONAUTICS AND SPACE ADMINISTRATION

FOREWORD

The work reported herein was performed under the sponsorship of the National Aeronautics and Space Administration, George C. Marshall Space Flight Center, Marshall Space Flight Center, Alabama, 35812. Mr. C. Loy is the Contracting Officers Representative.

The work was performed by the Advanced Composites Group of Grumman Aerospace Corporation, Bethpage, New York 11714. The Project Supervisor at Grumman is Mr. R.N. Hadcock and the Assistant Project Supervisor is Mr. J. Sicari.

The following Grumman personnel were the principal contributors to this report:

Mr. R.N. Hadcock	Manager, Advanced Composite Programs
Mr. S.J. Dastin	Deputy Manager, Advanced Composite Programs, Head, Advanced Chemical Processing and Composites Group
Mr. J. Sicari	Structural Systems
Mr. J. Suarez	Structural Mechanics
Mr. G. Golam	Materials and Processes
Mr. P. Palter	Elements Test
Mr. A. DeAngelis	Manufacturing Engineering
Mr. R. Collins	Quality Control

Approved by: 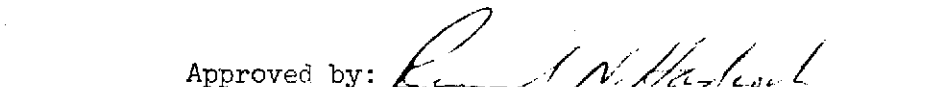
R.N. Hadcock Project Supervisor

ABSTRACT

This report describes the design, materials, tooling, manufacturing processes, quality control, test procedures and results associated with the fabrication and test of graphite/epoxy metering truss structure components exhibiting a near zero coefficient of thermal expansion.

Analytical methods were utilized, with the aid of a computer program, to define the most efficient laminate configurations in terms of thermal behavior and structural requirements. This was followed by an extensive material characterization and selection program; conducted for several graphite/graphite/hybrid laminate systems to obtain experimental data in support of the analytical predictions. Mechanical property tests as well as coefficient of thermal expansion tests were run on each laminate under study, the results of which were used as the selection criteria for the single most promising laminate. Further coefficient of thermal expansion measurement was successfully performed on three subcomponent tubes utilizing the selected laminate.

Five full size graphite/epoxy tubes were fabricated (using the selected laminate), all of which were dynamically tested, and a two member metering truss component was manufactured. The two member component was static tested successfully, verifying the structural integrity of the design concept.

CONTENTS

CONTENTS (Cont.)

ILLUSTRATIONS

ILLUSTRATIONS (Cont.)

ILLUSTRATIONS (Cont.)

TABLES

1.0 INTRODUCTION AND SUMMARY

The objectives of this program were to confirm the structural integrity, manufacturing feasibility, thermal response and environmental suitability of graphite/epoxy (Gr/Ep) structural members for use on a metering truss of a space operational optical system.

Of prime consideration on this program was the development of a graphite/graphite/hybrid laminate that would yield an almost zero coefficient of thermal expansion. This was necessary to meet the stringent thermal displacement criteria as set forth by the NASA. (Example: ± 2 micrometers (78.74×10^{-6} inches) axial displacement over a length of 5.51 m (217 inches).) The near zero coefficient of thermal expansion was achieved by the proper proportioning and orienting of a high modulus, negative coefficient graphite fiber (GY70) and a lower modulus slightly positive graphite fiber (Type A). A technique for the design of such laminates was developed as the IBM 1130 computer program ZERCO. The method involves a systematic search of laminates composed of layers 0 rad (0°), 1.57 rad (90°) and $\pm\theta$ radians. The angle of the angle plies ($\pm\theta$) is increased in .087 rad (5°) increments, and for each angle θ, a layup which results in a near zero coefficient of thermal expansion, is found for each of four cases; percent of 1.57 rad (90°) layers equal to 0, 5, 10 and 15.

Under the program the design of two components in particular, the tubular truss members and the apex fittings to which they attach, constituted the primary areas of design investigation. A design study was performed for the above noted members, which included consideration for strength, stiffness, weight, thermal expansion, some environmental effects, fabrication and joining techniques. Running concurrently with the design study, the theoretical analytical techniques were employed to conduct a coefficient of thermal expansion investigation. Coefficients were computed for a variety of material types and hybrid laminate orientations. Other design parameters such as member weights and stiffness requirements were also included in this investigation to provide practical limits for overall acceptability. The three most promising material/laminate configurations (designated laminates A, B and C) resulting from this study were then the object of an intensive material characterization and selection test program comprising approximately

165 specimens. Of primary importance for this portion of the program were the element coefficient of thermal expansion tests. Of the three laminate configurations tested only one, the B laminate, exhibited sufficient repeatability to meet the stringent requirements previously noted. An average value of .086 mm/mm/°C (.048 x 10^{-6} in/in/°F) was obtained over the applicable temperature range of -90°C to -23°C (-130°F to -9.5°F). This fell well within the maximum permissible value of .216 x 10^{-6} mm/mm/°C (.120 x 10^{-6} in/in/°F).

Following the successful completion of the elemental coefficient tests three subcomponent tubes utilizing the same laminate were fabricated. These subcomponent tubes, which were .152 m (6 inches) in length and .081 m (3.2 inches) in diameter, were used to verify the repeatability of the coefficient of thermal expansion in the anticipated structural shape. It should be noted that the three tubes were fabricated independently. Results of the three subcomponent tube tests were excellent, in fact, even better than the elemental tests insofar as the range over which a near zero coefficient was obtained was significantly larger. An average value of -.0050 x 10^{-6} mm/mm/°C (-.0028 x 10^{-6} in/in/°F) was obtained for the three tubes over the previously noted temperature range.

Subsequent to the subcomponent tube coefficient testing, five full size Gr/Ep tubes and a Gr/Ep apex fitting were fabricated. Of the five tubes fabricated, all underwent dynamic testing for natural frequency and damping characteristics. Behavior of the tubes was predictable and consistent.

Following completion of the dynamic testing two of the five tubes and the Gr/Ep apex fitting were assembled into a two member truss test component for structural verification of the apex fitting/joint design. Results of the test were satisfactory, with the structure far exceeding its design ultimate load of 28155 N (6330 lbs) axial compression. The remaining three tubes were sent to the NASA, MSFC for further testing.

2.0 CONCEPT DEFINITION AND DEVELOPMENT

2.1 Metering Truss Geometry and Structural Arrangement

The geometry and structural arrangement of the baseline metering truss for a space operational optical system is shown in Figure 2-1. The structure, which is 5.51 m (217 inches) in length overall, 3.35 m (132 inches) in diameter, is divided into three equal length bays of 1.83 m (72.3 inches) and has as its primary function, support of the secondary mirror relative to the primary under the action of both inertial and thermal loading. It is comprised of four basic structural components - tubes, apex fittings, rings and the secondary mirror support structure.

There are 48 tubes -1.949 m (76.77 inches) in length in the baseline configuration, 16 per bay, which serve as the longitudinal supports between the primary and secondary mirror. The tubes resist the primary axial and bending loads and are the predominant factor in controlling the thermal displacement of the secondary mirror. Four rings are also provided to resist the secondary loadings and enforce nodes for the longitudinal members. The tubes and rings intersect at eight points at the end of each bay, where they are joined by apex fittings which provide structural continuity in both the longitudinal and lateral directions. The secondary mirror support structure functions are to transmit the mirror inertia loads to the truss and to provide a thermally stable platform for mirror mounting. It is comprised of a centrally located ring and four strut members which mount to apex fittings at the uppermost ring.

For the purposes of this program, configuration studies were limited to the design of the tubes and the tube/ring/apex fitting intersection. Design of the entire structure was beyond the scope of this program.
scope.

2.2 Design Criteria

The general design criteria applicable to the components of the metering truss structure under investigation for this program were obtained from NASA, MSFC. The criteria are separated into two basic categories; load and stiffness requirements and temperature and dimensional stability requirements. The load and stiffness requirements are presented in Figure 2-2. The loads shown represent the most severe experienced by any single tube

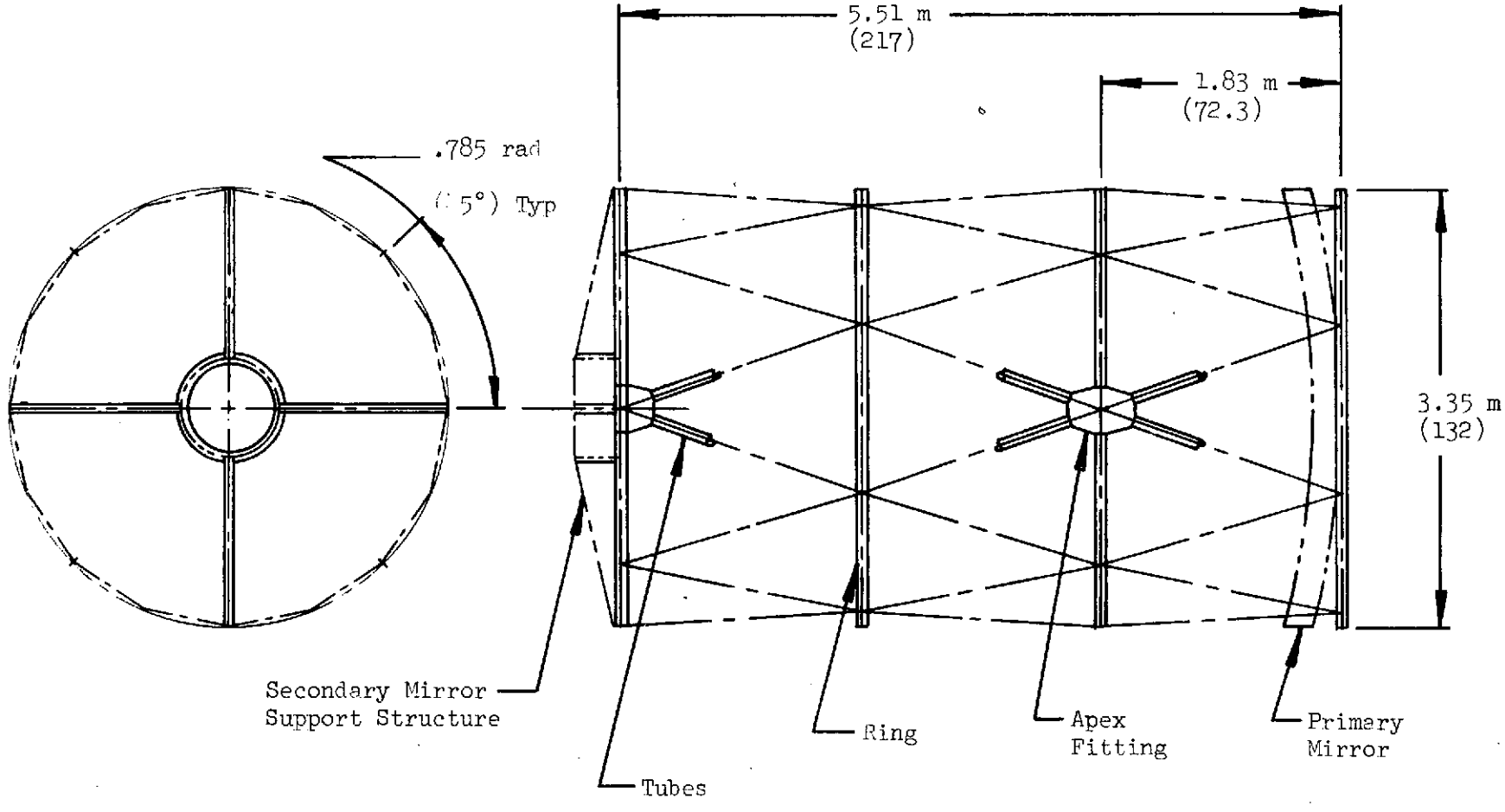

Figure 2-1 Metering Truss Geometry and Structural Arrangement

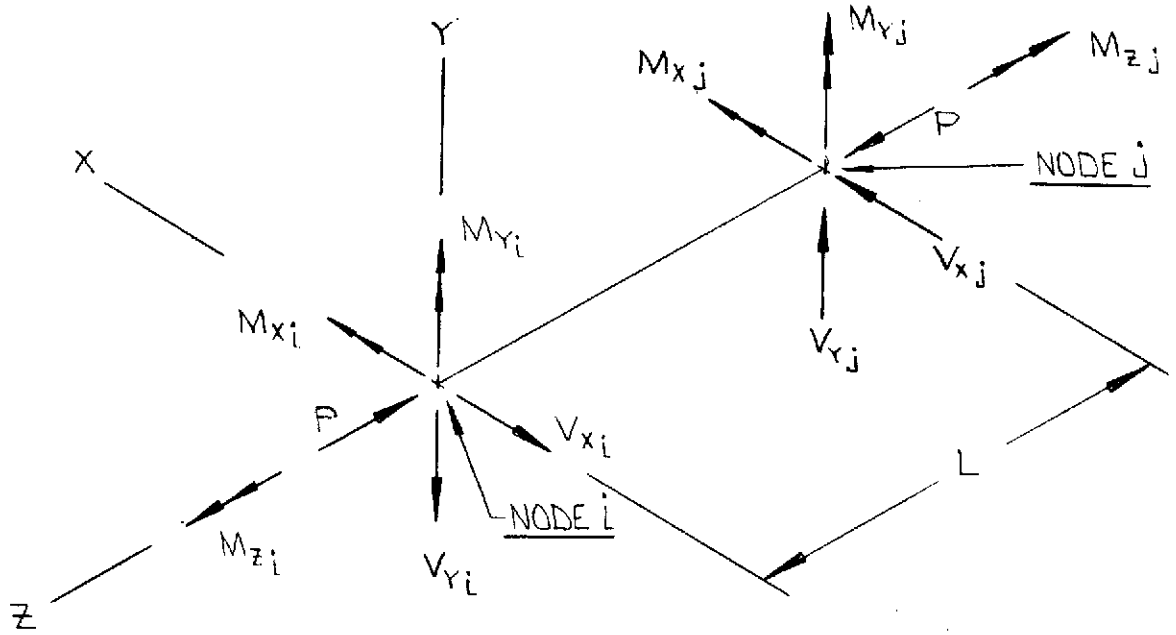

INTERNAL MEMBER LOADS-LIMIT

P= -4316.82N (-970.51 LB.)

NODE i		NODE j	
M_{xi}=	255.40 N-M (2261 IN-LB.)	M_{xj}=	84.54 N-M (748.34 IN-LB.)
M_{yi}=	14.28 N-M (126.4 IN-LB.)	M_{yj}=	29.81 N-M (263.89 IN-LB.)
M_{zi}=	2.49 N-M (22.08 IN-LB.)	M_{zj}=	-2.49 N-M (-22.08 IN-LB.)
V_{xi}=	22.64 N (5.09 LB.)	V_{xj}=	-22.64 N (-5.09 LB.)
V_{yi}=	-174.49 N (-39.23 LB.)	V_{yj}=	174.49 N (39.23 LB.)

(Factor of Safety = 1.4)

MINIMUM STIFFNESS REQUIREMENTS

EA= 27.057 x10^6 N (6.082 x10^6 LB.)

EI= 8.150 x10^3 N-M^2 (2.84 x10^6 LB-IN^2.)

L= 1.95 M (76.771 IN.)

Figure 2-2 Internal Member Loads and Stiffness Requirements

member in the structure. The temperature and dimensional stability requirements are listed below:

- Stabilized Structure Temperatures
  a. At secondary mirror = -90°C ± 1.7°C (-130°F ± 3°F)
  b. At primary mirror = -23.3°C ± 1.7°C (-10°F ± 3°F)
  c. Temperature gradient between primary and secondary-linear
- Dimensional Stability Requirements (Secondary Relative to Primary)
  a. Despace = ±2 μm (78.74×10^{-6} inches)
  b. Decenter = ±10 μm (393.7×10^{-6} inches)
  c. Tilt = 4.5 μ rad (2.58×10^{-4} degrees)
  d. Stability allowances - Prorated uniformly over a length of 5.511 m (217 inches), with each of the three bays charged one third the total allowance. This results in a unit allowance of 3.628×10^{-7} mm/mm (3.628×10^{-7} in/in)

2.3 Graphite/Epoxy Tube and Apex Fitting Design

Configuration studies were conducted for both the tube and apex fitting, fabricated entirely with Gr/Ep, which would result in representative flight structure. The major objectives of this study were:

- Develop a Gr/Ep tube with a near zero coefficient of thermal expansion
- Develop a tube/apex fitting design that would maintain a near zero thermal expansion across the joint
- Satisfy structural requirements
- Be compatible with overall system requirements
- Have low fabrication cost
- Provide for ease of assembly
- Allow fabrication of the tube with existing tooling without compromising the applicability of the basic design. Limitations imposed by the existing tube tooling were: (a) a maximum length of 1.12 m (44 inches) and (b) an outside diameter of 81.3 mm (3.2 inches)

In order to demonstrate the applicability of the tube/apex fitting design the members were sized for actual flight hardware (without regard for the existing tooling limitation imposed) and the configuration analyzed with the resultant geometry. Once the basic configuration was considered acceptable for flight structure the details were redesigned incorporating the length and diameter restrictions, but without changing the design concept.

The tube members were designed with a graphite/graphite/hybrid material system. This particular system was chosen to yield a laminate with a near zero coefficient of thermal expansion (C.T.E.), this being the primary objective of this program. Achievement of the near zero longitudinal C.T.E. was accomplished by the proper proportioning and orienting of a high modulus, negative coefficient graphite fiber (GY70) and a low modulus, slightly positive coefficient graphite fiber (Type A). The laminates were designed to be fiber controlled, by utilizing fibers in the 0 rad (0°), 1.57 rad (90°) and $\pm\theta$ rad ($\pm\theta$°) directions, thereby minimizing resin dependence for the C.T.E. In conjunction with the thermal criteria, the tubes were designed to meet all structural loading and stiffness requirements as presented in Figure 2-2. In order to match the given bending (EI) and axial (EA) stiffness coincidentally, E from both expressions were equated with the resulting equations solved for the radius. The solution for this expression is unique and resulted in a radius of 25.4 mm (1 inch). This radius yielded a required wall thickness of 1.45 mm (.057 inches) when a modulus of 134.43×10^9 N/m^2 (19.5×10^6 psi) was used (the value of the modulus noted is that which was obtained for the selected laminate $[\pm.907_A \text{ rad}/1.57_A \text{ rad}/0_{2\ GY70}\text{rad}]_s$ ($[\pm 52°_A/90°_A/0°_{2\ GY70}]_s$) exhibiting a near zero C.T.E.). Overall column and local stability modes were checked, as well as strength, using standard analytical techniques. Tube members actually fabricated for test had a diameter and length consistent with those imposed by the previously mentioned tooling restrictions; the wall thickness and laminate orientation, however, remained the same as that obtained for the flight members.

A cursory weight analysis was performed for the flight tubes, where the Gr/Ep members were compared to INVAR. Ground rules for the weight analysis performed are listed as follows:

- Lower bay (bay nearest the primary mirror) tubes were sized using the criteria presented in Figure 2-2. This is due to symmetry of the structure and the fact that the most severe loading can be experienced by anyone of the sixteen members
- All upper bay (bay nearest the secondary mirror) INVAR tubes were sized to a minimum gage wall thickness of .254 mm (.010 in.). The members are relatively lightly loaded
- The Gr/Ep minimum tube gage was considered to be 1.44 mm (.057 in.)
- All Gr/Ep tubes in the structure (48 members) were considered to be identical to provide a minimum cost design

Based on the aforementioned ground rules the Gr/Ep tubes reflect a 58% weight saving over the INVAR members. Weight of the Gr/Ep tubes were 5.78 N (1.3 lb/tube), while the INVAR tubes weighed in at 6.67 N (1.5 lbs/tube) for the lightly loaded members and 28.02 N (6.3 lbs/tube) for the more highly loaded members. It should be noted that for the INVAR tubes minimum stiffnesses for the more lightly loaded tubes was unknown, and the weights for these members may be unconservative.

The final configuration of the tube/apex fitting assembly is shown in Figures 2-3 through 2-5. Figures 2-3 and 2-4 depict the structure at a typical intersection, while Figure 2-5 shows the structure at one of the upper ring intersections where the secondary mirror support strut mounts. The assembly is an all bonded structure comprised of several detail components - clips, channel sections and gusset plates, all of which can be tailored to provide predictable and consistent coefficients of thermal expansion. The clips and channel sections provide shear paths from the tube into the ring in the plane 1.57 rad (90°) to the plane of the tubes. The gusset plates provide axial load continuity in the plane of the tubes, as well as moment continuity in both planes. The arrangement of the gusset is such that the larger of the moments is reacted by axial loads in the plates, while the smaller moment is resisted by plate bending. It should be noted that the laminate orientation of the gusset plate is the same as that of the tube, and therefore possesses the same near zero C.T.E. The shear in the plane of the tubes is resisted directly by the ring via the gusset plates. The tube/apex fitting assembly is totally adhesive bonded. This mode of assembly was selected to insure intimate contact between details,

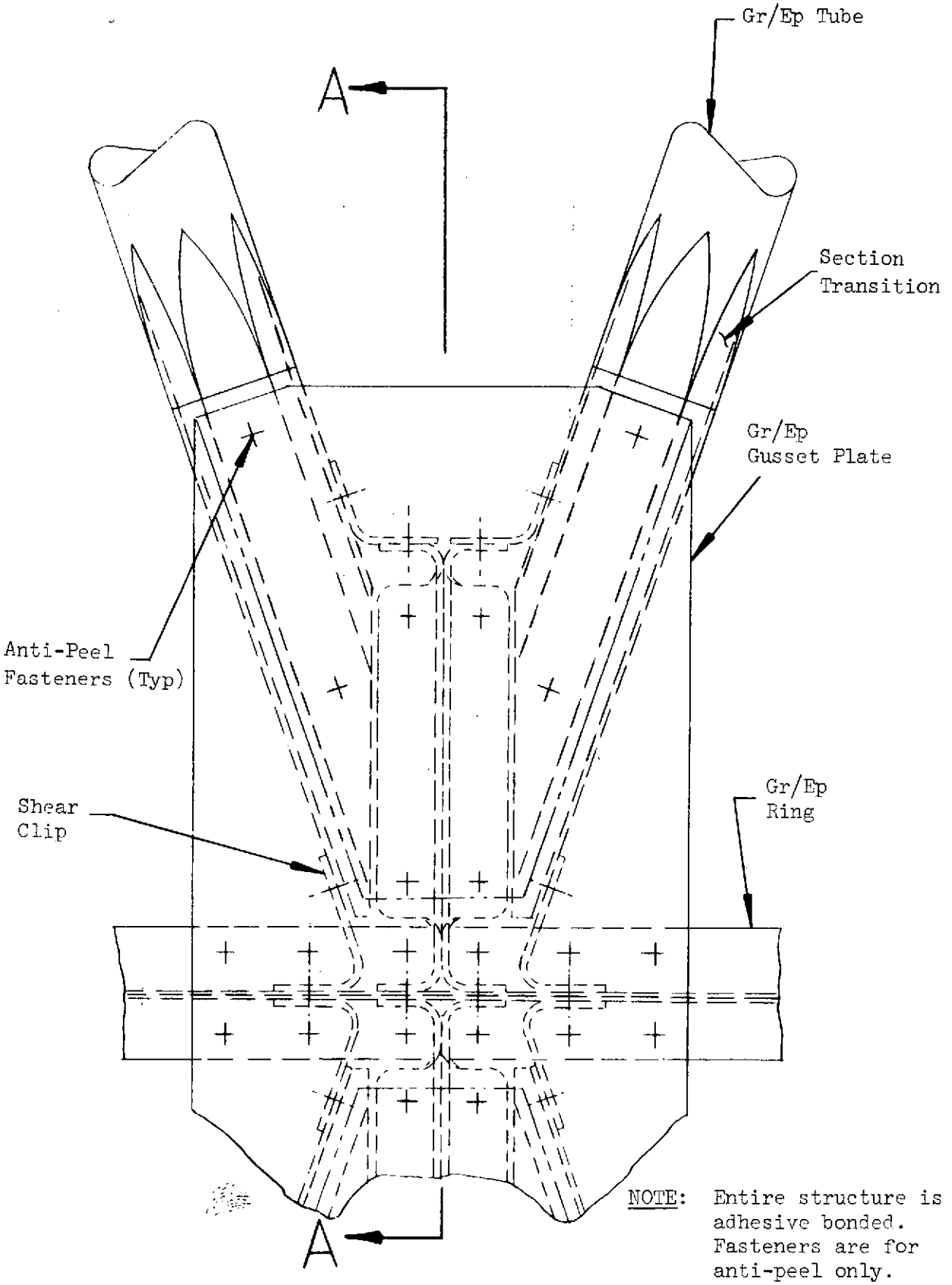

Figure 2-3 Tube/Apex Assembly, Typical Intersection - Front View

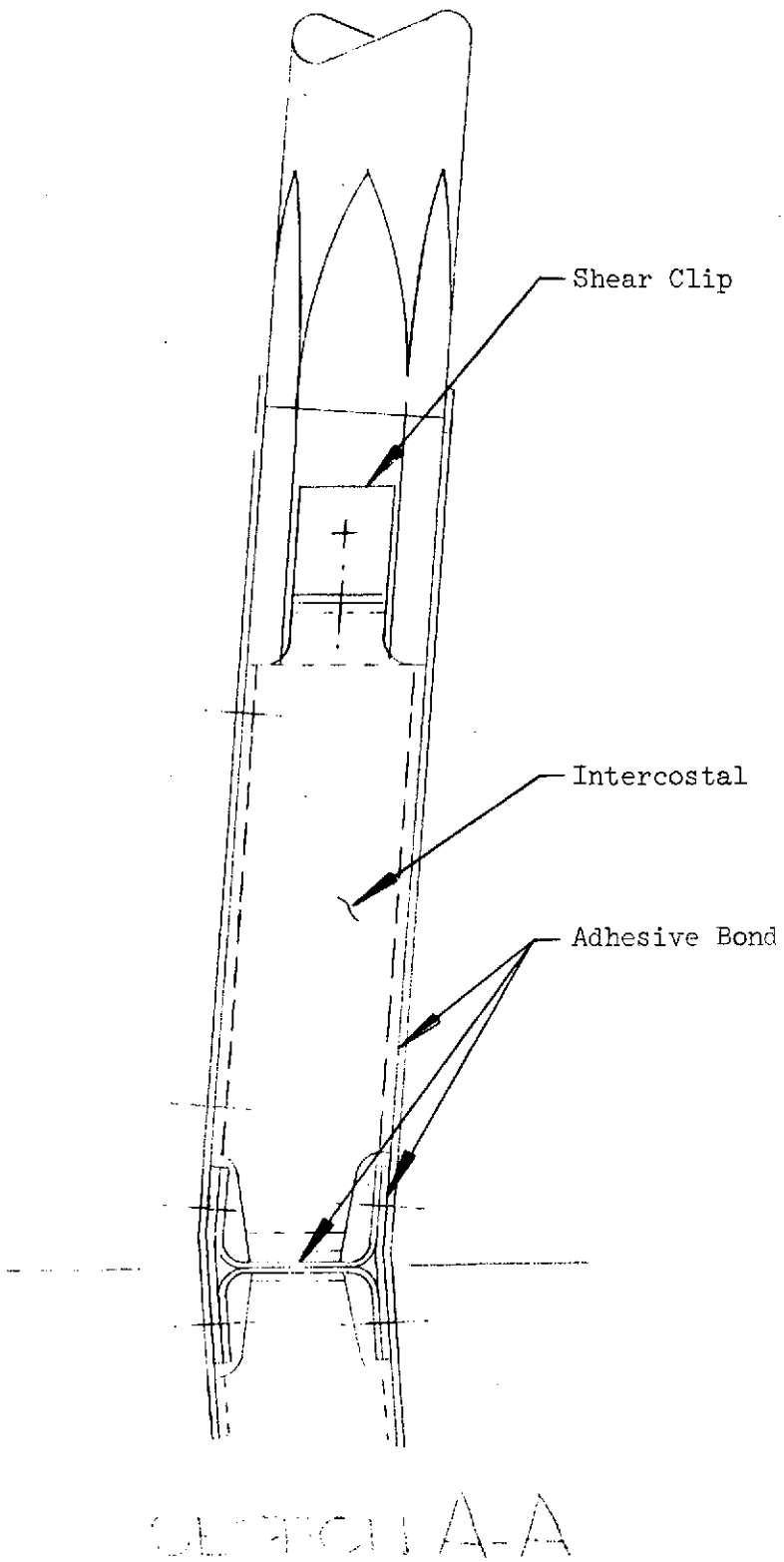

Figure 2-4 Tube/Apex Fitting Assembly, Typical Intersection - Side View

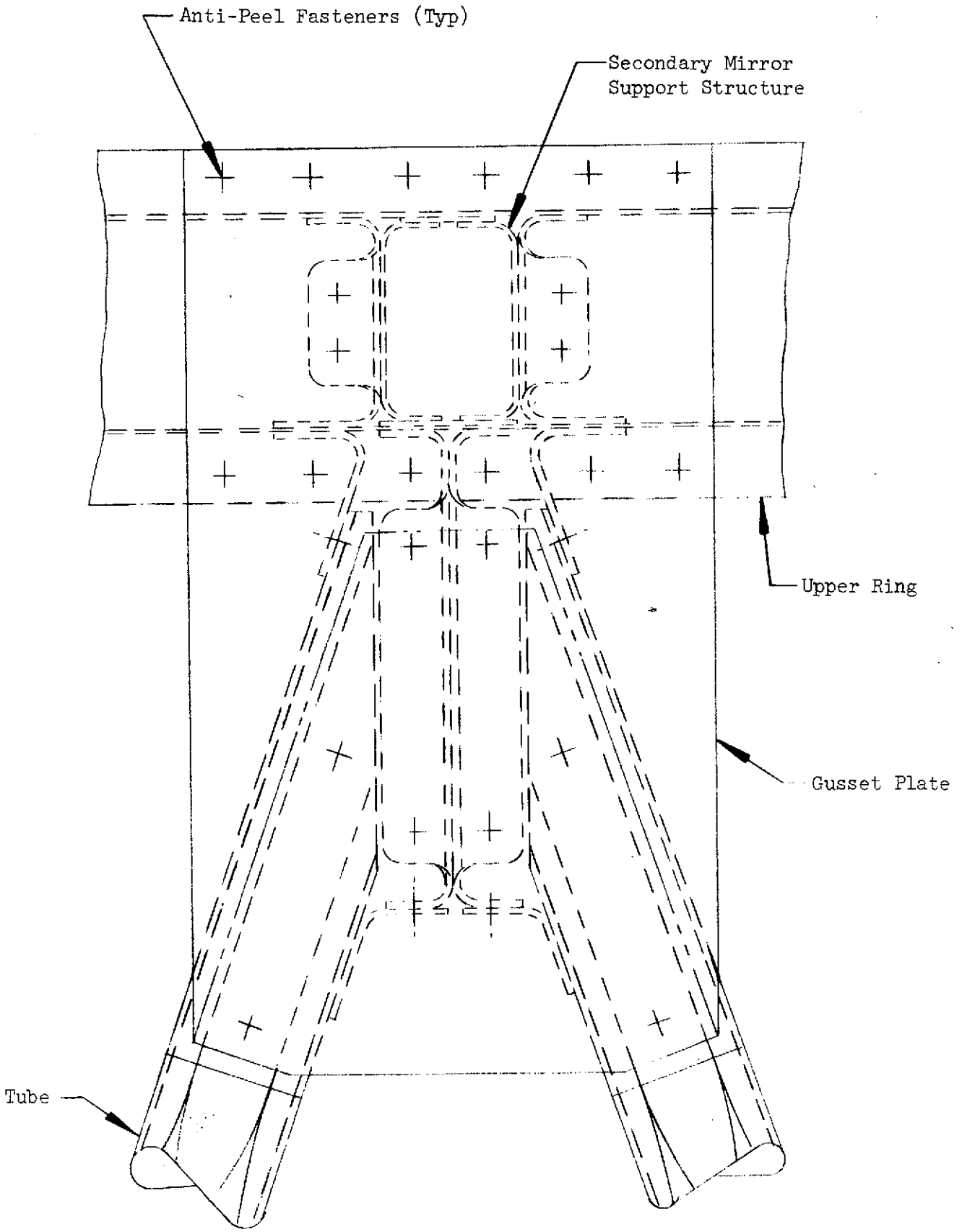

Figure 2-5 Tube/Apex Fitting Assembly, Upper Ring Intersection

eliminating such potential problem areas as bolt hole tolerances on thermal performance. All bonding of the tube/apex assembly is accomplished using a room temperature curing adhesive system and the double bonding technique. This technique involves application of the adhesive to one of the two faying surfaces (applying a release agent to the other), fitting up of the parts, curing, disassembling, inspection and finally application of the adhesive to the second faying surface for final assembly and curing. The system allows for visual bondline inspection and compensation for any mismatch prior to final bonding. As noted in Figures 2-3 through 2-5, fasteners are utilized in selected areas to resist any peel loads on the adhesive. The primary structural loads are resisted totally by the bonded joints. In order to utilize this concept, the tube end transitions from a round into an octagonal shape. The flats are created to provide the bond surfaces in conjunction with other features of the design concept. For the purposes of this program and in order to make use of the existing tube tooling, the flats were prepared by overwrapping the tube end oversize, in the round, with fiberglass and machining the flats to a wall thickness nominally greater than that of the basic tube. This closely approximates an integrally molded octagonal end shape that would be employed if all new tooling were fabricated. The two member test structure fabricated under this program is shown in Figure 2-6.

2.4 Materials Characterization and Selection

The materials used under this program consisted of two types of graphite fiber and a common epoxy matrix. The fibers are the Hercules Type A (low modulus) and the Celanese GY70 (high modulus), both of which were impregnated with the United States Polymeric E-702 resin system. The material characterization and selection program was conducted with three different laminate configurations (using a mix of both materials) for which analytical methods had predicted near zero coefficients of thermal expansion. The attainment of the near zero coefficient was the primary criteria in the selection process, other considerations however, such as mechanical properties also played a significant role. The program was setup such that an initial screening of all three multi-directional laminates was made, relative to tensile and compressive strength and modulus and of course the longitudinal and transverse C.T.E. Unidirectional properties were also run for the Type A and GY70 independently. All initial testing was done with

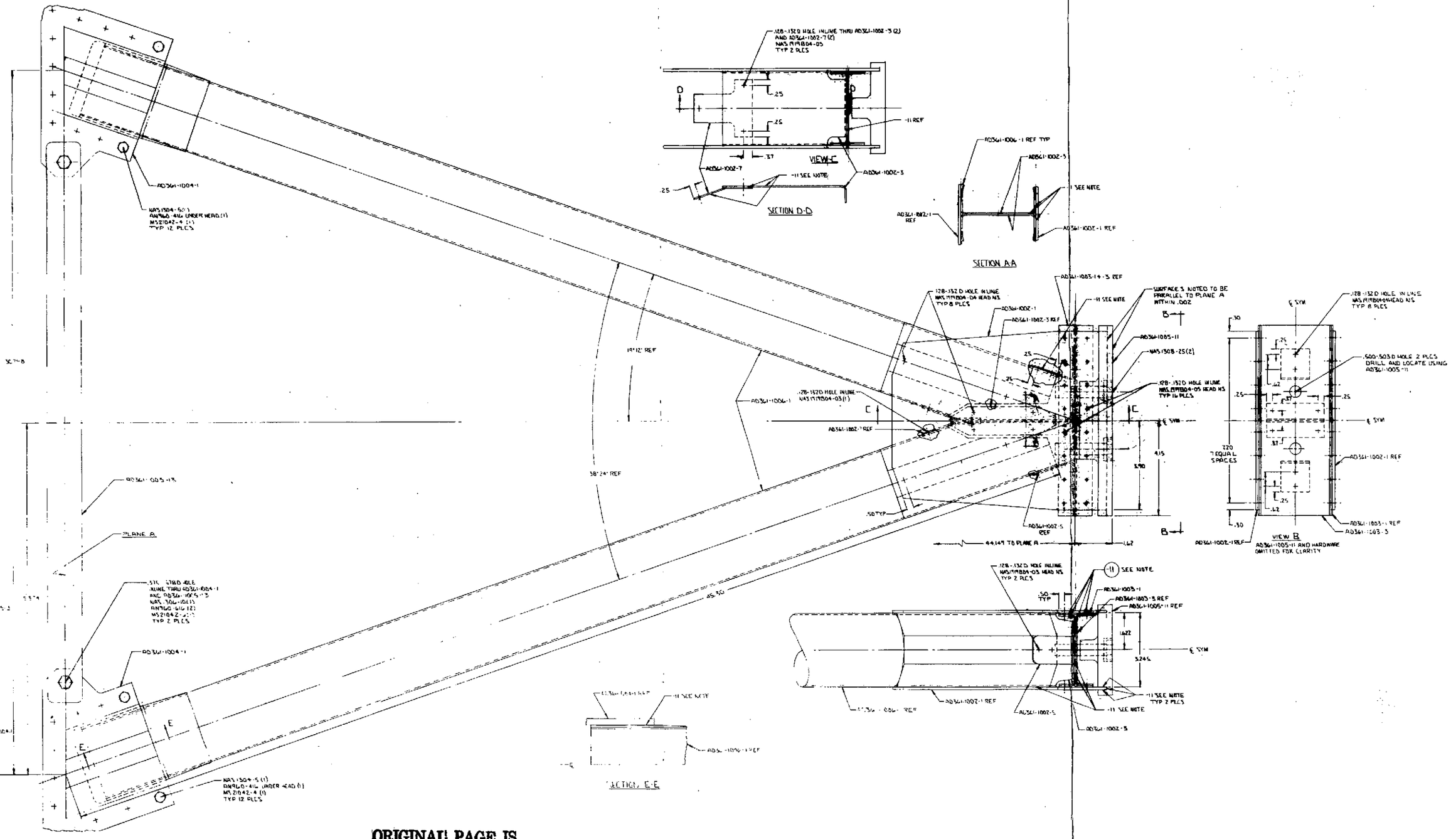

ORIGINAL PAGE IS
OF POOR QUALITY

FOLDOUT FRAME 1

Figure 2-6 Two Member Truss Component

FOLDOUT FRAME 2

the first buy of material - batch one. Subsequent to the results of the first tests one laminate, which exhibited the most consistent and predictable properties, was selected for further testing. The tests were environmental in nature (outgassing) followed by thermal coefficient testing. In order to determine the consistency of properties, both mechanical and physical, from material batch to batch, a second material buy was instituted. Further tests on the selected laminate (identical to the initial tests) were run and compared. For the purposes of identification the three laminates were denoted as A, B and C. The test matrix for the characterization and selection program is shown in Table 2-1 and represents all element tests performed, both planned and added.

Upon completion of the elemental tests three subcomponent tube specimens were fabricated using the selected laminates, and tested to determine the C.T.E. The intent was to compare the C.T.E. for these specimens, which were in the intended structural shape, to that of the flat rectangular elements.

The following sub-sections discuss in more detail the material characterization program and the results obtained.

2.4.1 Mechanical Properties Determination

The equations to predict multi-directional laminate structural behavior were developed in Reference 1.

The stress-strain relations for a single layer are given using functions of the multiples of the angle of rotation of the layer instead of powers of the angles. Sign conventions for stress and ply orientation are shown in Figure 2-7.

$$\begin{bmatrix} f_x \\ f_y \\ f_{xy} \end{bmatrix} = \begin{bmatrix} Q_{11} & Q_{12} & Q_{16} \\ Q_{21} & Q_{22} & Q_{26} \\ Q_{61} & Q_{62} & Q_{66} \end{bmatrix} \begin{bmatrix} \epsilon_x \\ \epsilon_y \\ \nu_{xy} \end{bmatrix} \qquad 1$$

where

f_x, f_y, and f_{xy} = Stresses applied to the layer

ϵ_x, ϵ_y, and γ_{xy} = Layer strains

Table 2-1 Test Matrix - Material Characterization and Selection Study

Property	Material Batch 1					Material Batch 2
	Laminate Configuration					Laminate Configuration
	A	B	C	Uni	Selected-B	Selected-B
F_1^t, E_{11}^t	5	5	5	6/6		5
F_2^t, E_{22}^t	5	5	5	5/5		5
F_1^c, E_{11}^c	5	5	5			5
F_2^c, E_{22}^c	5	5	5			5
F_1^b, E_{11}^b	5	5	5			5
F_2^b, E_{22}^b	5	5	5			5
F_{ILS}		5	5			
α_{11}	5(1)	6(1)	5(1)	5/5(1)		9(1)
α_{22}	3	3	3	3/3		
Outgassing at R.T					3	2
α_{11} (Post-Conditioned)					1	1
Outgassing at 65.5°C (150°F)					3	2
α_{11} (Post-Conditioned)					1	1
Humidity + Outgassing at R.T.					3	2
α_{11} (Post-Conditioned)					2	1
Humidity + Outgassing at 65.5°C (150°F)					3	2
α_{11} (Post-Conditioned)					2	1

(1) Includes Re-runs

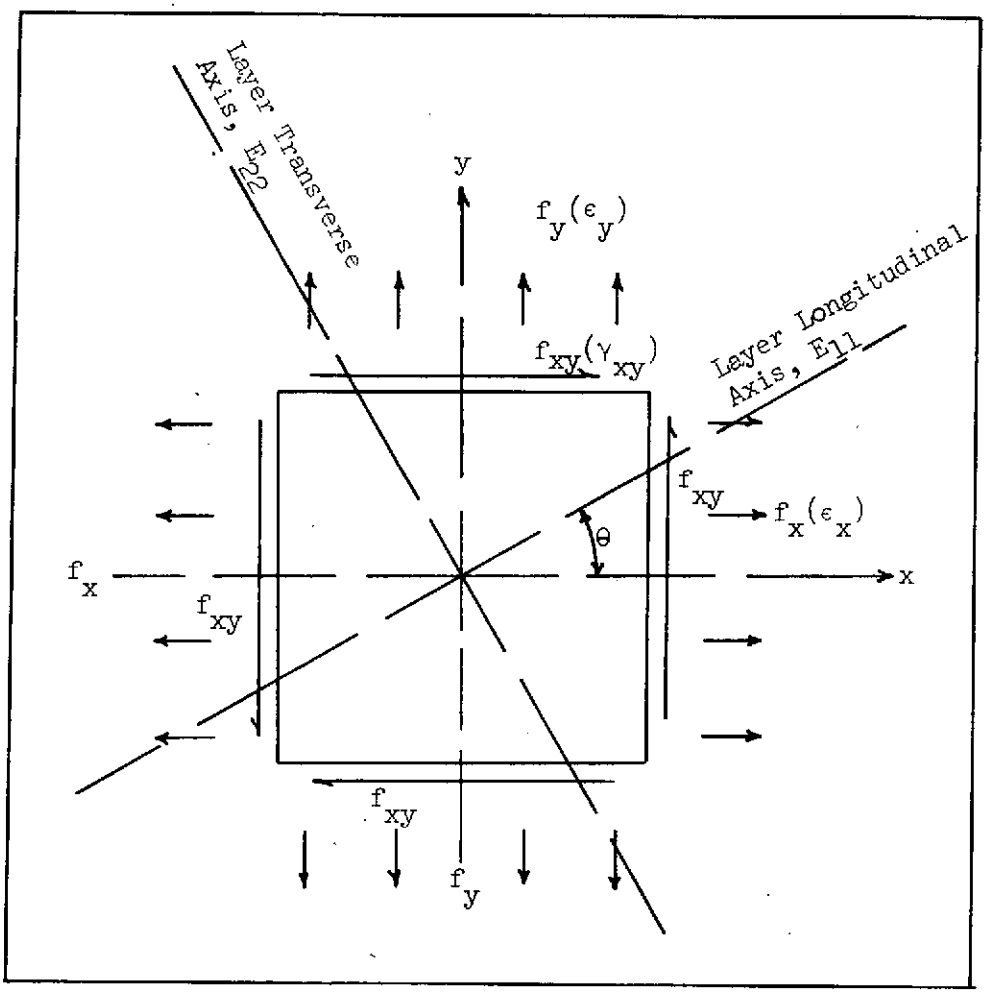

Figure 2-7 Layer Stress Conventions

and

$$Q_{11} = 3U_1 + U_2 + U_3\cos 2\theta + U_4\cos 4\theta$$

$$Q_{22} = 3U_1 + U_2 - U_3\cos 2\theta + U_4\cos 4\theta$$

$$Q_{21} = Q_{12} = U_1 - U_2 - U_4\cos 4\theta$$

$$Q_{66} = U_1 + U_2 - U_4\cos 4\theta \qquad (2)$$

$$Q_{61} = Q_{16} = -\frac{1}{2} U_3\sin 2\theta + U_4\sin 4\theta$$

$$Q_{62} = Q_{26} = -\frac{1}{2} U_3\sin 2\theta - U_4\sin 4\theta$$

θ = Angle between layer axis and laminate axis.

and

$$U_1 = \frac{1}{8\psi} \left[E_{11} + E_{22} + \nu_{21}E_{11} + \nu_{12}E_{22}\right]$$

$$U_2 = \frac{1}{2\psi} \left[G_{12} - \frac{1}{2} \left(\nu_{21}E_{11} + \nu_{12}E_{22}\right)\right] \qquad (3)$$

$$U_3 = \frac{1}{2\psi} \left[E_{11} - E_{22}\right]$$

$$U_4 = \frac{1}{8\psi} \left[E_{11} + E_{22} - \left(\nu_{21}E_{11} + \nu_{12}E_{22}\right) - 4\psi G_{12}\right]$$

where

E_{11}, E_{22}, and G_{12} = Layer longitudinal, transverse, and shear moduli

ν_{12} = Major Poisson's ratio

ν_{21} = Minor Poisson's ratio

$\psi = 1 - \nu_{12}\nu_{21}$

Considering the [0/1.57/$\pm\theta$] ([0/90/$\pm\theta$]) laminates with equal numbers of layers in the $+\theta$- and $-\theta$-degree directions, using ℓ, m, and n to denote the proportion by thickness of layers in the 0, 1.57 and $\pm\theta$ rad (0,90, and $\pm\theta$ degree) directions, assuming plain strain through the laminate and using the relations for equilibrium, then:

$$\ell f_x^{L} + m f_x^{M} + n f_x^{N} = f_x$$

$$\ell f_y^{L} + m f_y^{M} + n f_y^{N} = f_y \qquad (4)$$

$$\ell f_{xy}^{L} + m f_{xy}^{M} + n f_{xy}^{N} = f_{xy}$$

where f_x, f_y, and f_{xy} are respectively the longitudinal, transverse, and shear stresses applied to the laminate; f_{ij}^{L} and f_{ij}^{M} are the 0 and 1.57 rad (0 and 90 degree) layer stresses and f_{ij}^{N} is the stress in the $\pm\theta$ rad (degree) pair of layers.

Substituting Eq. 1 into Eq. 4 results in:

$$f_x = (\Sigma RQ_{11}^{R})\,\epsilon_x + (\Sigma RQ_{12}^{R})\,\epsilon_y = A_{11}\,\epsilon_x + A_{12}\,\epsilon_y$$

$$f_y = (\Sigma RQ_{12}^{R})\,\epsilon_x + (\Sigma RQ_{22}^{R})\,\epsilon_y = A_{12}\,\epsilon_x + A_{22}\,\epsilon_y \qquad 5$$

$$f_{xy} = (\Sigma RQ_{66}^{R})\,\gamma_{xy} = A_{66}\,\gamma_{xy}$$

where RQ_{ij}^{R} represents the summation of the proportion of each layer thickness multiplied by its stress-strain coefficient, that is:

$$RQ_{11}^{R} = \ell Q_{11}^{L} + mQ_{11}^{M} + nQ_{11}^{N}$$

Inverting Eq. 5, the strain-stress relations become:

$$\epsilon_x = \frac{\left[\Sigma RQ_{22}^{R}\right] f_x - \left[\Sigma RQ_{12}^{R}\right] f_y}{\left[\Sigma RQ_{11}^{R}\right]\left[\Sigma RQ_{22}^{R}\right] - \left[\Sigma RQ_{12}^{R}\right]^2}$$

$$\epsilon_y = \frac{-\left[\Sigma RQ_{12}^{R}\right] f_x + \left[\Sigma RQ_{11}^{R}\right] f_y}{\left[\Sigma RQ_{11}^{R}\right]\left[\Sigma RQ_{22}^{R}\right] - \left[\Sigma RQ_{12}^{R}\right]^2} \qquad 6$$

$$\gamma_{xy} = \frac{f_{xy}}{\Sigma RQ_{66}^{R}}$$

The laminate overall elastic properties in the elastic range are given by:

$$A_{11} = A_x = \frac{E_x}{1 - \nu_{xy}\nu_{yx}} = \Sigma RQ_{11}^{R}$$

$$A_{22} = A_y = \frac{E_y}{1 - \nu_{xy}\nu_{yx}} = \Sigma RQ_{22}^{R} \qquad 7$$

$$A_{12} = \frac{\nu_{yx}E_x}{1 - \nu_{xy}\nu_{yx}} = \frac{\nu_{xy}E_y}{1 - \nu_{xy}\nu_{yx}} = \Sigma RQ_{12}^{R}$$

$$A_{66} = A_{xy} = G_{xy} = \Sigma RQ_{66}{}^{R}$$

$$\nu_{xy} = \frac{\Sigma RQ_{12}{}^{R}}{\Sigma RQ_{22}{}^{R}} \qquad 7 \text{ (Cont.)}$$

$$\nu_{yx} = \frac{\Sigma RQ_{12}{}^{R}}{\Sigma RQ_{11}{}^{R}}$$

The stress applied to each layer is obtained by substituting Eq. 6 into Eq. 1, which results in:

$$f_x{}^{R} = \frac{\left[Q_{11}{}^{R}\,\Sigma RQ_{22}{}^{R} - Q_{12}{}^{R}\,\Sigma RQ_{12}{}^{R}\right] f_x - \left[Q_{11}{}^{R}\,\Sigma RQ_{12}{}^{R} - Q_{12}{}^{R}\,\Sigma RQ_{11}{}^{R}\right] f_y}{\left[\Sigma RQ_{11}{}^{R}\right]\left[\Sigma RQ_{22}{}^{R}\right] - \left[\Sigma RQ_{12}{}^{R}\right]^2} \qquad 8$$

$$f_y{}^{R} = \frac{-\left[Q_{22}{}^{R}\,\Sigma RQ_{12}{}^{R} - Q_{12}{}^{R}\,\Sigma RQ_{22}{}^{R}\right] f_x + \left[Q_{22}{}^{R}\,\Sigma RQ_{11}{}^{R} - Q_{12}{}^{R}\,\Sigma RQ_{12}{}^{R}\right] f_y}{\left[\Sigma RQ_{11}{}^{R}\right]\left[\Sigma RQ_{22}{}^{R}\right] - \left[\Sigma RQ_{12}{}^{R}\right]^2}$$

$$f_{xy}{}^{R} = \frac{Q_{66}{}^{R} f_{xy}}{\Sigma RQ_{66}{}^{R}}$$

The longitudinal tension strength, $F_x{}^{tu}$, for $[0/1.57/\pm\theta]$ ($[0/90/\pm\theta]$) laminates is obtained from Eq. 8

$$F_x^{tu} = F_x^{L} \frac{\left[\Sigma RQ_{11}^{R}\right]\left[\Sigma RQ_{22}^{R}\right] - \left[\Sigma RQ_{12}^{R}\right]^2}{\left[Q_{11}^{R}\,\Sigma RQ_{22}^{R} - Q_{12}^{R}\,\Sigma RQ_{12}^{R}\right]}$$

where $F_x{}^{L}$ is the composite layer strength.

The equation for laminate modulus of elasticity, E_x, of multi-directional laminates is obtained from Eq. 6.

$$E_x = \Sigma RQ_{11}^R - \frac{\left[\Sigma RQ_{12}^R\right]^2}{\Sigma RQ_{22}^R}$$

The analysis was programmed as the IBM 1130 computer program 'PRPCK'. Mechanical properties and strengths for the laminates with configurations 'A', 'B', and 'C' were obtained using the above program.

Table 2-2 lists the unidirectional properties of GY70/E702 and Type A/E702 Gr/Ep used in the analysis of the multi-directional laminates 'A', 'B', and 'C'. The moduli values, E_L, E_T, G_{LT} reflect the latest available test data. The transverse modulus, E_T, is the average of the tension and compression moduli. The transverse tension and compression moduli from References 2 and 3 are 11.0 x 10^9 N/M^2 (1.6 x 10^6 psi) and 20.0 x 10^9 N/M^2 (2.9 x 10^6 psi), respectively. The difference between the tension and compression moduli in the longitudinal direction is only on the order of 10 percent. This average transverse modulus gives better correlation in the evaluation of the coefficient of thermal expansion.

A discussion of the test results vs. predictions, for the various material properties of the 'A', 'B', and 'C' laminate configurations are presented as follows:

- Tensile Strength and Modulus - The tensile specimens were 12.7 mm (.50 inches) wide and 279.4 mm (11.00 inches) long with fiberglass gripping tabs adhesively bonded to each side of both ends of the otherwise rectangular, uniform cross-section. These tabs extend beyond the length of the specimen to assure proper alignment during test. Pins placed in the holes at the ends of the tabs, mate with grooves in the top surface of laterally self-aligning grips to assure alignment. The specimens were subjected to axial loading.

  The results of the tension element tests are summarized in Tables 2-3 and 2-4, and compared to predicted values. The ratios of average test to predicted modulus in the longitudinal direction

Table 2-2

Unidirectional Properties of GY70/E702 and Type A/E702 Graphite/Epoxy

Property	GY70/E702 Gr/Ep			
	RT		-50°C (-58°F)	
	Max	Min	Max	Min
E_L, N/m^2 (psi)	290 x 10^9 (42.0 x 10^6)		*	
E_T, N/m^2 (psi)	6.90 x 10^9 (1.00 x 10^6)		*	
G_{LT}, N/m^2 (psi)	4.83 x 10^9 (.700 x 10^6)		*	
ν_{LT}	.25		*	
F^{tu}, N/m^2 (psi)	621 x 10^6 (90 x 10^3)		*	
α_L, m/m/°C (in/in/°F)	-.900 x 10^{-6} (-.500 x 10^{-6})	-1.08 x 10^{-6} (-.600 x 10^{-6})	-.954 x 10^{-6} (-.530 x 10^{-6})	-1.13 x 10^{-6} (-.630 x 10^{-6})
α_T, m/m/°C (in/in/°F)	30.6 x 10^{-6} (17.0 x 10^{-6})	28.2 x 10^{-6} (15.7 x 10^{-6})	25.9 x 10^{-6} (14.4 x 10^{-6})	23.8 x 10^{-6} (13.2 x 10^{-6})
t, m (inches)	1.60 x 10^{-4} (.0063)			
	Type A/E702 Gr/Ep			
E_L, N/m^2 (psi)	128 x 10^9 (18.5 x 10^6)		*	
E_T, N/m^2 (psi)	15.5 x 10^9 (2.25 x 10^6)		*	
G_{LT}, N/m^2 (psi)	4.83 x 10^9 (.700 x 10^6)		*	
ν_{LT}	.25		*	
F^{tu}, N/m^2 (psi)	1455 x 10^6 (211 x 10^3)		*	
α_L, m/m/°C (in/in/°F)	.540 x 10^{-6} (.300 x 10^{-6})	.259 x 10^{-6} (.144 x 10^{-6})	.191 x 10^{-6} (.106 x 10^{-6})	.120 x 10^{-6} (.0666 x 10^{-6})
α_T, m/m/°C (in/in/°F	28.4 x 10^{-6} (15.8 x 10^{-6})	25.9 x 10^{-6} (14.4 x 10^{-6})	23.0 x 10^{-6} (12.8 x 10^{-6})	19.8 x 10^{-6} (11.0 x 10^{-6})
t, m (inches)	1.33 x 10^{-4} (.00525)			

Table 2-3 Theoretical and Test Tension Moduli
For Laminates 'A', 'B' and 'C'

Laminate	Orientation	E^t_{test} $10^9 N/M^2$ (msi)	E^t_{test} (Avg) $10^9 N/M^2$ (msi)	E_{pred} $10^9 N/M^2$ (msi)	E_{test}/E_{pred}
A	longitudinal	150.97 (21.9) 155.11 (22.5) 160.63 (23.3) 177.17 (25.7)	161.31 (23.4)	155.80 (22.6)	1.04
A	transverse	17.85 (2.59) 18.61 (2.70 22.54 (3.27) 23.57 (3.42) 25.09 (3.64)	21.57 (3.12)	27.78 (4.03)	.776
B	longitudinal	132.36 (19.2) 135.12 (19.6) 144.08 (20.9) 144.08 (20.9) 146.15 (21.2)	140.63 (20.4)	139.25 (20.2)	1.01
B	transverse	35.71 (5.18) 39.15 (5.68) 43.77 (6.35 44.05 (6.39) 44.46 (6.45)	41.43 (6.01)	47.29 (6.86)	.876
C	longitudinal	125.47 (18.2) 127.53 (18.5) 132.36 (19.2) 166.14 (24.1)	137.88 (20.0)	141.32 (20.5)	.975
C	transverse	63.35 (9.19) 69.62 (10.1) 71.69 (10.8) 74.45 (10.8)	69.62 (10.1)	76.52 (11.1)	.909

Table 2-4 Theoretical and Test Tension Strength
For Laminates 'A', 'B' and 'C'

Laminate	Orientation	F^{ult} test $10^6 N/M^2$	(KSI)	F^{ult} test (AVG) $10^6 N/M^2$	(KSI)	F^{ult} pred $10^6 N/M^2$	(KSI)	F^{ult}/F^{ult} test pred
A	longitudinal	340	(49.3)					
		356	(51.7)					
		380	(55.1)					
		351	(50.9)					
		349	(50.6)	355	(51.5)	332	(48.2)	1.07
A	transverse	Tab Failure				197	(28.6)	
B	longitudinal	262	(38.0)					
		225	(32.6)					
		316	(45.8)					
		261	(37.9)					
		291	(42.2)	271	(39.3)	296	(43.0)	.914
B(1)	longitudinal	279	(40.5)					
		294	(42.6)					
		292	(42.4)					
		369	(53.5)					
		284	(41.2)	303	(44.0)	296	(43.0)	1.02
B(1)(2)	transverse	240	(34.8)					
		235	(34.1)					
		245	(35.6)					
		233	(33.8)					
		251	(36.4)	272	(39.4)	349	(50.6)	.779
C	longitudinal	203	(29.4)					
		248	(36.0)					
		329	(47.7)					
		255	(37.0)					
		199	(28.8)	247	(35.8)	303	(44.0)	.814
C	transverse	138	(20.0)					
		155	(22.5)					
		140	(20.3)					
		132	(19.1)					
		105	(15.3)	134	(19.4)	163	(23.7)	.819

(1) Second Batch Material

(2) Failure by splitting of laminate in the tab region

for laminates 'A', 'B', and 'C', are 1.035, 1.009, and .975, respectively. These ratios show excellent agreement between theory and test. In the transverse direction the agreement between theory and test is only fair. The ratios of average test to predicted modulus in the transverse direction for laminates 'A', 'B', and 'C', are .776, .876, and .909, respectively. This discrepancy can be explained as being the result of using the average of the transverse tension and compression moduli rather than the transverse tension modulus. Laminate 'A' which has layers of Type A Gr/Ep in the 1.57 rad (90°) and $\pm$.264 rad ($\pm$15° 07') degree directions shows the largest difference between theory and experiment. In addition to using a much higher unidirectional transverse modulus for the Type A graphite this laminate because of the orientation of its angle plies at $\pm$.264 rad ($\pm$15° 07') exhibits considerable edge effects. The experimentally obtained moduli range between 17.9×10^9 N/M^2 (2.59×10^6 psi) and 25.1×10^9 N/M^2 (3.64×10^6 psi). The use of the lower transverse tension modulus for the Type A graphite yields laminate moduli closer to the test results.

Tension strength test results listed in Table 2-4 show fairly good agreement with predicted values. Excellent correlation was obtained for laminates 'A' and 'B' in the longitudinal directions. Test strengths for laminate 'C' showed a wide scatter. Results for the transverse 'A' and 'B' (first batch) laminates are not included since all failures were in the tab area.

- Compression Strength and Modulus - The compression properties were determined on specimens subjected to direct end loading. They were of the rectangular, constant section "Northrop" configuration, with adhesively bonded fiberglass tabs at both ends, acting as spacers during test and allowing for installation of strain gages on the center of the specimen. During test the load was applied axially with the specimen supported in the Northrop type fixture.

The results of the compression element tests are summarized and compared to predicted values in Tables 2-5 and 2-6. The ratios of average test to predicted modulus for the three material/laminate configurations range from .827 to 1.14. A large scatter in the compression test results was observed. The compression test moduli are lower than the tension test moduli. Because both tension and compression moduli for unidirectional graphite/epoxy are equal, the same moduli for tension and compression for laminates 'A', 'B', and 'C' have been listed under design properties in Table 2-8. Table 2-5 lists compression strength test results and the predicted values.

- Flexural Strength and Modulus - The specimens were 1016 mm (4 inches) long by 12.7 mm (.50 inch) wide uniform bars of rectangular cross-section which were tested as simply supported beams. The specimens were tested under single point center loading at a span-to-thickness ratio ($\frac{L}{t}$) of 32:1 and symmetric two point loading over a span of 44t (secondary span of 18t). During test the center deflections of the specimens were measured using an LVDT type deflectometer.

  Flexure tests were performed on coupons of type 'A', 'B' and 'C' laminates. Results of these tests are presented in Table 2-7. These coupons were analyzed by considering the individual layers comprising the coupons. Stress in each layer is determined by distributing the bending moment to each layer proportionately according to the layer modulus and to the distance from the neutral axis. The ratios of average test to predicted flexure strength for the three material/laminate configuration vary from .925 to 1.225. Flexural test moduli are not compared to predicted values due to improper failure mode (the specimens failed in interlaminar shear).

- Horizontal Shear - The horizontal shear specimens were 22.8 mm (90 inch) long by 6.35 mm (250 inch) wide uniform bars of constant cross-section. They were tested as center loaded simply supported beams over a span-to-thickness ratio of 5:1.

Table 2-5 Theoretical and Test Compression Moduli
For Laminates 'A', 'B' and 'C'

Laminate	Orientation	E^c_{test} $10^9 N/M^2$ (msi)	E^c_{test} (Avg) $10^9 N/M^2$ (msi)	E_{pred} $10^9 N/M^2$ (msi)	E_{test}/E_{pred}
A	longitudinal	97.89 (14.2) 125.47 (18.2) 129.60 (18.8) 133.74 (19.4) 159.25 (23.1)	129 (18.7)	156 (22.6)	.827
A	transverse	20.26 (2.94) 20.54 (2.98) 26.61 (3.86) 30.19 (4.38)	31.7 (4.60)	27.8 (4.03)	1.14
B	longitudinal	96.51 (14.0) 119.26 (17.3) 122.02 (17.7) 144.08 (20.9) 163.38 (23.7)	129 (18.7)	139 (20.2)	.926
B	transverse	39.29 (5.70) 40.26 (5.84) 41.08 (5.96) 44.67 (6.48) 47.22 (6.85)	42.5 (6.17)	47.3 (6.86)	.899
C	longitudinal	113.75 (16.5) 115.81 (16.8) 124.09 (18.0) 124.78 (18.1) 140.63 (20.4)	124 (18.0)	141 (20.5)	.878
C	transverse	58.32 (8.46) 61.70 (8.95) 63.49 (9.21) 67.35 (9.77) 68.38 (9.92)	63.8 (9.26)	76.5 (11.1)	.834
B(1)	longitudinal	118.7 (17.2) 122.8 (17.8) 122.0 (17.7) 110.3 (16.0 126.1 (18.3)	120 (17.4)	139 (20.2)	.862
B(1)	transverse	38.6 (5.6) 42.7 (6.2) 40.0 (5.8) 46.9 (6.8) 40.7 (5.9)	41.8 (6.06)	47.3 (6.86)	.885

(1) Batch No. 2

Table 2-6 Theoretical and Test Compression Strength
For Laminates 'A', 'B' and 'C'

Laminate	Loading	No. Tests	F^{ult}_{test} (Avg.)[1] $10^6 N/m^2$	(ksi)	F^{ult}_{pred} $10^6 N/m^2$	(ksi)	$F^{ult}_{test}/F^{ult}_{pred}$
A	Longitudinal	5	498	(72.2)	332	(48.2)	1.50
A	Transverse	5	207	(30.0)	197	(28.6)	1.05
B	Longitudinal	5	353	(51.2)	296	(43.0)	1.19
B	Transverse	5	453	(65.7)	349	(50.6)	1.30
B[2]	Longitudinal	5	299	(43.4)	288	(43.0)	1.01
B[2]	Transverse	5	432	(62.6)	488	(50.6)	1.24
C	Longitudinal	5	374	(54.2)	303	(44.0)	1.23
C	Transverse	5	202	(29.3)	163	(23.7)	1.24

[1] Based upon nominal per ply thicknesses of .160mm (.0063) for GY70, and .133mm (.00525 in) for Type A.

[2] Batch No. 2

Table 2-7 Theoretical and Test Flexural Strength
For Laminates "A", "B" and "C"

Laminate	Loading	No.of Tests	$F_{b_{test}}^{ult}$(Avg) $10^6 N/m^2$(ksi)	$F_{b_{pred}}^{ult}$ $10^6 N/m^2$(ksi)	F_{test}/F_{pred}	Critical Layer Material and Angle Between Load and Filament
A	Longitudinal	5	681.1 (98.8)	620.5 (90)	1.09	GY70 at 0 RAD (0°)
A	Transverse	5	78.5 (11.39)	68.9 (10)	1.14	Type A at 1.3 RAD (75°)
B	Longitudinal	5	698.4 (101.3)	620.5 (90)	1.225	GY70 at 0 RAD (0°)
B	Transverse	5	19.1 (2.77)	20.7 (3)	.925	GY70 at 1.57 RAD (90°)
C	Longitudinal	5	22.1 (3.20)	20.7 (3)	1.07	GY70 at 1.57 RAD (90°)
C	Transverse	5	710.1 (103)	620.5 (90)	1.14	GY70 at 0 RAD (0°)

The results of the horizontal shear tests are given in Appendix B. These tests are used primarily for material qualification and the results which varied from 24.1×10^6 N/m^2 (3.5 ksi) to 30.5×10^6 N/m^2 (4.43 ksi) are considered acceptable. The horizontal (interlaminar) shear strength of unidirectional GY70 Gr/Ep is 37.3×10^6 N/m^2 (5.4 ksi), but for multi-directional laminates this value is considerably reduced. Assuming a trend similar to that observed in boron/epoxy this reduction is of the order of 40 percent.

Table 2-8 lists design properties for laminates 'A', 'B' and 'C'. Strength allowables are given as 80 percent of predicted values.

2.4.2 Coefficient of Thermal Expansion Investigation

A preliminary investigation to determine the thermal expansion characteristics of graphite composites was performed using available unidirectional mechanical and physical data. The goal was to obtain a near-zero coefficient of thermal expansion by combining high-strength and high modulus graphite/epoxy layers in an orthotropic laminate. Laminates with at least four layer orientations, 0 rad (0°), 1.57 rad (90°) and $\pm\theta$ rad (θ°) were chosen in order to have a "filament controlled laminate" not primarily resin dependent.

A search technique, programmed as the IBM 360/67 computer program "ZERCO", was utilized to find laminates with zero coefficient of thermal expansion. In the analysis, the elastic and thermal response of each layer of the multi-directional laminates in a state of plane stress is given by

$$\begin{bmatrix} \sigma_L \\ \sigma_T \\ \tau_{LT} \end{bmatrix} = \begin{bmatrix} Q_{11} & Q_{12} & 0 \\ Q_{12} & Q_{22} & 0 \\ 0 & 0 & 2Q_{66} \end{bmatrix} \begin{bmatrix} \epsilon_L - \alpha_L \Delta T \\ \epsilon_T - \alpha_T \Delta T \\ \frac{1}{2}\gamma_{LT} \end{bmatrix} \qquad 9$$

where

$$\begin{aligned} Q_{11} &= E_L/(1 - \nu_{LT}\,\nu_{TL}) \\ Q_{12} &= \nu_{LT}\,E_T/(1 - \nu_{LT}\,\nu_{TL}) \\ Q_{22} &= E_T/(1 - \nu_{LT}\,\nu_{TL}) \\ Q_{66} &= G_{LT} \end{aligned} \qquad 10$$

Table 2-8 Design Properties for Laminates 'A', 'B' and 'C' at RT

GY70 0-rad (0°) Layers; Type A 1.57-rad (90°), ±θ Layers

A. [2/1/4] θ = .264-rad (15° 07')
B. [4/2/4] θ = .908-rad (52° 02')

GY70 0-rad (0°) and 1.57-rad (90°) layers; Type A ±θ Layers

C. [4/2/4] θ = .721-rad (41° 18')

Property \ Configuration	A	B	C
L, 0-rad (0°) Layers*	.324 (GY70)	.444 (GY70)	.429 (GY70)
M, 1.57-rad (90°) Layers*	.135 (Type A)	.185 (Type A)	.214 (GY70)
N, ±θ Layers*	.541 (Type A)	.371 (Type A)	.357 (Type A)
θ, Radians (Degrees)	.264 (15° 07')	.908 (52° 02')	.721 (41° 18')
α_L, m/m/°C(in/in/°F)**	$-.09\times10^{-6}$ ($-.05\times10^{-6}$)	$.26\times10^{-6}$ ($.14\times10^{-6}$)	$.3\times10^{-6}$ ($.17\times10^{-6}$)
α_L m/m/°C (in/in/°F)	11.2×10^{-6} (6.20×10^{-6})	4.05×10^{-6} (2.25×10^{-6})	1.44×10^{-6} (0.80×10^{-6})
E_L, N/m^2 (psi)	156×10^9 (22.6×10^6)	139×10^9 (20.2×10^6)	141×10^9 (20.5×10^6)
E_T, N/m^2 (psi)	27.8×10^9 (4.03×10^6)	47.3×10^9 (6.86×10^6)	76.5×10^9 (11.1×10^6)
G_{LT}, N/m^2 (psi)	8.81×10^9 (1.28×10^6)	15.0×10^9 (2.18×10^6)	15.1×10^9 (2.19×10^6)
ν_{LT}	.255	.271	.164
ν_{TL}	.046	.092	.089
F^{tu}, N/m^2 (psi)	$.266\times10^9$ (38600)	$.237\times10^9$ (34400)	$.242\times10^9$ (44000)
F^{cu}, N/m^2 (psi)	$.266\times10^9$ (38600)	$.237\times10^9$ (34400)	$.242\times10^9$ (44000)
F^{su}, N/m^2 (psi)	$.148\times10^9$ (21500)	$.253\times10^9$ (36700)	$.253\times10^9$ (36700)
Buckling Coefficients			
$F^{crit} = K\,(\frac{t}{b})^2$			
K_c, N/m^2 (psi)	141×10^9 (20.5×10^6)	202×10^9 (29.3×10^6)	239×10^9 (34.7×10^6)
K_s, N/m^2 (psi)	133×10^9 (19.3×10^6)	221×10^9 (32.1×10^6)	301×10^9 (43.7×10^6)

*Decimal fractions are based on relative thicknesses

**Average Test Values

E_L, E_T and G_{LT} are the longitudinal-transverse- and in-plane shear-moduli, respectively. ν_{LT} and ν_{TL} are the major and minor Poisson's ratios.

Using a coordinate transformation the stress-strain relation for a layer when the applied stress makes an angle θ with respect to the natural layer axis is given by

$$\begin{bmatrix} \sigma_x \\ \sigma_y \\ \tau_{xy} \end{bmatrix} = \begin{bmatrix} Q^1 \end{bmatrix} \begin{bmatrix} \epsilon_x - \alpha_x \Delta T \\ \epsilon_y - \alpha_y \Delta T \\ \frac{1}{2}\gamma_{xy} - \frac{1}{2}\alpha_{xy} \Delta T \end{bmatrix} \qquad 11$$

where

$$[Q^1] = [T]^{-1} [Q][T] \qquad 12$$

and

$$[T] = \begin{bmatrix} \cos^2\theta & \sin^2\theta & 2\sin\theta\cos\theta \\ \sin^2\theta & \cos^2\theta & -2\sin\theta\cos\theta \\ -\sin\theta\cos\theta & \sin\theta\cos\theta & \cos 2\theta \end{bmatrix} \qquad 13$$

For a laminated composite consisting of n layers symmetrically laminated about the middle surface of the laminate (no coupling between in-plane loading and out-of-plane deformation) the following expression is obtained

$$[N] = [A][\epsilon] - [B]\Delta T \qquad 14$$

where N_x, N_y and N_{xy} are the stress resultants and the matrices $[A]$ and $[B]$ are given by the following expressions

$$A_{ij} = \sum_{k=1}^{n} {Q_{ij}}^{1(k)} (h_{k+1} - h_k)$$

$$B_i = \sum_{k=1}^{n} ({Q_{ij}}^{1(k)} \alpha_j^{(k)}) (h_{k+1} - h_k) \qquad 15$$

$$i = 1, 2, 3$$

$$j = 1, 2, 3$$

where
$$\alpha_1^{(k)} = \alpha_x^{(k)}$$
$$\alpha_2^{(k)} = \alpha_y^{(k)} \qquad 16$$
$$\alpha_3^{(k)} = \tfrac{1}{2}\,\alpha_{xy}^{(k)}$$

The coefficients of thermal expansion α_x, α_y, α_{xy} for the laminate are obtained from Eq. 14 by setting the resultant stresses, $\lceil N \rceil$, equal to zero.

$$\begin{bmatrix} \alpha_x \\ \alpha_y \\ \alpha_{xy} \end{bmatrix} = [A]^{-1}\,\lceil B \rceil \qquad 17$$

The program involves a systematic search of laminates composed of layers at 0 rad (0°), 1.57 rad (90°) and $\pm\theta$ rad (θ°). The angle of the angle plies ($\pm\theta$ rad) is increased by .0875 rad (5°) increments and for each angle θ, a layup which results in a coefficient of thermal expansion, α, equal to zero is found for each of four cases (proportion of 1.57 rad (90°) layers equal to 0, 5, 10, and 15 percent). For some cases no combination of 0-rad (0°) and $\pm\theta$-rad (θ°) layers can result in a zero coefficient. Figure 2-8 presents a typical carpet plot of variation of coefficient of thermal expansion (C.T.E.) vs. orientation of angle plies. Each laminate configuration which resulted in a zero coefficient of thermal expansion was then checked against minimum stiffness requirements and adjusted maintaining $\alpha = 0$.

From the above preliminary investigation eleven laminates were selected for further study. Figure 2-9 shows a plot of the longitudinal coefficient of thermal expansion versus orientation of the angle plies for six laminates composed of GY70 0-rad (0°) layers and Type A 1.57-rad (90°) and $\pm\theta$-rad (θ) with the E702 resin system at room temperature. Figure 2-10 shows a similar plot of the longitudinal coefficient of thermal expansion versus orientation of the angle plies for five laminates composed of GY70 0- and 1.57-rad (0° and 90°) layers and Type A $\pm\theta$-rad (θ°) layers with the E702 resin system at room temperature.

Three material/laminate configurations, 'A', 'B', and 'C' were selected for fabrication and test.

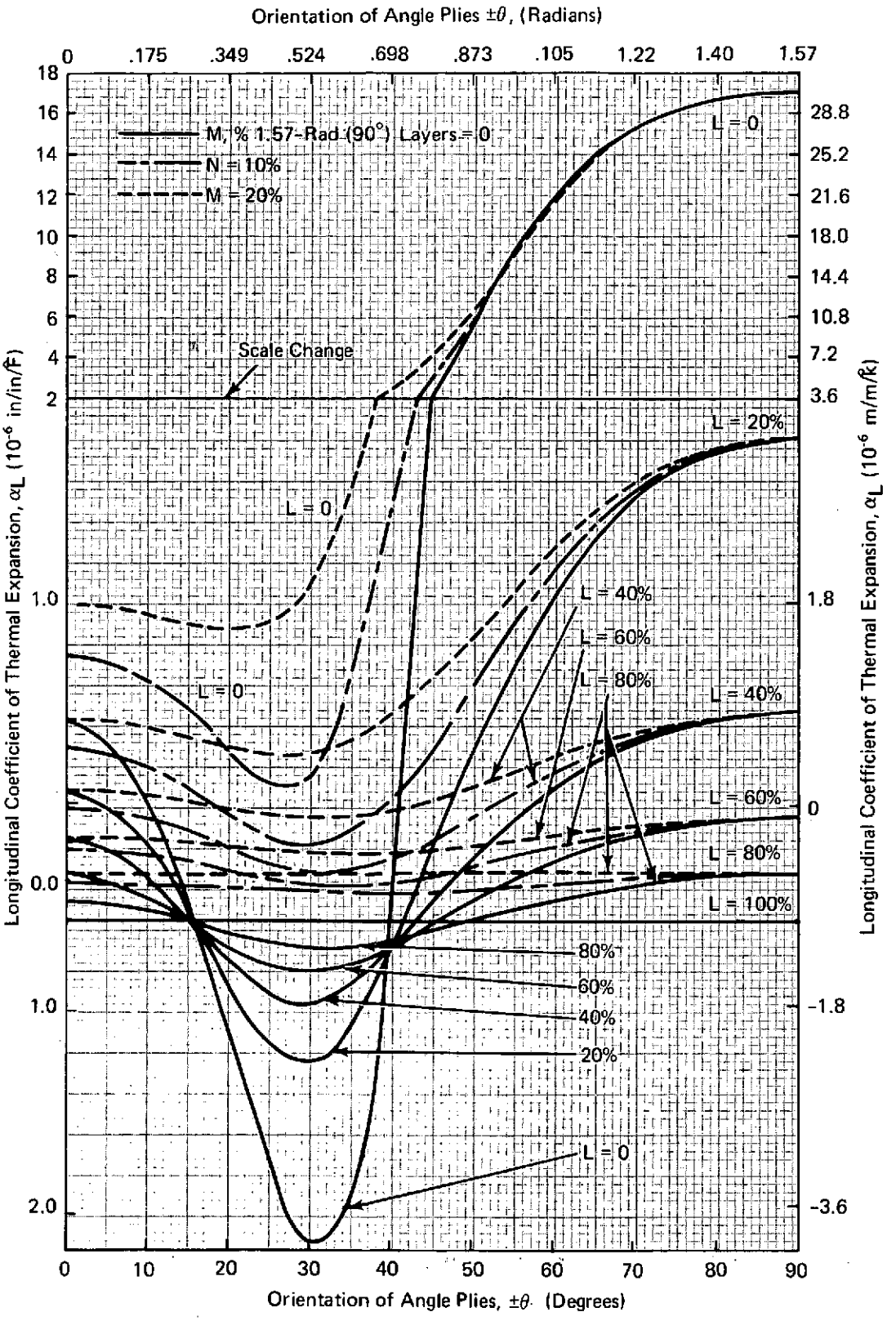

Figure 2-8 Typical Carpet Plot of Coefficient of Thermal Expansion Vs. Orientation of Angle Plies

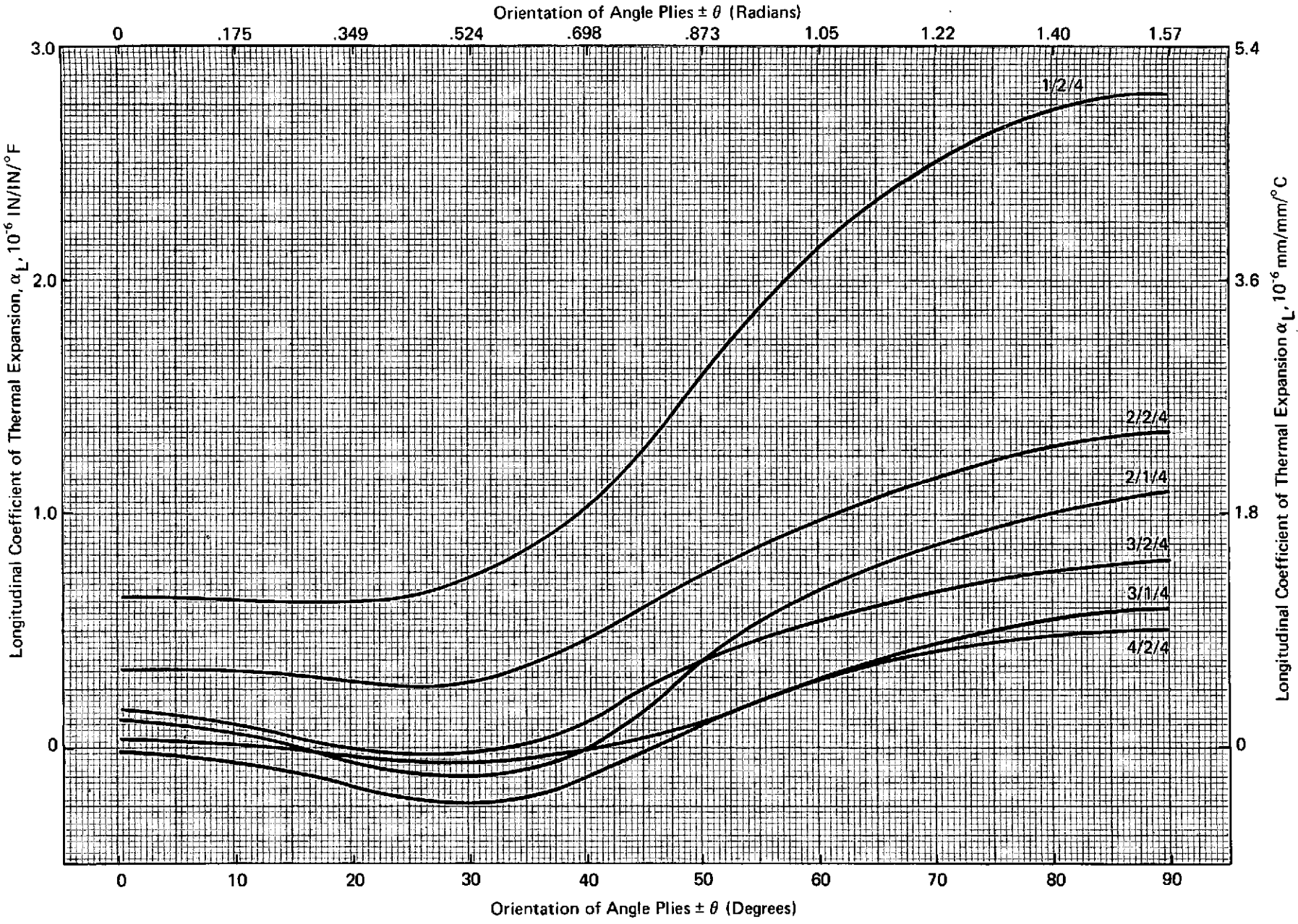

Figure 2-9 Coefficient of Thermal Expansion of Laminates Composed of GY70 0-Rad (0°) Layers Type A1.57 Rad 90° ± θ Layers With the E702 Resin System Using R.T. Properties

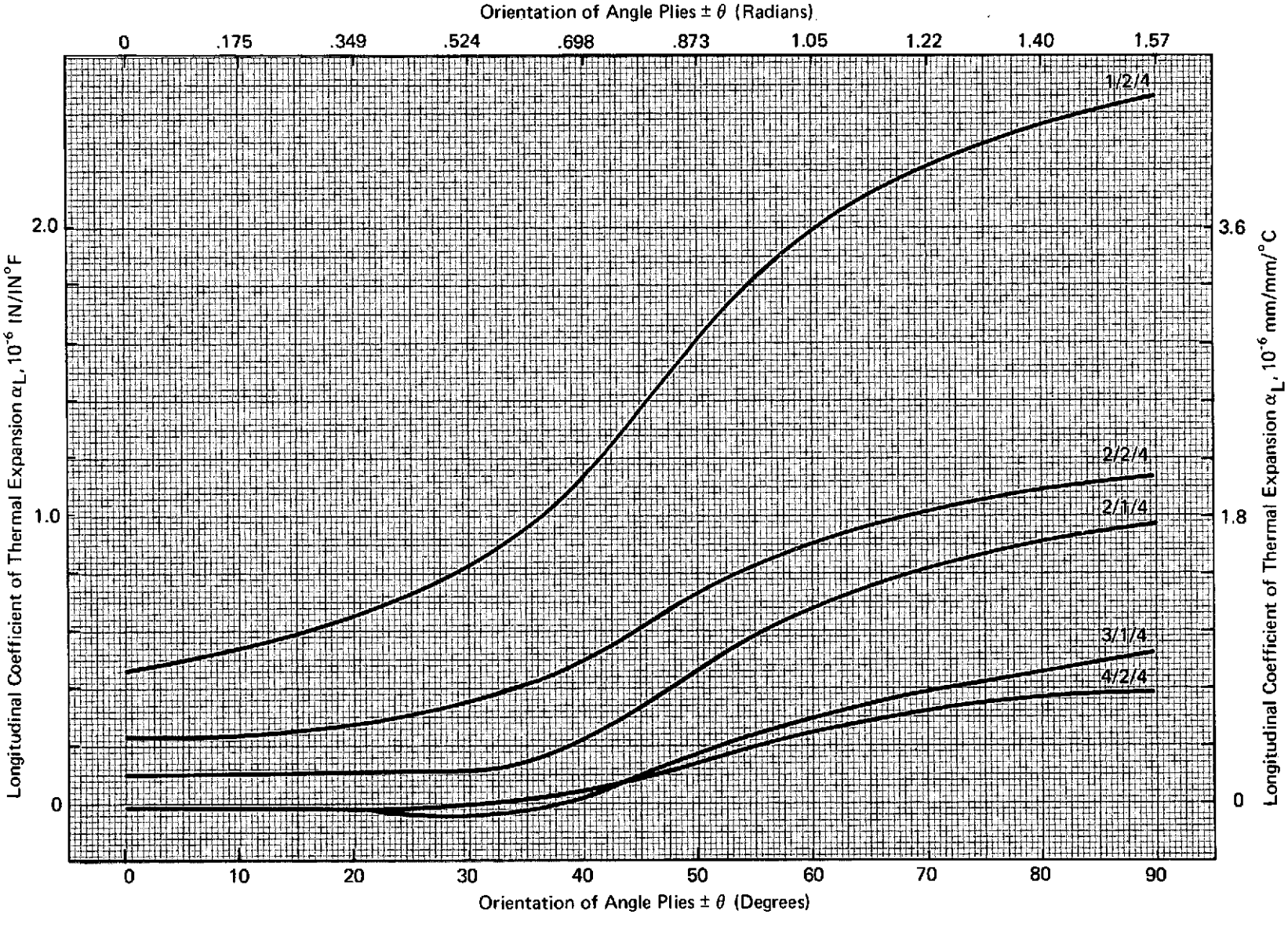

Figure 2-10 Coefficient of Thermal Expansion of Laminates Composed of GY70 0 & 1.57 Rad (0° & 90°) Layers, Type A ± θ Layers With The E702 Resin System Using R.T. Properties

Factors affecting selection of these specific configurations were the slope of the curve - a relatively gentle slope was desired in order to minimize variation in the coefficient for slight variation in orientation (manufacturing tolerances), laminate symmetry-to minimize distortions in the cured parts and to avoid large built-in interlaminar stresses, and a sufficiently different $\pm\theta$ orientation - to yield data over the broadest possible spectrum, within program scope.

Configuration 'A' consists of two GY70 0-rad (0°) layers, one Type A 1.57-rad (90°) layer and four $\pm$.264-rad ($\pm$15° 07') layers. Configuration 'B' consists of four GY70 0-rad (0°) layers, two Type A 1.57-rad (90°) layers and four $\pm$.908-rad ($\pm$52° 02') layers. Configuration 'C' consists of four 0-rad (0°) and two 1.57-rad (90°) layers of GY70 and four Type A $\pm$.721-rad ($\pm$41° 18') layers.

Analytical checks of the three selected laminates were made, in the tubular configuration, and indicated that all design criteria were either met or exceeded i.e., EI_{min} EA_{min}, column buckling, local buckling and strength requirements.

Subsequent to analytical selection of the three laminate configurations the test program was begun. At the initiation of the test program some problems developed relative to the test procedures, apparatus and lack of specimen pre-conditioning. The problems and their resolution are discussed in succeeding paragraphs.

Initially, the coefficient of thermal expansion tests were conducted at GAC. The test specimens were uniform bars of rectangular cross-section, 76.3 mm (3.0 in) in length and 12.7 mm (.50 in) in width. Testing was conducted in a high precision Theta Industries vitreous silica dilatometer which was calibrated after every third run with an NBS quartz standard. A heating and cooling chamber was used to provide the necessary thermal environment, -40°C to 65°C (-40°F to +150°F), with specimen temperature monitored by a thermocouple positioned close to the mid-point of the specimen. Both specimen temperature and length change were continuously monitored and plotted on a Texas Instruments dual-pen recorder. The specimens were cooled from ambient room temperature to -40°C (-40°F) and maintained at this temperature until stabilization occurred. The specimens were then heated to

-15°C, +10°C, +35°C (+5°F, -50°F, +95°F) and finally to 65°C (+150°F) and the same stabilization procedure followed.

The values for the quartz standard are based upon the "Certificate of Analysis" for Standard Reference Material 739 (fused-silica) published by the National Bureau of Standards.

The initial results obtained from the Type A/E702 longitudinal coefficient tests showed a major discrepancy from the predicted values. At this time, one specimen was sent to the IIT Research Institute to be tested and a thorough investigation of Grumman's test set up was conducted. This investigation showed that while system operation was proper, it exhibited a lack of sensitivity and response, thus precluding sufficiently accurate results. As a result of the IITRI test and the equipment check, a decision was made to run all future coefficient of thermal expansion specimens at Theta Industries, Inc.

The test measurements made by Theta were conducted on a high precision Theta Industries differential silica dilatometer with active temperature control for all critical system components. The specimen configuration was modified to 50.8 mm (2.0 in) in length by 6.4 mm (.25 in) in accordance with Theta's requirements. The expansion calibration was carried out with a 0.010 inch thick gage block, having an inaccuracy of 0.01%. The linearity of the differential transformer is better than 0.25%. A Digitec Model 1268 Voltmeter was used for a continuous read out. A copper versus copper-nickel thermocouple (Type T) was used for temperature measurement. During the expansion test measurements, the junction temperature was held at +35°C $\pm$ 0.5°C (95°F $\pm$ .9°F). An NBS quartz standard was used as the reference material (see Figure 2-11 for test set-up). The temperature range of the tests was -100°C to +20°C (-148°F to +68°F).

After the specimen and reference standard were loaded inside the test tube, the system was evacuated for approximately 10 minutes. Air passing thru phospherus pentoxide (to remove the moisture) was then filled into the system at a rate of 0.5 liter/minute. The system was then stabilized for approximately 15 hours. Liquid nitrogen was then filled into the double walled protection tube to cool the specimen and reference. The nitrogen

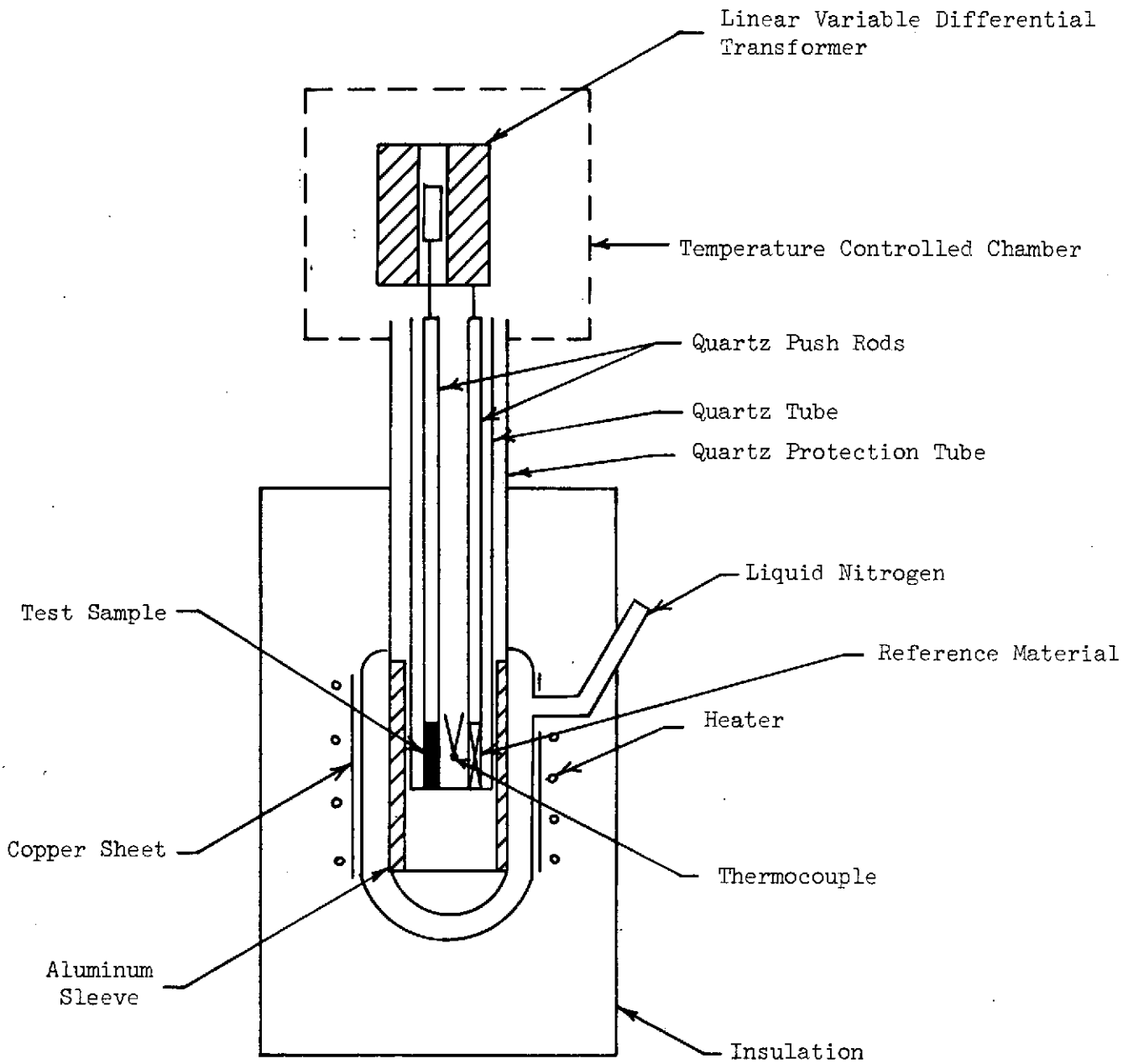

Figure 2-11 Schematic of Theta Dilatometer

was filled in intervals to achieve a cooling rate of approximately 4° C/min (7.2°F). From -100°C to -60°C (-148°F to -76°F) the inside tube (containing the specimen and reference) warmed up by itself; after that the tube was heated to achieve a heat-up rate of approximately 3/4°C/min (1.35°F/min).

Initial test results from Theta for the Type A unidirectional specimens indicated that after a re-run of the tests a change of the measured coefficient was observed. As a result of this phenomenon all further test specimens were thermally stabilized for a period of one hour at -100°C (-148°F) prior to testing.

The test apparatus for the measurement of the coefficient of thermal expansion consists basically of two push rods in parallel. One push rod measures the expansion (or contraction) of the test specimen and the other push rod measures the quartz standard. Thus, the specimen growth is measured relative to the known growth of the quartz standard. Once all problems were resolved the test program was begun in earnest. Priority was given to C.T.E. testing the unidirectional GY70 and Type A laminates (both longitudinal and transverse) first. This was done so that test correlation data could be developed for the multi-directional laminates.

In order to analytically predict the coefficient of thermal expansion of multi-directional laminates it is necessary to have accurate values of the mechanical and physical properties of the unidirectional composite systems making up the laminate.

Figure 2-12 shows the longitudinal coefficient of thermal expansion of unidirectional GY70/E702 Gr/Ep specimens as a function of temperature. Scatter in the test results is significant. Values as low as -1.27×10^{-6} mm/mm/°C ($-.695 \times 10^{-6}$ in/in/°F) and as high as -1.05×10^{-6} mm/mm/°C ($-.584 \times 10^{-6}$ in/in°F) at -50°C (-58F) were obtained. Figure 2-13 shows the longitudinal coefficient of thermal expansion of unidirectional Type A/E702 Gr/Ep specimens as a function of temperature. Scatter in the test results is very significant at the higher temperatures. At 5°C (41°F) the value of α_L ranges between 0.56×10^{-6} mm/mm/°C ($.311 \times 10^{-6}$ in/in/°F) and 0.23×10^{-6} mm/mm/°C ($.128 \times 10^{-6}$ in/in/°F). Similarly Figures 2-14 and 2-15 show the transverse coefficients of thermal expansion at temperature

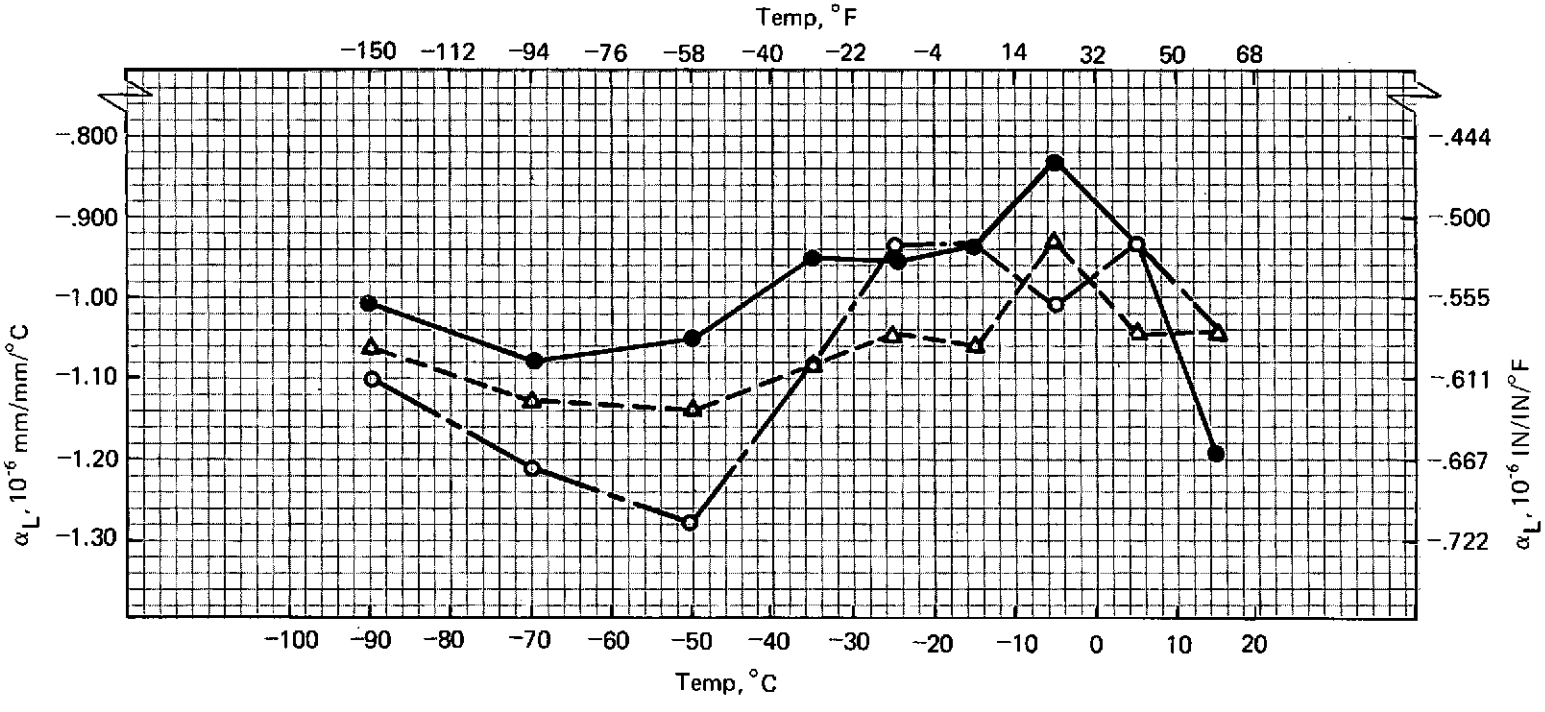

Figure 2-12 Coefficient of Thermal Expansion GY70/E702 Gr/Ep (Unidirectional)

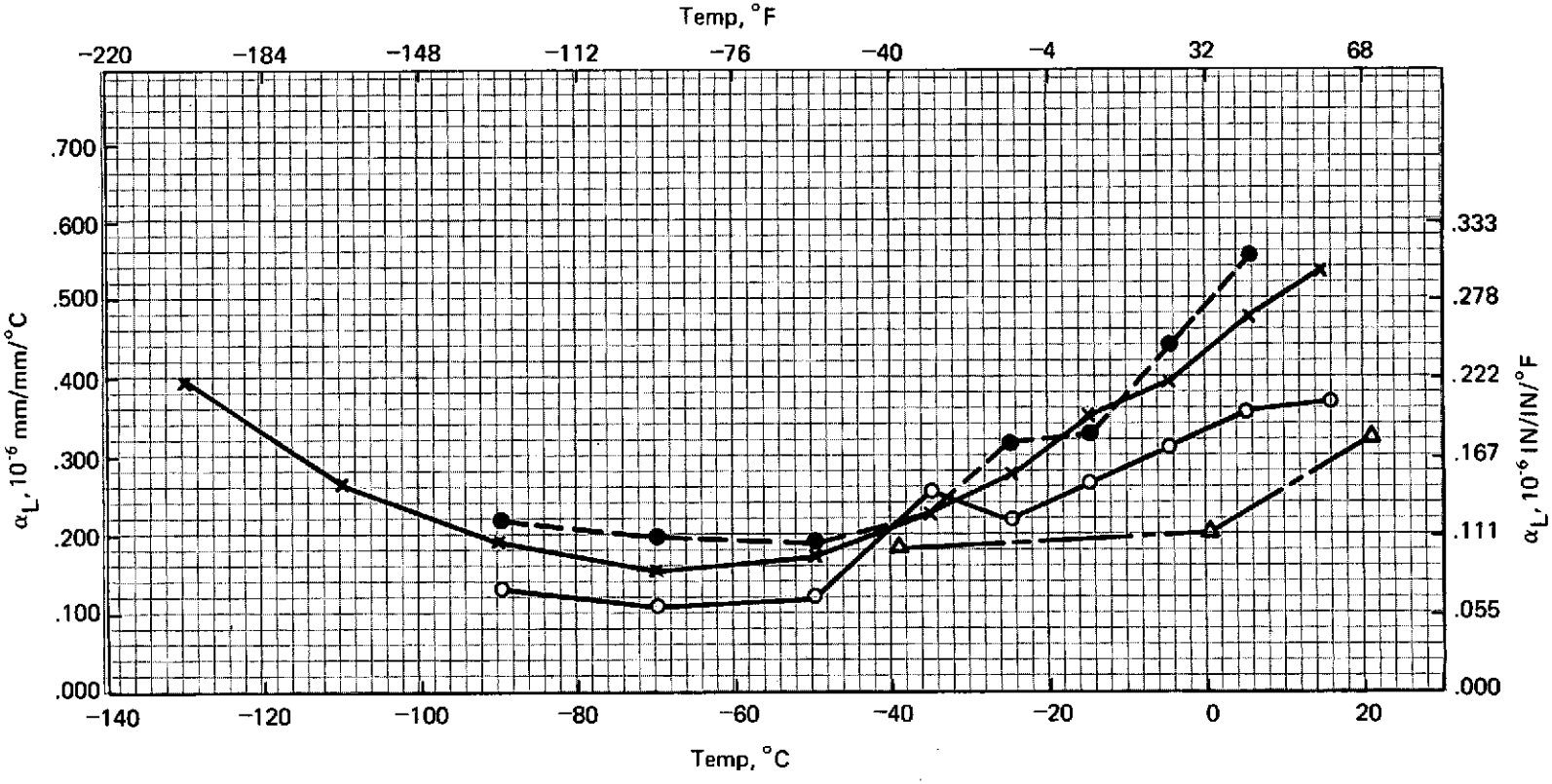

Figure 2-13 Coefficient of Thermal Expansion Type A/E702 Gr/Ep (Unidirectional)

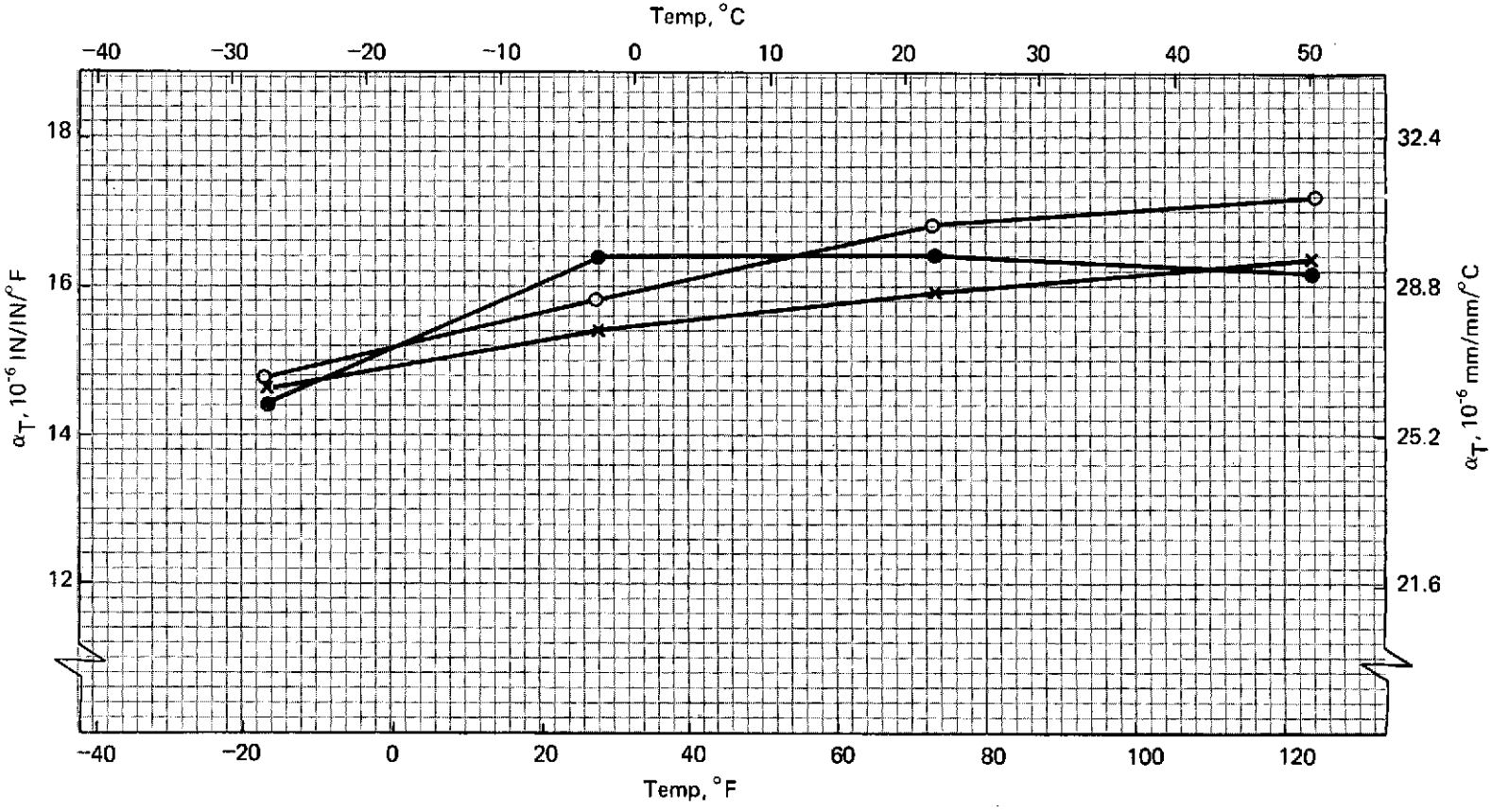

Figure 2-14 Transverse Coefficient of Thermal Expansion GY70/E702 Gr/Ep (Unidirectional)

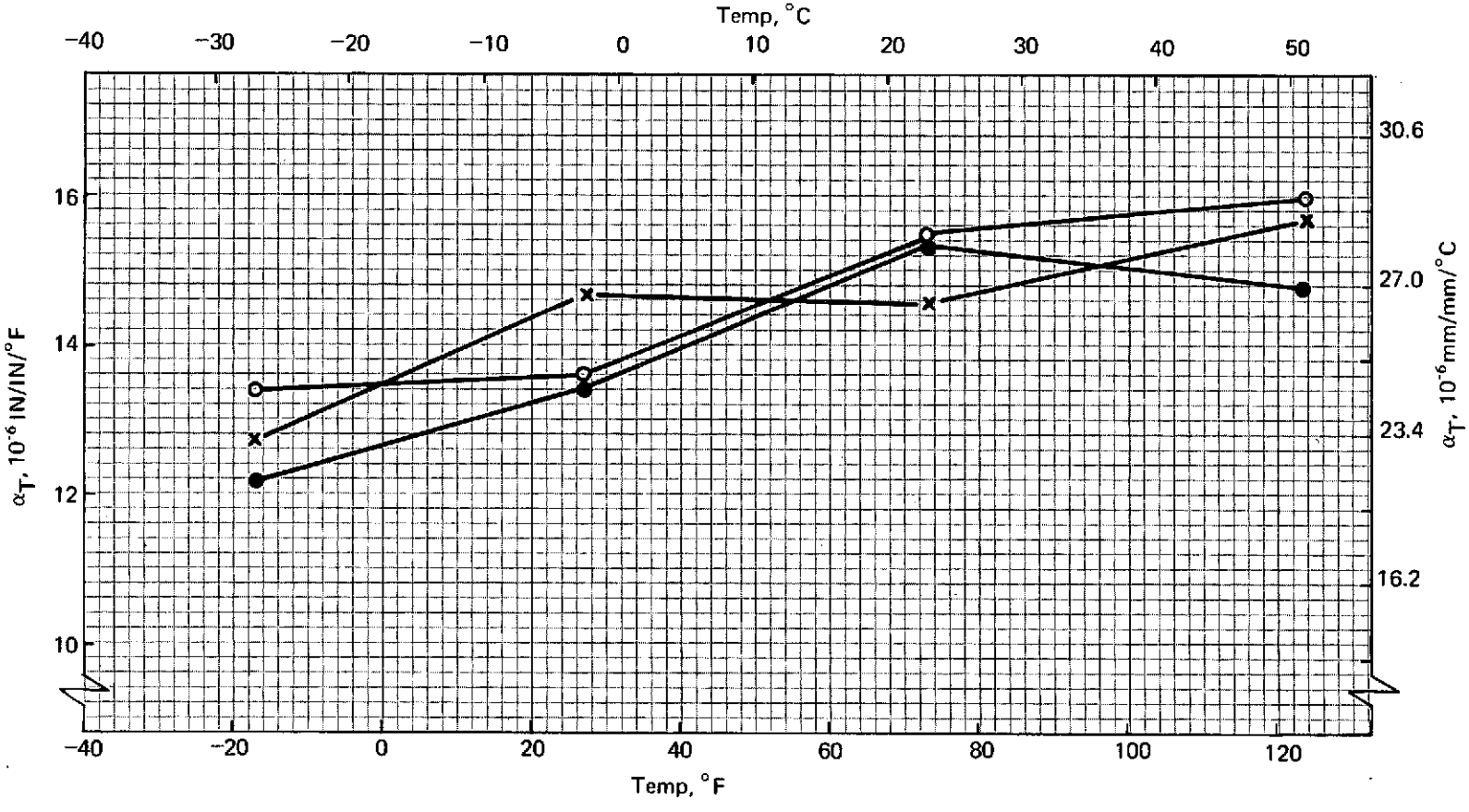

Figure 2-15 Transverse Coefficient of Thermal Expansion Type A/E702 Gr/Ep (Unidirectional)

for unidirectional specimens of GY70/E702 and Type A/E702 Gr/Ep, respectively. Variations in the transverse coefficient of thermal expansion are of the order of 10%, considerably less than those observed for the longitudinal coefficient of thermal expansion, as expected. In the longitudinal direction, slight misalignment can significantly affect the test results, not so in the transverse direction which is basically resin-controlled. But, because the transverse coefficient of thermal expansion is approximately two orders of magnitude greater than the longitudinal coefficient of thermal expansion, these small percent variations cause very large differences in the prediction of coefficients of thermal expansion for multi-directional laminates.

Table 2-2 of Section 2.4.1 lists the unidirectional properties of GY70/E702 and Type A/E702 Gr/Ep used in the analysis of the multi-directional laminates 'A', 'B', and 'C'. The moduli values, E_L, E_T, G_{LT} are the ones used to predict the mechanical properties of 'A', 'B' and 'C' laminates. The transverse modulus, E_T, is the average of the tension and compression moduli. The transverse tension and compression moduli are 11.0 x 10^9 N/m^2 (1.6 x 10^6 psi) and 20.0 x 10^9 N/m^2 (2.9 x 10^6 psi), respectively. The coefficient of thermal expansion is given over a range (max-min) as obtained from Figures 2-12 through 2-15.

Using the properties listed in Table 2-2 and the IBM 360/67 computer program THRM9, transverse and longitudinal coefficients of thermal expansion were generated for the multi-directional laminates 'A', 'B' and 'C'.

Figures 2-16 through 2-18 show plots of the transverse coefficient of thermal expansion at temperature, experimentally obtained for laminates 'A', 'B' and 'C', respectively. The analytical predictions are superimposed as heavy solid lines. The curves labeled 1 and 2 bound the band of possible transverse coefficients of thermal expansion for nominal thickness laminates. Laminate 'A' shows good correlation between test and theory at R.T. Test results at R.T. range between 11.0 x 10^{-6} mm/mm/°C (6.1 x 10^{-6} in/in/°F) and 11.4 x 10^{-6} mm/mm/°C (6.37 x 10^{-6} in/in/°F), and predictions between 10.4 x 10^{-6} mm/mm/°C (5.75 x 10^{-6} in/in/°F) and 11.0 x 10^{-6} mm/mm/°C (6.1 x 10^{-6} in/in/°F). Figure 2-17 shows the good correlation obtained between test and theory for the transverse coefficient of thermal expansion for the 'B'

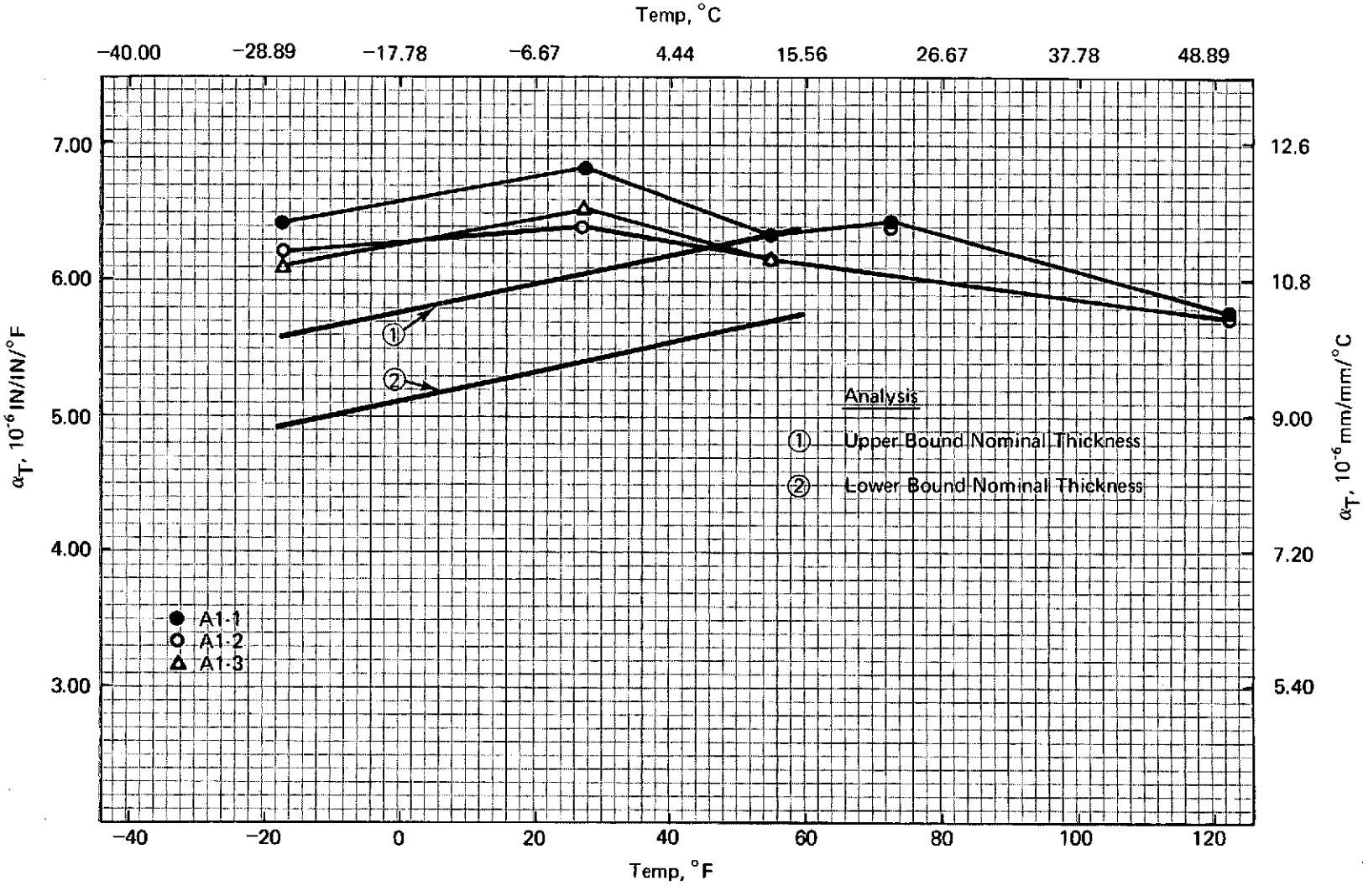

Figure 2-16 Transverse Coefficient of Thermal Expansion Type A/GY70/E702 Gr/Ep Laminate "A"

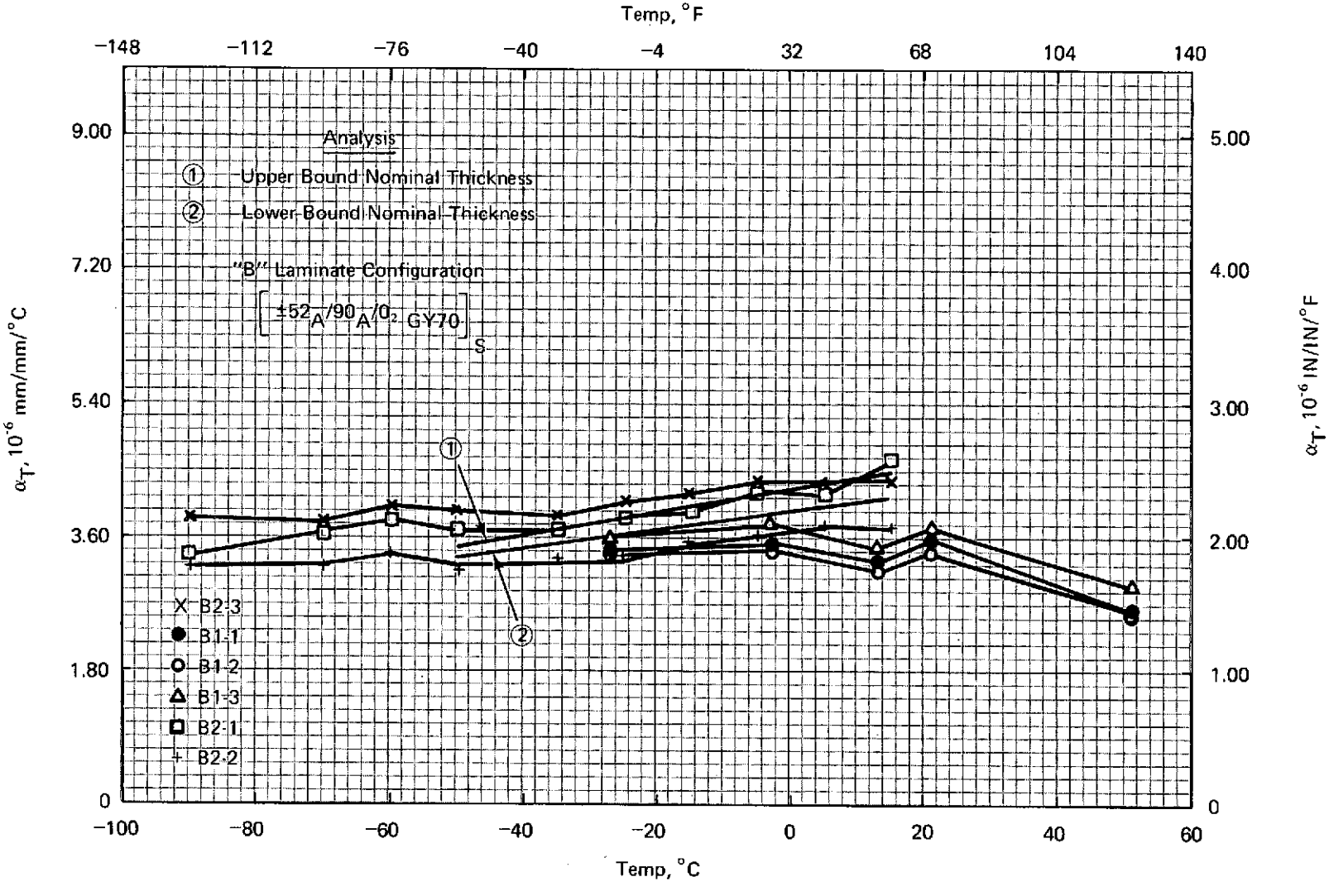

Figure 2-17 Transverse Coefficient of Thermal Expansion Type A/GY70/E702 Gr/Ep Laminate "B"

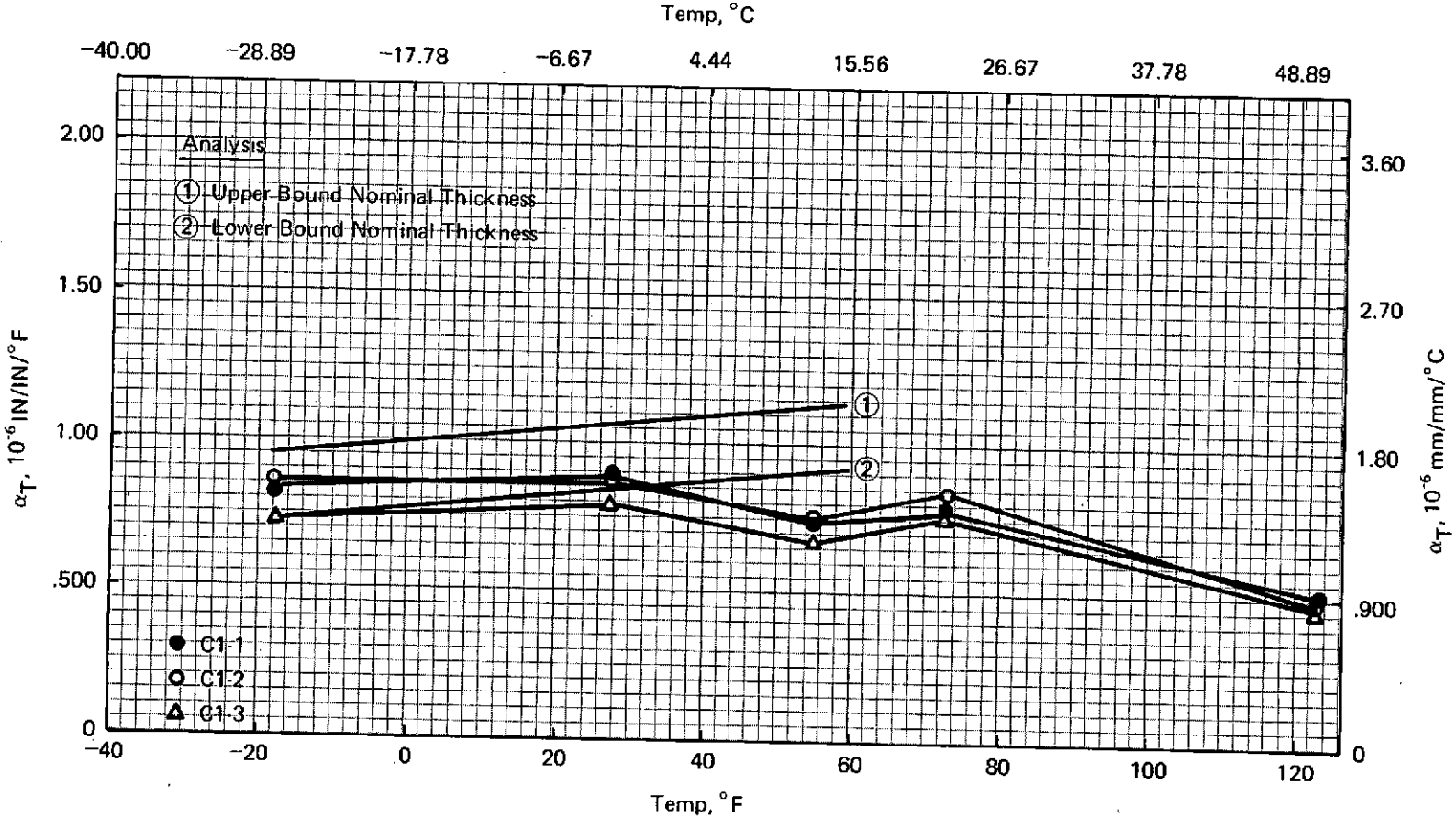

Figure 2-18 Transverse Coefficient of Thermal Expansion Type A/GY70/E702 Gr/Ep Laminate "C"

laminate. At R.T. test results ranged from a low of 3.15 x 10^{-6} mm/mm/°C (1.75 x 10^{-6} in/in/°F) to a high of 4.59 x 10^{-6} mm/mm/°C (2.56 x 10^{-6} in/in/°F). Predicted values range from a low of 4.14 x 10^{-6} mm/mm/°C (2.3 x 10^{-6} in/in°F) to a high of 4.5 x 10^{-6} mm/mm/°C (2.5 x 10^{-6} in/in/°F). Figure 2-18 shows the analytically predicted transverse coefficient of thermal expansion for laminate 'C' to lie on the high side at R.T. Test results range from 1.26 x 10^{-6} mm/mm/°C (.70 x 10^{-6} in/in/°F) and 1.40 x 10^{-6} mm/mm/°C (.78 x 10^{-6} in/in/°F), and analytical predictions from 1.62 x 10^{-6} mm/mm/°C (.90 x 10^{-6} in/in/°F) to 2.04 x 10^{-6} mm/mm/°C (1.14 x 10^{-6} in/in/°F). The agreement is excellent at -29°C (-20°F).

Figures 2-19 through 2-22 show plots of the longitudinal coefficient of thermal expansion at temperature, experimentally obtained for laminates 'A', 'B' and 'C'. Again, analytical predictions are superimposed as heavy solid lines. These lines labeled 1 and 2 span the range of possible coefficients of thermal expansion for nominal thickness laminates based on the maximum-minimum physical properties for unidirectional graphite/epoxy listed in Table 2-2.

Figure 2-19 shows the band of analytically predicted coefficients of thermal expansion to lie within the scatter band of test results throughout the entire temperature range. The agreement between test and theory is very good considering that the test results are estimated to be accurate to within $\pm$.145 x 10^{-6} mm/mm/°C ($\pm$.081 x 10^{-6} in/in/°F). This is explained as follows:

The test apparatus for the measurement of the coefficient of thermal expansion consists basically of two push rods in parallel. One push rod measures the growth of the test specimen and the other push rod measures the growth of the quartz standard. Thus, the specimen growth is measured relative to the known growth of the quartz standard. The best estimate of the possible error in the test set up is $\pm$0.05 x 10^{-6} mm/mm/°C (.028 x 10^{-6} in/in/°F), of which $\pm$.03 x 10^{-6} mm/mm/°C ($\pm$.0167 x 10^{-6} in/in/°F) is due to the quartz standard. Interchanging the location of the test specimen and the quartz standard should have no effect on the results, but tests show that this reversal causes significant change in the test values obtained for the 'B' laminate. It is tentatively assumed on the basis of these results that a further test error exists of $\pm$.140 x 10^{-6} mm/mm/°C ($\pm$.077 x 10^{-6} in/in/°F).

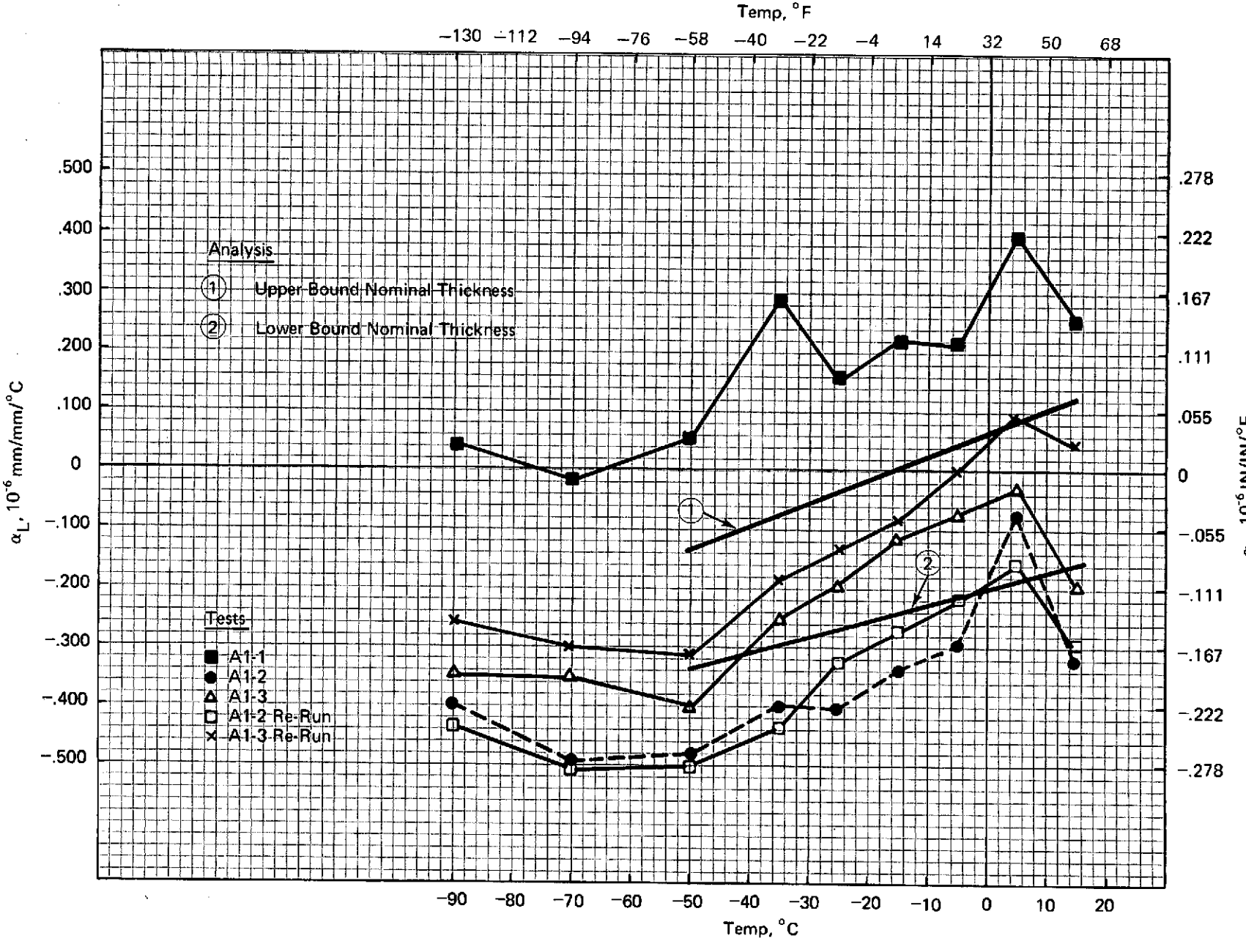

Figure 2-19 Longitudinal Coefficient of Thermal Expansion - Type A/GY70/E702 Gr/Ep Laminate "A"

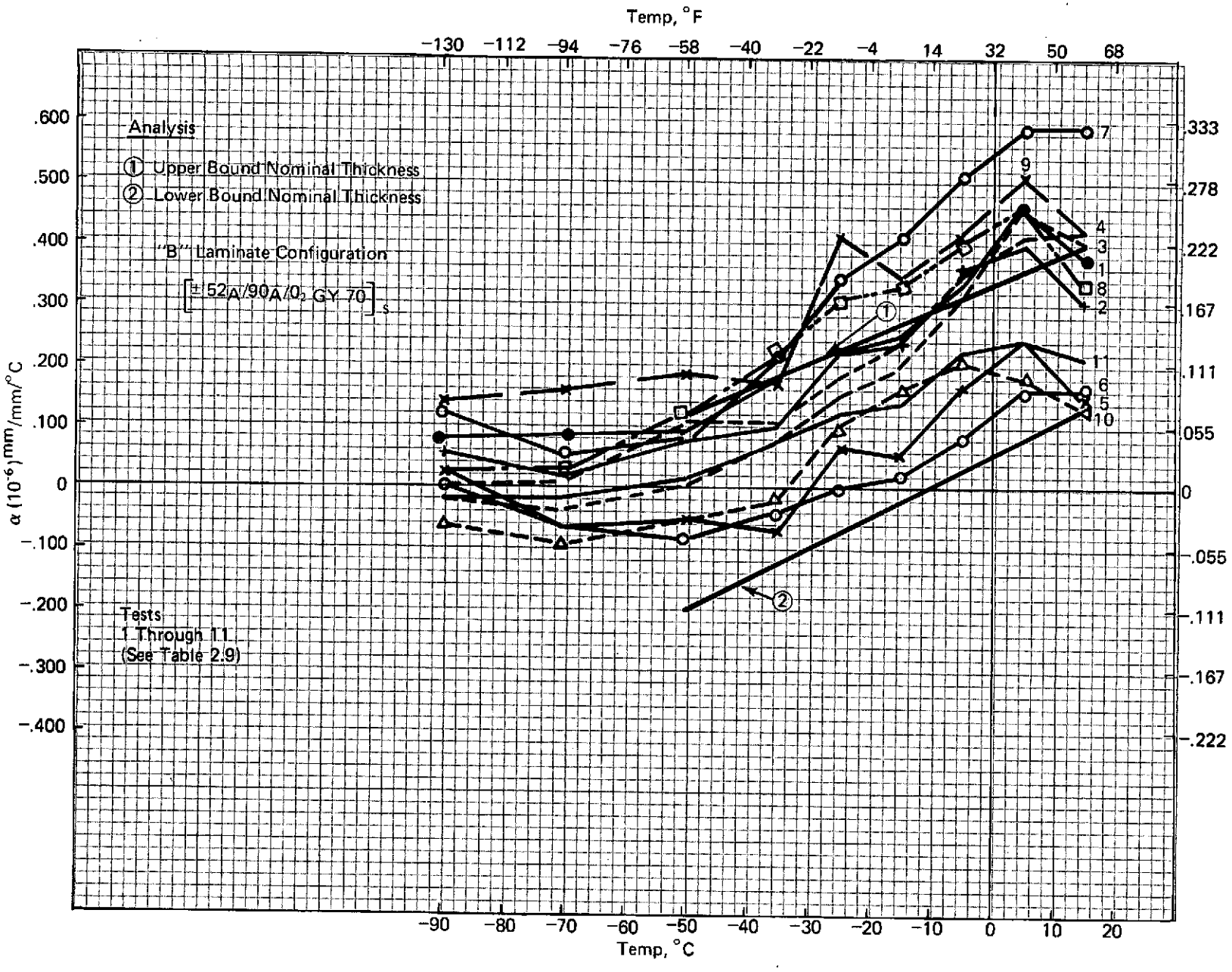

Figure 2-20a Longitudinal Coefficient of Thermal Expansion - Type A/GY70/E702 Gr/Ep Laminate "B"

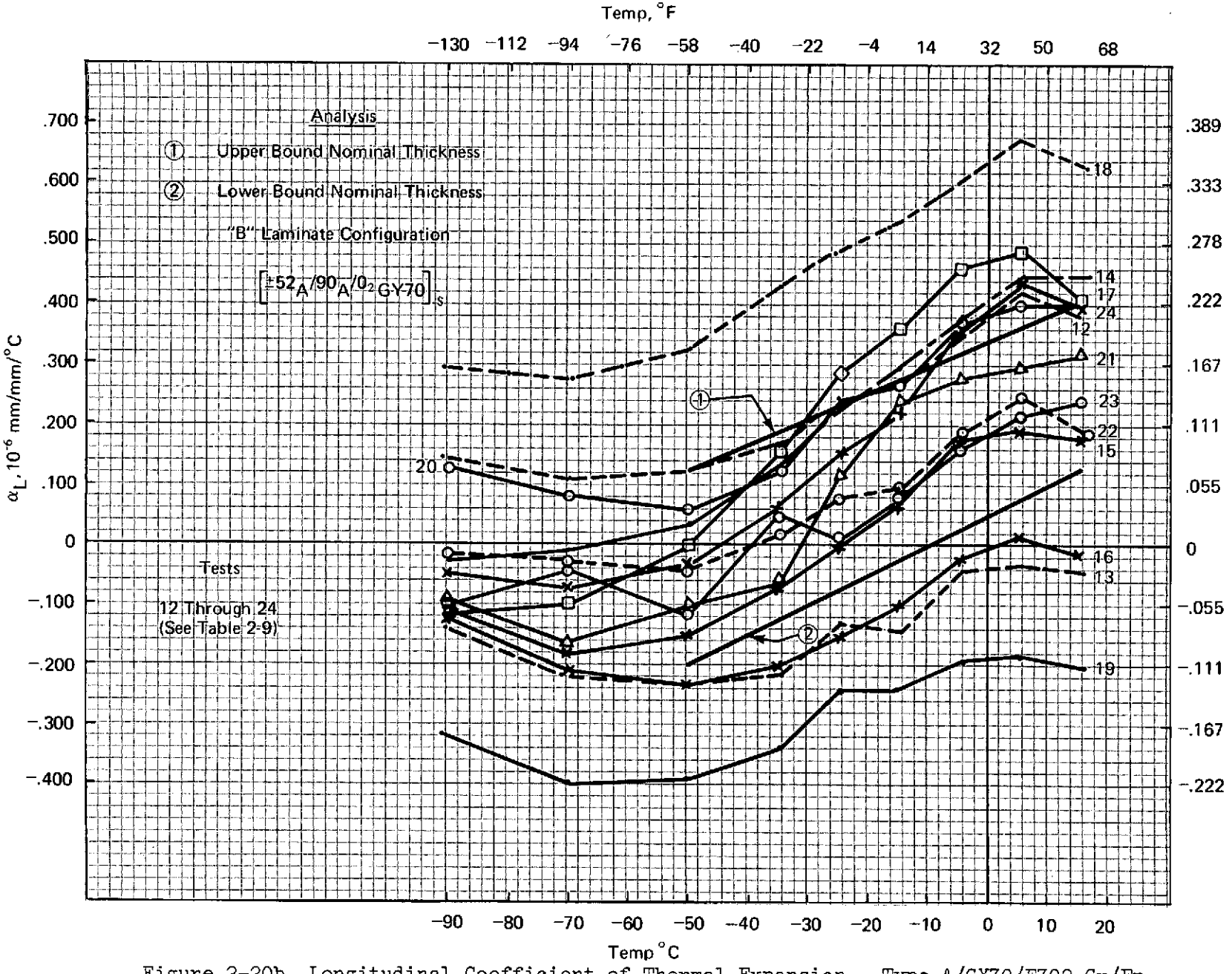

Figure 2-20b Longitudinal Coefficient of Thermal Expansion - Type A/GY70/E702 Gr/Ep Laminate "B"

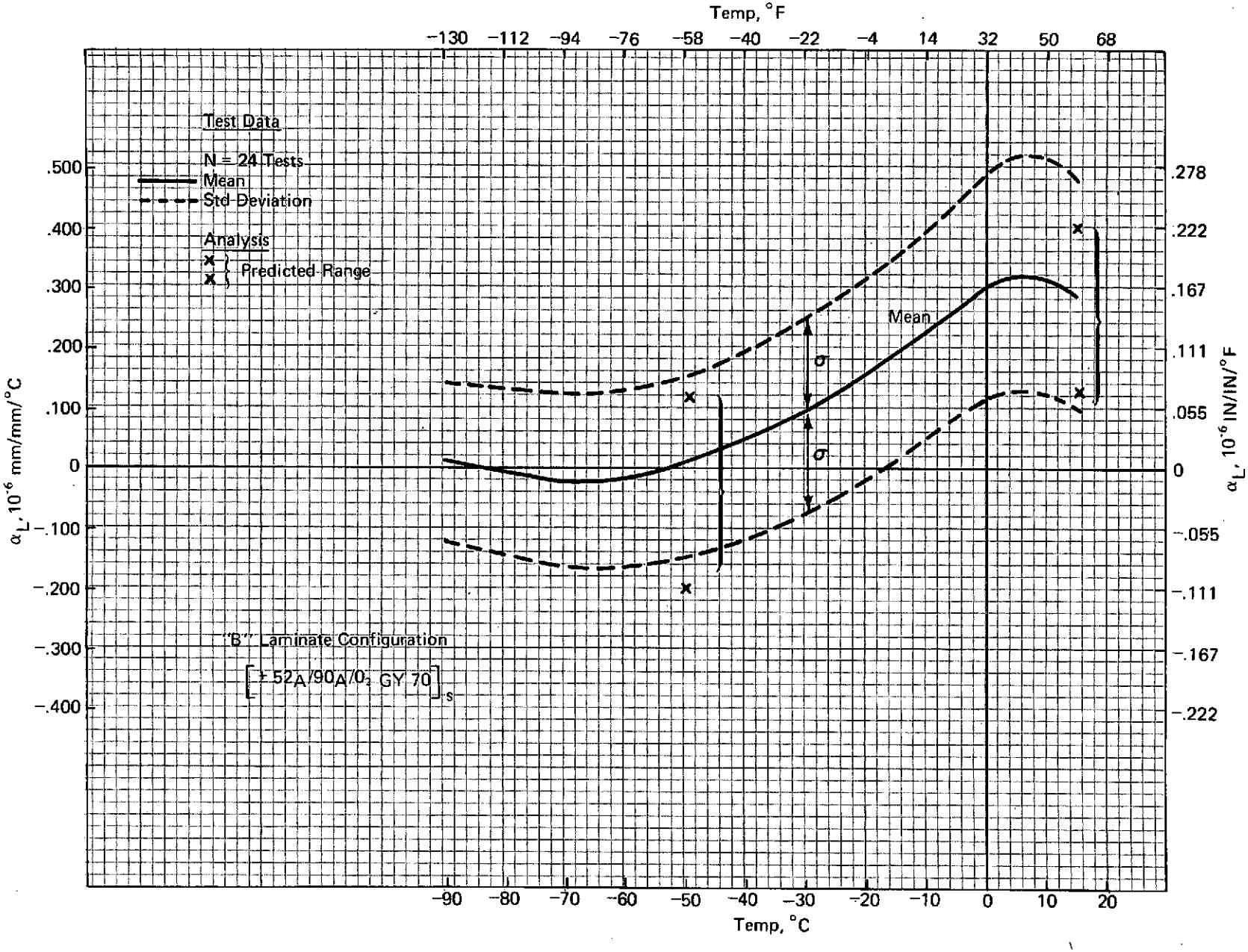

Figure 2-21 Normal Distribution of the Longitudinal Coefficient of Thermal Expansion for Laminate "B"

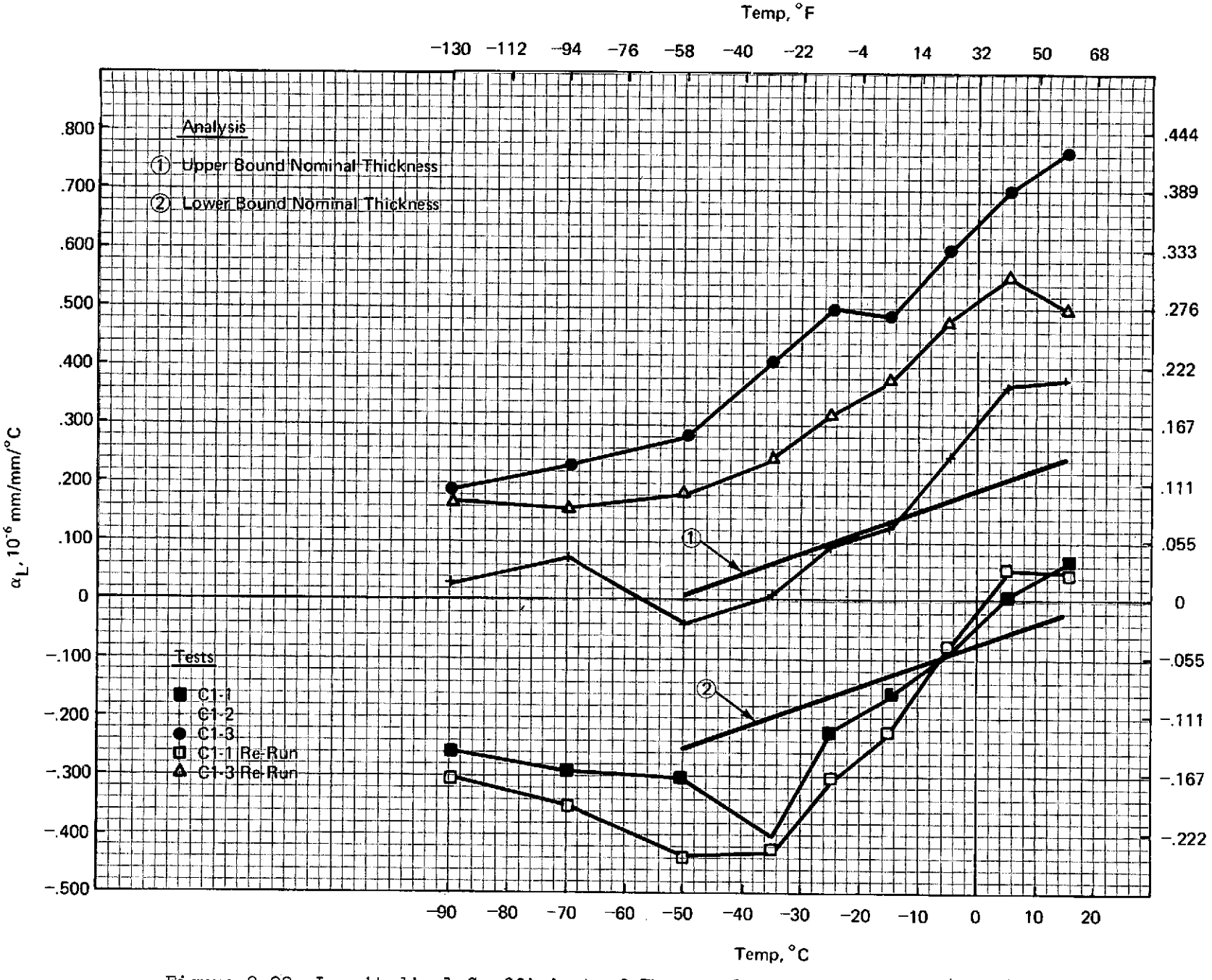

Figure 2-22 Longitudinal Coefficient of Thermal Expansion - Type A/GY70/E702 Gr/Ep Laminate "C"

The predicted range of values at R.T. for laminate 'A' is -.160 x 10^{-6} mm/mm/°C (-.088 x 10^{-6} in/in/°F) to +.120 x 10^{-6} mm/mm/°C (+.066 x 10^{-6} in/in/°F), and the range of test results -.320 x 10^{-6} mm/mm/°C (-.178 x 10^{-6} in/in/°F) to +.260 x 10^{-6} mm/mm/°C (+.145 x 10^{-6} in/in/°F).

Figures 2-20A and 2-20B show plots of 24 test runs of specimens of configuration B. This laminate was selected as the most desirable of the three in the selection program. Selection, of necessity, was made early in the characterization program and based upon the few initial test results both mechanical and C.T.E. Consistency of results was the prime deciding factor. Successive data proved the selection to be proper. These two plots include specimens originally tested, re-tested, after environmental exposure and from two material batches. Table 2-9 identifies all 24 test curves plotted in Figures 2-20A and 2-20B. As can be seen from the data there is no discernable difference between the C.T.E. for specimens having undergone environmental exposure (outgassing or humidity), or from different material batches, relative to the norm. The analytically predicted band of possible values for the longitudinal coefficient of thermal expansion again lies within the band of all test results. At R.T. the range of test results is -.200 x 10^{-6} mm/mm/°C (-.111 x 10^{-6} in/in/°F) to +.630 x 10^{-6} mm/mm/°C (+.350 x 10^{-6} in/in/°F), and the range of predicted values +.130 x 10^{-6} mm/mm/°C (+.072 x 10^{-6} in/in/°F) to +.400 x 10^{-6} mm/mm/°C (+.222 x 10^{-6} in/in/°F). Figure 2-21 shows a plot of the normal distribution of the longitudinal coefficient of thermal expansion for laminate 'B'. The graph shows the mean value and one standard deviation as a function of temperature. Plots of test data at temperature show it to be approximately normally distributed. The range of predicted possible values for the longitudinal coefficient of thermal expansion is also indicated at R.T. and at -50°C (-58°F). The agreement, considering again the possible test error of $\pm$.145 x 10^{-6} mm/mm/°C ($\pm$.081 x 10^{-6} in/in/°F) is very good. The mean value of α_L for laminate 'B' at R.T. is +.290 x 10^{-6} mm/mm/°C (+.160 x 10^{-6} in/in/°F). The standard deviation is 0.191 x 10^{-6} mm/mm/°C (0.105 x 10^{-6} in/in/°F). The mean value of α_L at -50°C (-58°F) is +0.010 x 10^{-6} mm/mm/°C (+.005 x 10^{-6} in/in/°F) and the standard deviation 0.155 x 10^{-6} mm/mm/°C (0.085 x 10^{-6} in/in/°F).

Table 2-9 Specimen Description 'B' Laminate

Specimen No.	Specimen Description
1	B1-1/N/P
2	B1-2/N/P
3	B1-3/N/P
4	B1-1/N/P
5	B1-1/R/P
6	B1-1/R/P
7	B1-1/N/G70 (R1-1)
8	B2-1/N/P
9	B2-1/N/P
10	B2-1/N/P
11	B2-1/R/P
12	B1-1/N/H150 (HF1-1)
13	B2-1/R/P
14	B2-2/N/P
15	B2-2/R/P
16	B2-3/R/P
17	B2-3/N/P
18	B2-1/N/G70 (R2-1)
19	B2-1/N/G150 (F2-1)
20	B1-2/N/H70 (HR1-2)
21	B2-2/N/H70 (HR2-2)
22	B2-1/N/H150 (HF2-1)
23	B1-2/N/H150 (HF1-2)
24	B1-1/N/H70 (ER1-1)

Code

Mat'l Batch - Spec. No/Test Configuration/Environ. Exposure

B1 = Batch 1
B2 = Batch 2
N = Specimen and Standard in Normal Position
R = Specimen and Standard in Reversed Position
P = Plain - No Exposure
G70 = Subjected to Outgassing at R.T.
G150 = Subjected to Outgassing at 65.5°C (150°F)
H70 = Subjected to Humidity Then Outgassing at R.T.
H150 = Subjected to Humidity Then Outgassing at 65.5°C (150°F)

Figure 2-22 shows the longitudinal coefficient of thermal expansion for laminate 'C' as a function of temperature. The scatter in the test results is quite large. The re-run of specimen C1-3 indicates that curve C1-3 might be quite wrong and the spread in test results not as bad as seen at first glance. Not enough specimens were tested to allow for any meaningful statistical distribution. In general the predicted values for α_L lie on the band of test results.

A thickness effect is noticeable in the test results obtained. In general the thicker specimens show lower coefficients of thermal expansion. Because of the good agreement obtained between predicted and test values for the coefficient of thermal expansion of laminate 'B' it is thought at this time that the thickness effect is already included in the spread of values obtained from unidirectional specimens, and used as input to predict the physical properties of multilayer composites. Table 2-10 lists measured thicknesses of typical specimens 'A', 'B' and 'C' at three locations, at the ends and center. In addition, the possible misalignment of fibers by as much as .035 rad (2°) was investigated. This possible but unlikely misalignment results in a maximum change in α_L for laminates 'A' and 'B' of approximately $.036 \times 10^{-6}$ mm/mm/°C ($.020 \times 10^{-6}$ in/in/°F), and for laminate 'C' of $.015 \times 10^{-6}$ mm/mm/°C ($.008 \times 10^{-6}$ in/in/°F).

In conclusion than, the element test results for the selected 'B' laminate show that for the applicable temperature range of -90°C to -23°C (-130°F to -9.5°F) an average coefficient of thermal expansion of $.086 \times 10^{-6}$ mm/mm/°C ($.048 \times 10^{-6}$ in/in/°F) was obtained. This fell well within the maximum permissible value of $.216 \times 10^{-6}$ mm/mm/°C ($.120 \times 10^{-6}$ in/in/°F). Further, predictions of the C.T.E. were in generally good agreement with the test results.

The next planned program progression was to fabricate three tubular specimens of the 'B' laminate .304 m (12 inches) in length and 81.2 mm (3.2 inches) in diameter for C.T.E. measurement. The tubular configuration was the anticipated structural shape for use in the metering truss. Planning called for these tests to be run at G.A.C., however, numerous attempts to make the measurements proved unsuccessful. The test procedure used to

Table 2-10 Specimen Thickness - Actual Vs Nominal

Specimen	Test Thickness MM (Inches)			Average Thickness MM (Inches)	Nominal Thickness MM (Inches)
	End 1	Center	End 2		
A1-1	1.017 (.0400)	1.083 (.0427)	1.068 (.0420)	1.058 (.0416)	0.9875 (.03885)
A1-2	1.142 (.0450)	1.020 (.0402)	1.092 (.0430)	1.083 (.0427)	
A1-3	1.169 (.0460)	1.245 (.0490)	1.194 (.0470)	1.202 (.0473)	
B1-1	1.500 (.0590)	1.545 (.0608)	1.576 (.0620)	1.540 (.0606)	1.440 (.0567)
B1-2	1.525 (.060)	1.450 (.057)	1.525 (.0600)	1.500 (.0590)	
B1-3	---	1.538 (.0605)	1.550 (.0610)	1.544 (.0608)	
C1-1	1.765 (.0695)	1.715 (.0675)	1.728 (.0680)	1.735 (.0683)	1.495 (.0588)
C1-2	1.452 (.0572)	1.538 (.0605)	1.627 (.0640)	1.540 (.0606)	
C1-3	1.531 (.0603)	1.500 (.0590)	1.591 (.0627)	1.541 (.0607)	

try and make the measurement involved the use of two laser interferometers. The interferometer measuring corner cubes were mounted at each end of the tube to measure relative growth between the two ends. The cubes were mounted to the tubes using double back tape (small flats were created on the inside diameter with potting compound for mounting), in order to facilitate removal and usage on other tubes. The member rested on a 'vee' block with teflon mounting pads, such that expansion could freely take place. The tube was placed in a thermal vacuum chamber and the chamber isolated from the floor by air spring isolators. The lasers/detectors were located outside, but rigidly mounted to the chamber and pointed through an optically flat window. Positioning of the lasers was maintained as close to the window as possible to minimize the effect of temperature, pressure or humidity change on the air path length of the beam outside the chamber. Measurement accuracy of 254×10^{-6} mm (10×10^{-6} inches) was expected. During the actual running of the tests, a random drift of $5080\text{-}7620 \times 10^{-6}$ mm ($200\text{-}300 \times 10^{-6}$ inches) was experienced; which represented a reading an order of magnitude higher than the value to be measured.

In order to determine whether the instrument or the specimen was at fault, an aluminum tube was placed in the chamber for measurement. Results indicated that over the range of temperature change investigated ($\Delta T = 5.5°C$ ($10°F$)) accuracy was only on the order of 10-20%. This was significant in that the coefficient of thermal expansion of aluminum is two orders of magnitude greater than the measurement being attempted on the graphite tubes. Further, upon cool down the laser readings indicated additional specimen growth - an impossible condition.

Based upon these findings it was determined that the equipment available did not possess sufficient sensitivity to make these extremely fine measurements. A program decision was made to subcontract the thermal coefficient measurement of the subcomponent tubes. The Perkin-Elmer Corp. was contacted, given the measurement requirements and expressed an ability to effectively obtain the desired values. The only change necessary to the specimen configuration was to reduce its length to .152 m (6 inches). This was necessary to make the specimen compatible with an existing test set-up at Perkin-Elmer.

The technique used by Perkin-Elmer was primarily that of the attached reference. The specimen was used as an etalon spacer in a multiple beam Fizeau interferometer. The configuration is shown in Figure 2-23. The chamber used for this measurement series had internal coils which carried liquid or gaseous nitrogen as the heat exchanging fluid. These cooling coils surrounded a black anodized aluminum tube, which is used as a thermal diffuser to allow a thermally uniform surface for radiant heat transfer to the tubular specimen. The coil, diffuser and specimen are concentric with each other and with the chamber wall. The chamber is lined with aluminized mylar and an aperture baffle of the same material is also provided to minimize thermal losses to atmosphere. The fully assembled system is shown in Figure 2-24.

Specimens were installed in the chamber and were pumped down overnight to a vacuum of 40 millitorr or less. During a run, liquid nitrogen was circulated through the coil to cool the sample by radiation and conduction. Heatup was accomplished by circulating heated nitrogen gas through the coils. Samples were cooled to -101°C (-150°F) in about four hours. Through cool down a few random and approximate data points were obtained.

Data taking during a run consisted of temperature measurements (thermocouples attached to sample with aluminum tape) as read from a portable millivolt potentiometer, and interferograms taken on polaroid film at the appropriate temperatures. The total fringe motion was monitored by eye on the ground glass screen to observe both direction of fringe motion, and whole numbers of fringes.

Fringe count was converted to $\Delta L/L$ using the relationship:

$$\frac{\Delta L}{L} = \frac{N\lambda}{2L_o}$$

where $\Delta L/L$ is length change per unit length
N is the fringe shift
$\lambda/2$ is 3.16×10^{-7} M (12.45×10^{-6} inches), the length represented by a 1/2 wave fringe of HeNe laser light
L_o is the original sample length, approximately .152 M (six inches)

The data are presented in Figures 2-25, 2-26 and 2-27. For the cooling runs, the reference point is room temperature while for the heating

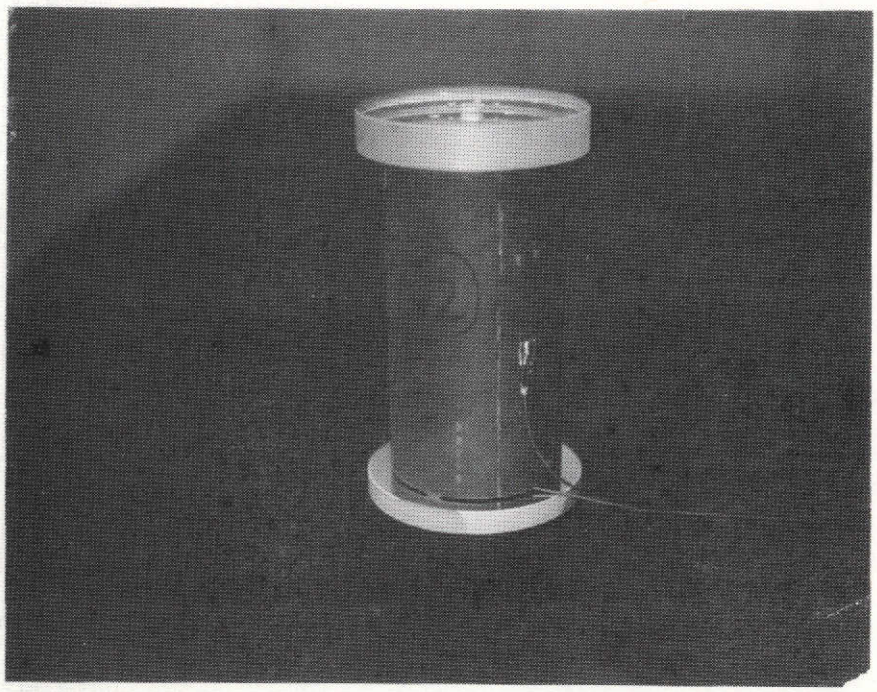

Figure 2-23 Specimen Configuration Showing Fizeau Mirrors and Thermocouple Attachment

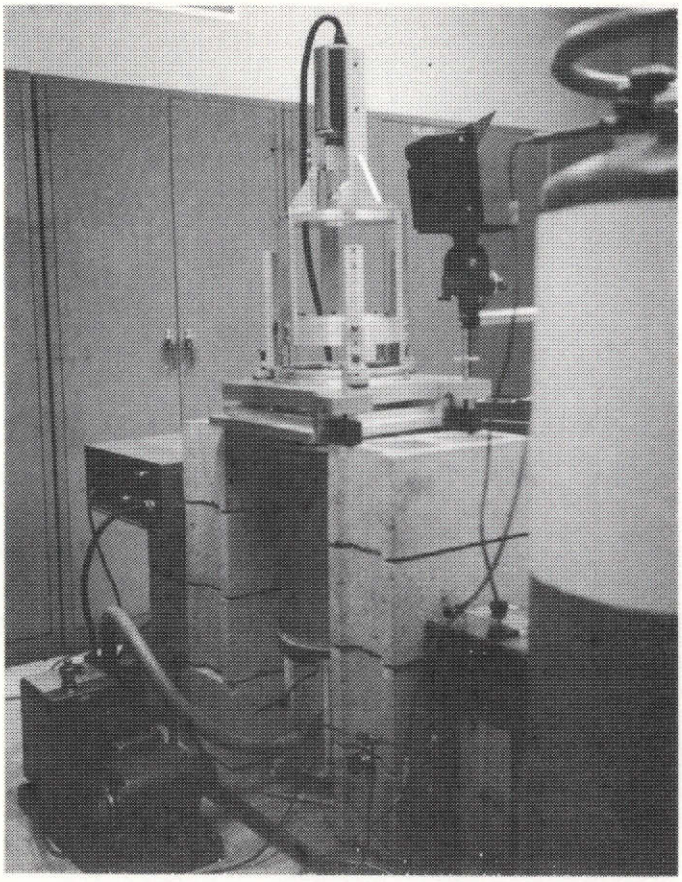

Figure 2-24 Overall View of Laser Interferometric Dilatometer

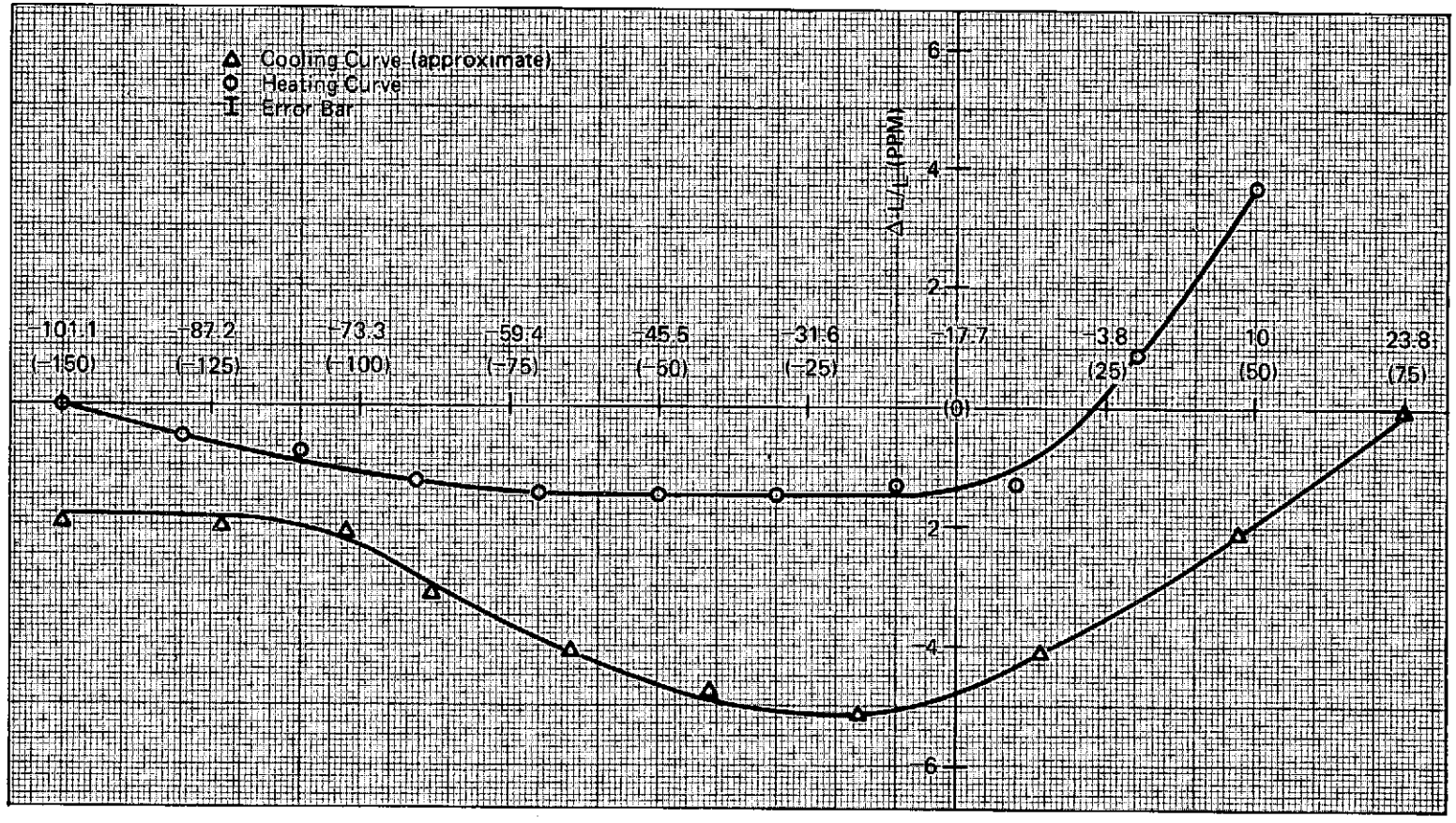

Figure 2-25 Expansivity of Gr/Ep Tube Number 1

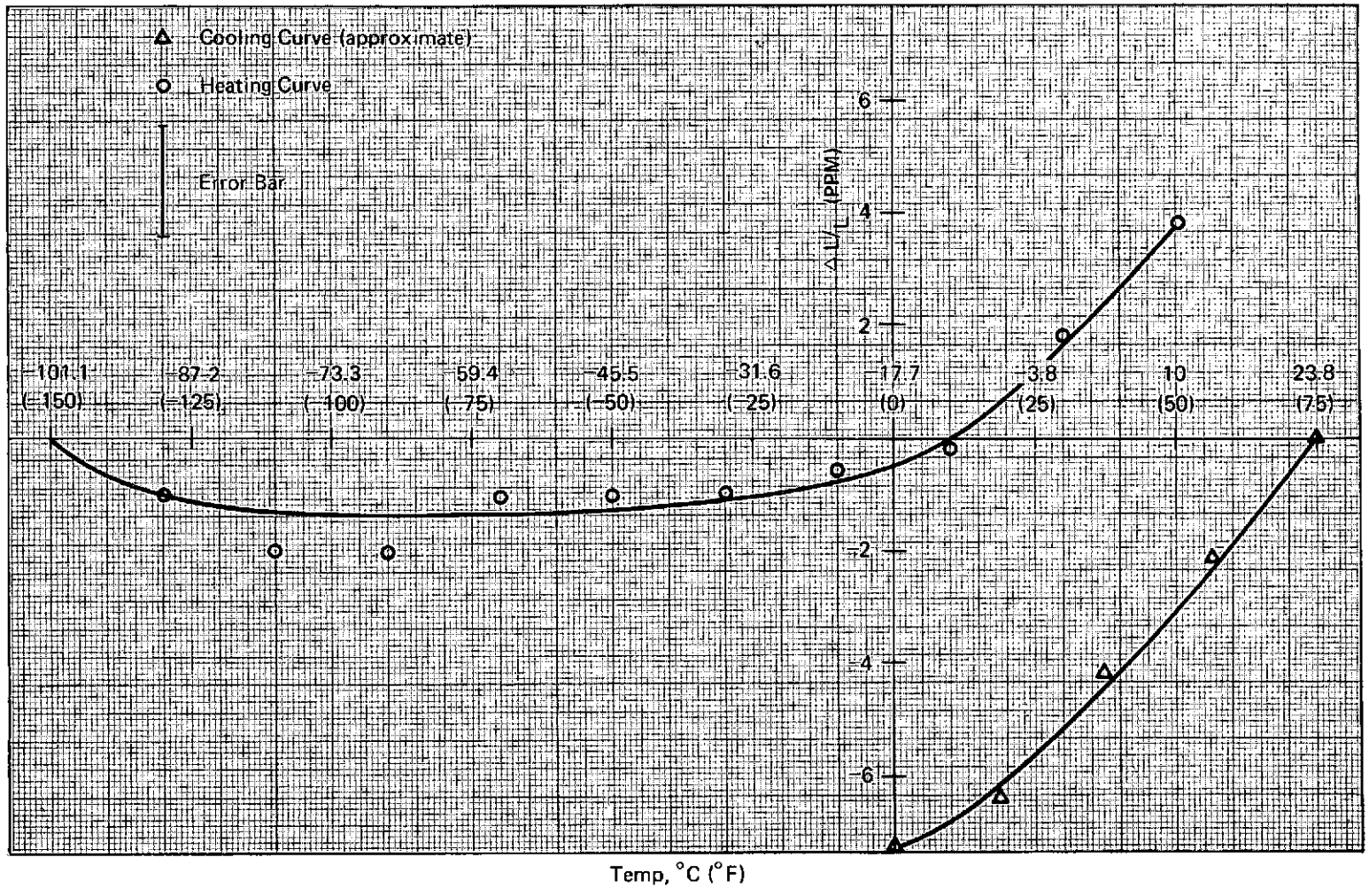

Figure 2-26 Expansivity of Gr/Ep Tube Number 2

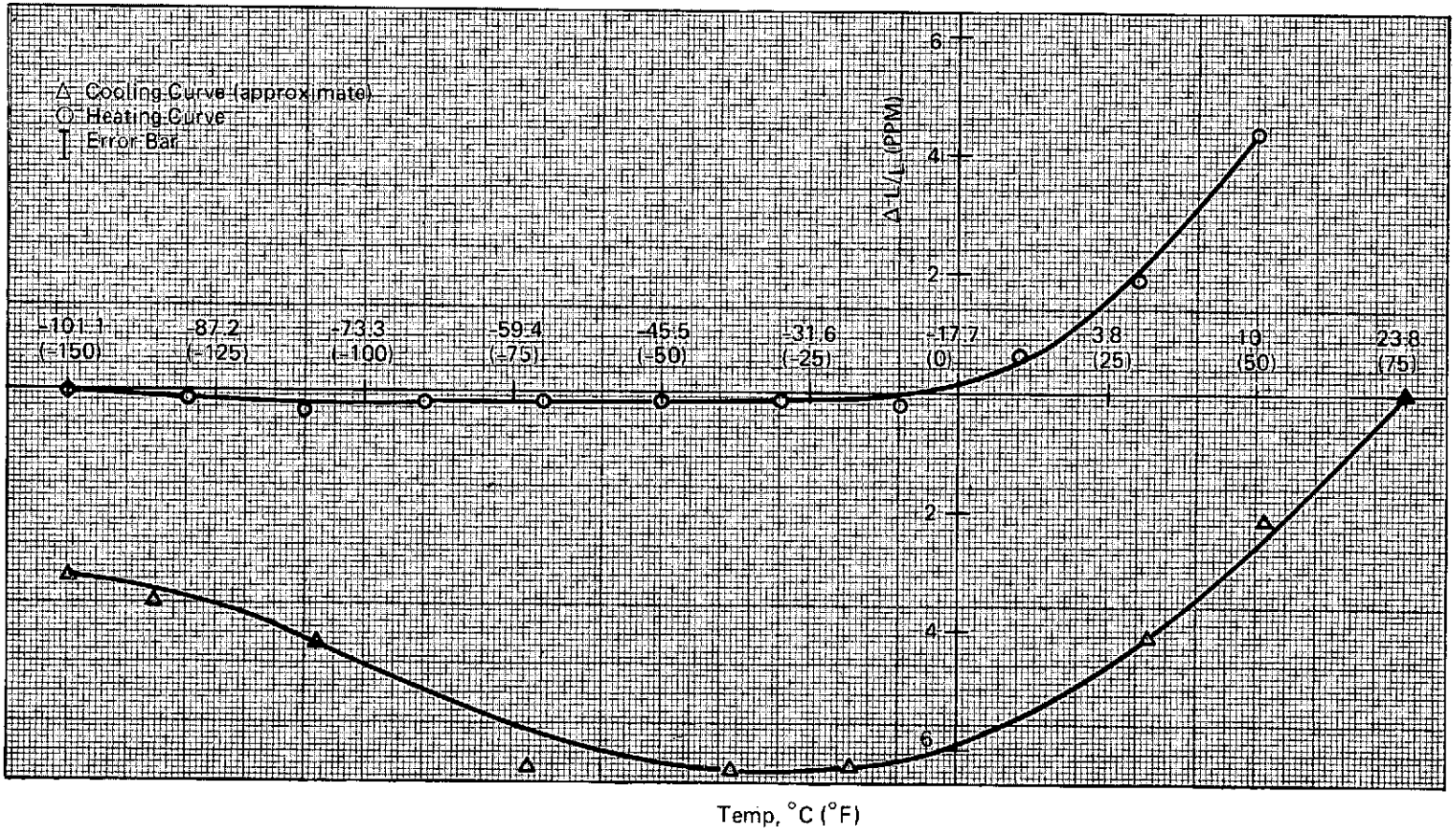

Figure 2-27 Expansivity of Gr/Ep Tube Number 3

runs, the reference is the -101°C (-150°F) condition. This data presentation eliminates overlap of the two curves in the figures. Error bars are given in each figure and are explained below.

The data show the same type of behavior for all three specimens:

(a) On cooling from room temperature to approximately -17.7°C (0°F), there is a contraction of 5 to 7 ppm (positive CTE),

(b) Further cooling to -101°C (-150°F) showed an expansion of approximately 3 ppm (negative CTE),

(c) On heating from -101°C (-150°F), there is an initial contraction of up to 2 ppm (negative CTE), followed by,

(d) An expansion of approximately 5 ppm between -17.7°C (0°F) and +10°C (+50°F)(positive CTE).

The data seem to show a change in length due to the non-reversible nature of the expansion on cooling in the -45.5°C (-50°F) to -101°C (-150°F) range. The specimens apparently increased in length by approximately 4.57×10^{-7} M (18×10^{-6} inches) as a result of the testing. This was deduced from the data but not measured directly. The deduction has as its basis the cooling curve, however, data points for this curve are only approximate and therefore suspect, especially when dealing with such small values.

Measurement accuracy is primarily affected by two factors: specimen CTE homogeneity and fringe readability. CTE homogeneity in the specimen is dependent on uniform fiber packing and orientation. Because of the nature of composite materials, if bonds are broken between fiber and matrix in the vicinity of the support points, or any other area for that matter, the area with broken bonds will have the expansion coefficient of the matrix. This may have happened in specimen number 2, since the interferograms taken at three temperatures showed a change in fringe orientation and spacing. This indicates a much higher CTE for that point. This behavior for this specimen was repeatable, and a second cycle provided semiquantitative confirmation. Due to this behavior, the estimated error for fringe count for specimen 2 is substantially greater than for the other samples. For specimens 1 and 3, fringe count was ± 0.12, for an error in $\Delta L/L$ of ± 0.25 ppm. For specimen 2, the fringe count error is approximately ± 0.5 for a ± 1 ppm error in $\Delta L/L$.

The fringe readibility was not a problem except for the -34.4°C (-30°F) and -23.3°C (-10°F) readings during heating. In this range there was a condensation of an unidentified substance on one or other of the mirrors within the specimen ID. This phenomena was repeated for all three specimens in an identical manner. Film growth started at -67.7°C (-90°F) and spread slowly, obscuring a small portion of the interferogram. The obscuration did not entirely cover the fringe pattern, so that data could be taken. The film disappeared before reaching -12.2°C (+10°F).

Subsequent to the analysis of data received from Perkin-Elmer, C.T.E. curves were generated for the three subcomponent specimens. Values were calculated utilizing the heating cycle curves depicted on Figures 2-25, 2-26 and 2-27, and plotted over the normal distribution of longitudinal CTE curves generated from previous element data. The results which are presented in Figure 2-28, show good agreement with the element data. Further, the consistency of test of results for the three independently fabricated tubes is very encouraging. It should be noted that when compared to the element test data, the range of temperature over which an effectively zero ($<10^{-8}$) coefficient is exhibited is greatly increased. It is felt that this may be attributed to specimen size, since any imperfection or flaw in a specimen 50 mm x 6.35 mm (2in. x .25 in.) will exhibit a much greater impact than the same flaw in a specimen 152 mm x 81 mm in diameter (6 in. x 3.2 in.). Specimen size may also provide for equalization, or averaging of any imperfection impact on the CTE. Over the temperature range of -90°C to -23°C (-130°F to -9.5°F) an average value of $-.0050 \times 10^{-6}$ mm/mm/°C ($-.0028 \times 10^{-6}$ in/in/°F) was obtained for the three tubes.

2.4.3 Environmental Testing

A series of outgassing and humidity tests were performed on the 'B' laminate fabricated from both material batches 1 and 2. The objective of these tests were to confirm the suitability of the Gr/Ep material for use in a space environment as part of a precision optical system. The tests conducted established the degree of outgassing in vacuum at room temperature and 65.5°C (150°F) as well as the degree of water absorption in a 95% RH, 37.7°C (100°F) environment. Also determined was amount of water retention during subsequent vacuum exposure. Specimen identification and test conditions are presented in Table 2-11, while a description of the tests and results follow.

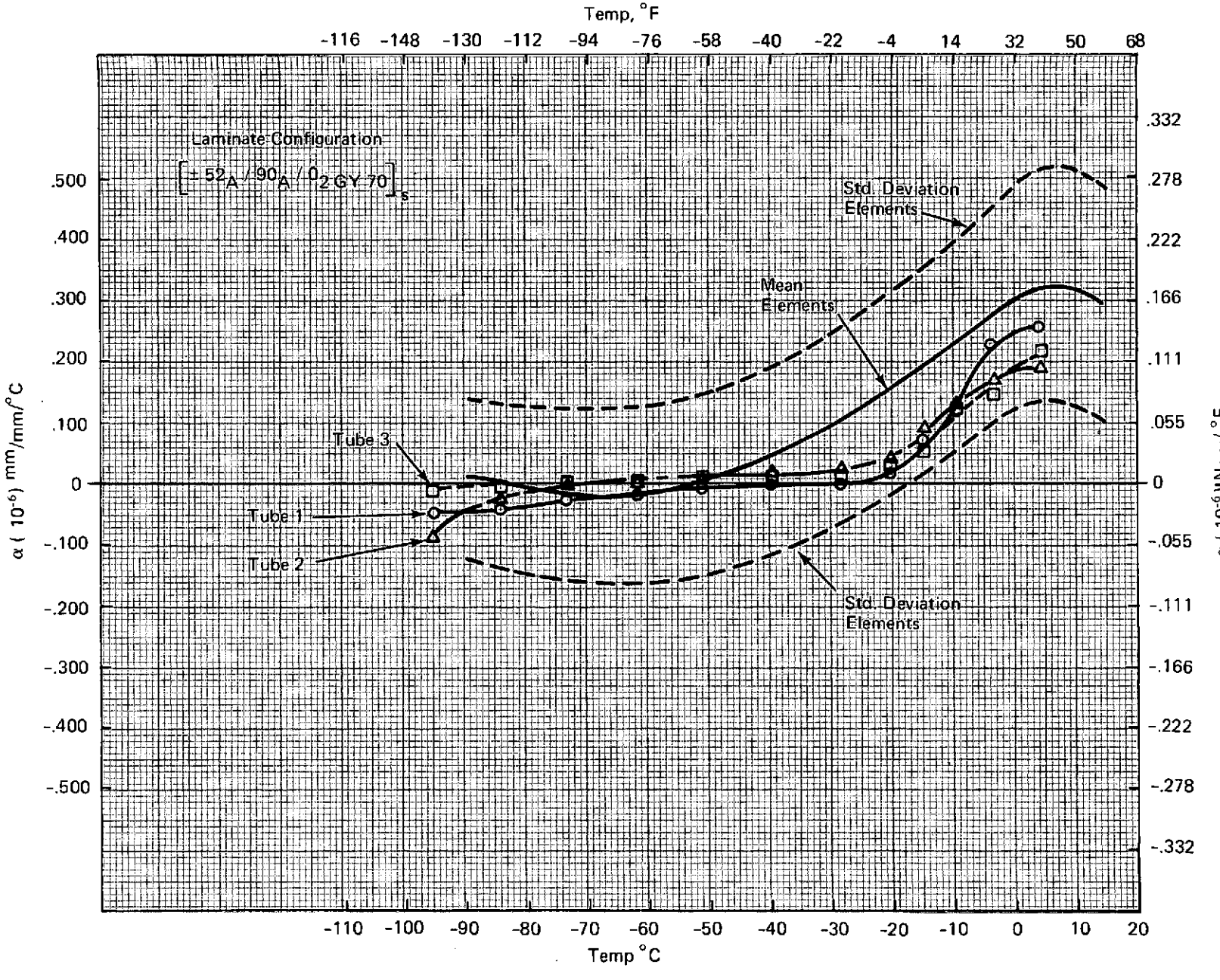

Figure 2-28 Coefficient of Thermal Expansion for "B" Laminate Gr/Ep Tubes

Table 2-11. Specimen Identification and Test Conditions for 'B' Laminate Environmental Tests

	Specimen No.	Batch No.	Test Conditions
OUTGASSING	R1-1*	1	RT, 120 hours, 10^{-5} torr
	R1-2	1	
	R1-3	1	
	R2-1	2	
	R2-2	2	
	F1-1	1	65.5°C (150°F), 120 hours, 10^{-5} torr
	F1-2	1	
	F1-3	1	
	F2-1	2	
	F2-2	2	
HUMIDITY AND OUTGASSING	HR1-1	1	37.8°C (100°F), 95% RH for 100 hours followed by RT outgassing
	HR1-2	1	
	HR1-3	1	
	HR2-1	2	
	HR2-2	2	
	HF1-1	1	37.8°C (100°F), 95% RH for 100 hours followed by 65.5°C (150°F) outgassing
	HF1-2	1	
	HF1-3	1	
	HF2-1	2	
	HF2-2	2	

* Sample R1-1 was exposed for 99 hours.

- Outgassing - The test procedure called for specimens to be exposed in a glass bell-jar vacuum system employing a liquid nitrogen baffled diffusion pump coupled to a Welch rotary pump. The sample was suspended in a small furnace enclosure, weight change being detected and measured by a Cahn electrobalance at frequent intervals during the outgassing period. A thermocouple junction was mounted within the furnace to measure temperature. The test plan was as follows:

  Expose specimens to 10^{-5} torr at room temperature until no weight loss is detected for a thirty minute period.

  Raise temperature to 65.5°C (150°F) at a rate not exceeding 1.1°C (2°F) per minute.

  Expose specimen at 65.5°C (150°F) for 120 hours.

  Prior to exposure, a thickness profile of the specimen was made to detect possible thickness changes as a result of the outgassing. No significant change was noted. Results of the tests were very encouraging, showing extremely small amounts of outgassing for this material system. Figure 2-29 shows a plot of specimen weight loss versus time at 65.5°C (150°F). As can be seen, total outgassing is on the order of .35% for a 99 hour exposure. The balance of data are presented in Table 2-12, covering 10 specimens from both material batches. The data shows, as expected, a relatively large change in outgassing with increase in temperature. Also as expected, there was no change in outgassing behavior from batch to batch.

- Humidity Exposure and Subsequent Outgassing - Specimens for humidity exposure were suspended in a thermotron humidity chamber at 95% RH and 37.8°C (100°F) for one hundred hours. The specimens were weighed prior to and following exposure, with each specimen being wiped free of surface water before re-weighing. Specimen thickness was also checked before and after test. Following this, the specimens were placed in the high vacuum enclosure and were exposed at either room temperature or 65.5°C (150°F) until no weight change

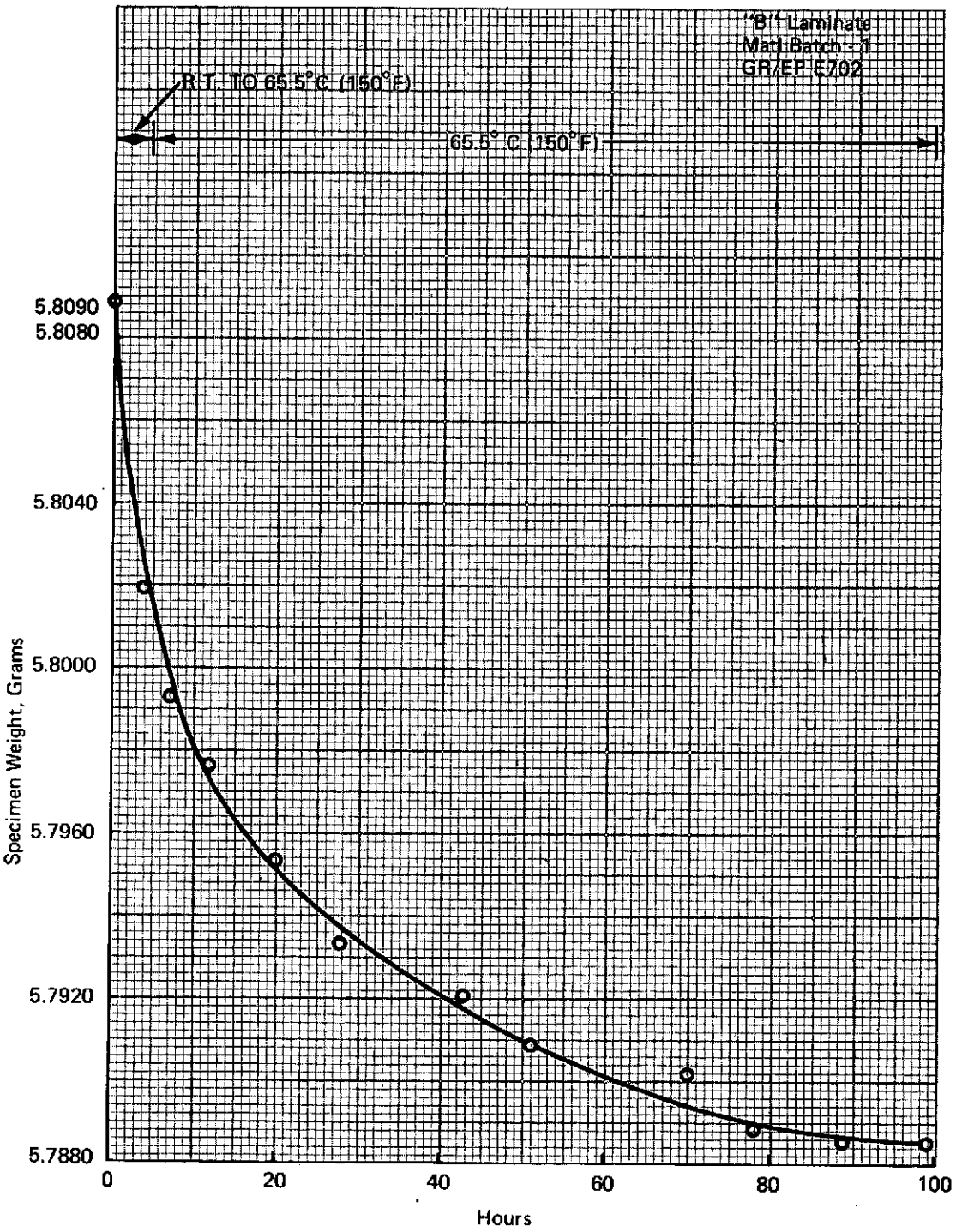

Figure 2-29 Outgassing, Weight Loss vs Time

Table 2-12 Outgassing Exposure-Test Results

Sample No.	Orig. Wt.,g	Temp.	Final Wgt.,g	% Outgassing Total	% Outgassing/Cm^2/HR R.T.to 65.5°C(150°F)
R1-1 (1)	.7663	RT	.7654	0.17	
R1-2	.7268		.7267	0.014	
R1-3	.7467		.7465	0.027	
R2-1 (1)	.7611		.7604	0.092	
R2-2	.7462		.7458	0.054	
F1-1 (1)	5.8090	65.5°C	5.7886	0.35	0.087
F1-2	4.6435	(150°F)	4.6263	0.37	0.11
F1-3	4.9670		4.9482	0.38	0.124
F2-1 (1)	6.9683		6.9397	0.41	0.089
F2-2	8.0710		8.0452	0.32	0.057

(1) Specimens subsequently measured for α_τ

occurred over a four hour period. The results, which are shown in Table 2-13, indicated an extremely small amount of moisture absorption under the conditions of test. The time necessary to reach equilibrium during vacuum treatment after exposure to humidity was dependent on the specimen temperature. Those specimens exposed at room temperature required from 20-24 hours, while those exposed at 65.5°C (150°F) reached constant weight after 8-12 hours. The vacuum tests were terminated when the specimens reached their approximate starting weights. In conclusion, the tests have shown that humidity exposure at 37.8°C (100°F) and 95% RH for 100 hours resulted in a weight increase of about .27%. No dimensional changes were noticed. Relatively little, if any, moisture was retained in the specimen following subsequent, brief, vacuum treatment.

2.5 Dynamic Response Testing

Dynamic response testing was accomplished on the five Gr/Ep tubes fabricated under this program. The tubes were 81.28 mm (3.2 inches) in diameter and 1.12 m (44.25 inches) long. Testing was conducted to identify and measure the dynamic response, mode shape and damping.

Each tube was instrumented with seven accelerometers suspended with lacing cord at the first mode node points and attached to a shaker at the tube mid point. The test set-up is shown in Figure 2-30. The specimens was subjected to low level constant force sinusoidal frequency sweeps as the output of accelerometer No. 1 (located at tube end) was being recorded as Co-Quad response. Each Co-Quad resonant condition was investigated for pure mode. After the pure mode condition was established, the amplitude and phase relationship of the seven accelerometers was recorded and the mode shape developed. The damping for each mode was determined by the 3db point method (Δf at the Co-Quad equivalence).

Pure mode condition could only be established for the first bending mode and is presented in Table 2-14. A typical tube fundamental mode shape is presented in Figure 2-31.

Table 2-13. Humidity Exposure Followed by Vacuum-Test Results

Sample No.	Orig. Wt.,g	Wt. after Humidity Exposure, g.	Wt. after Vacuum, g	Temp. in Vacuum
HR1-1 (1)	5.8131	5.8278	5.8137	RT
HR1-2 (1)	4.7323	4.7435	4.7325	
HR1-3	5.2373	5.2535	5.2394	
HR2-1	5.6360	5.6468	5.6349	
HR2-2 (1)	.7250	.7262	.7244	
HF1-1 (1)	.7372	.7339	.7320	65.5°C
HF1-2	.7418	.7423	.7419	(150°F)
HF1-3	.7462	.7469	.7451	
HF2-1 (1)	.7497	.7508	.7488	
HF2-2	.7399	.7405	.7394	

(1) Specimens subsequently measured for α_T

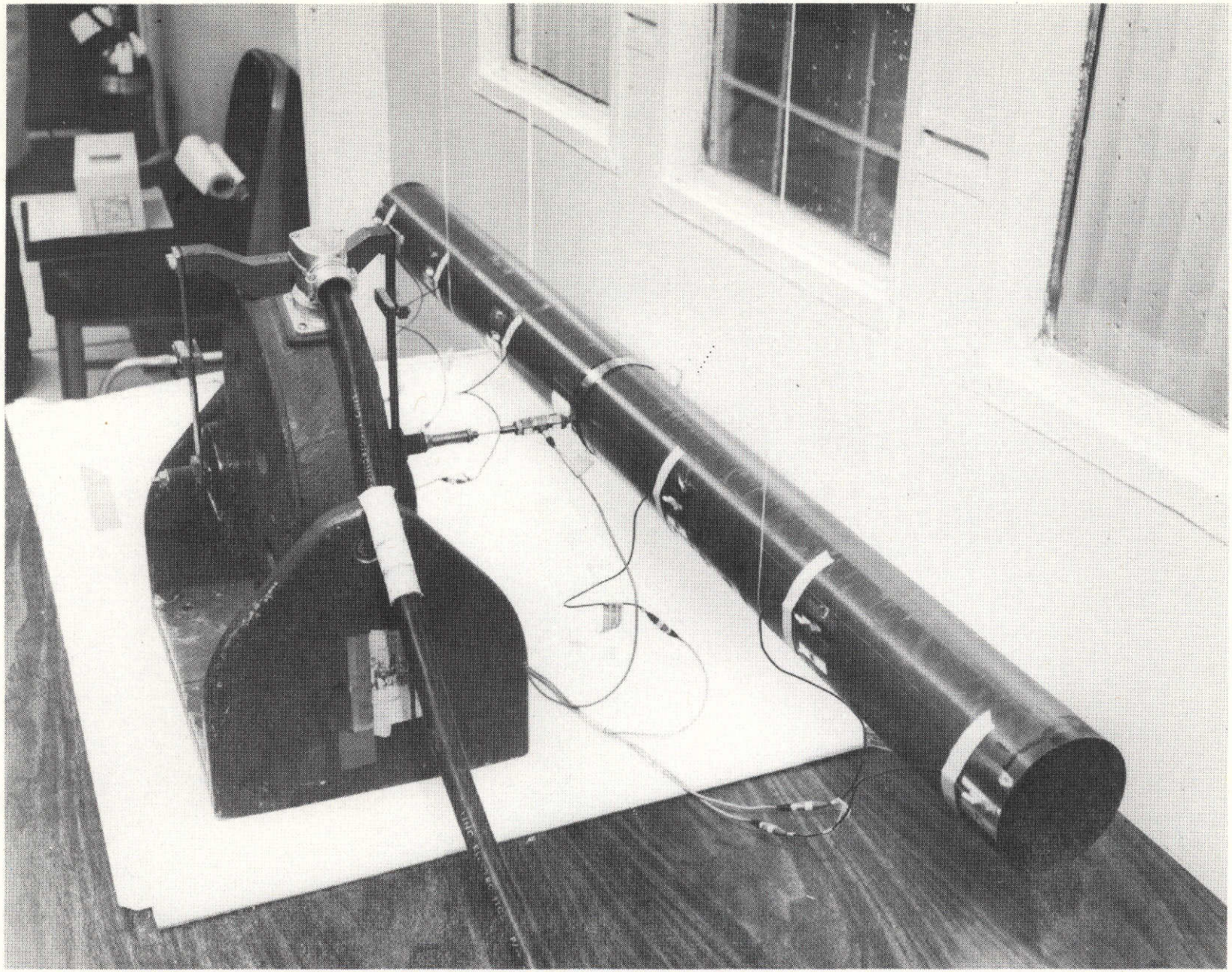

Figure 2-30 Dynamic Test Set-Up, Gr/Ep Tube

Table 2-14 Dynamic Test Results

Specimen	f Force, N (lb.)	F_N, HZ	Damping
1	1.112 (.25)	576.8	.00433
	2.224 (.5)	577.0	.00364
2	.444 (.1)	579.8	.00396
	1.112 (.25)	579.7	.00430
	2.224 (.50)	579.8	.00414
3	.444 (.1)	578.2	.00380
	1.112 (.25)	578.3	.00449
	2.224 (.5)	578.2	.00415
4	1.112 (.25)	575.7	.00432
	2.224 (.50)	575.5	.00455
5	1.112 (.25)	584.1	.00445
	2.224 (.5)	584.0	.00393

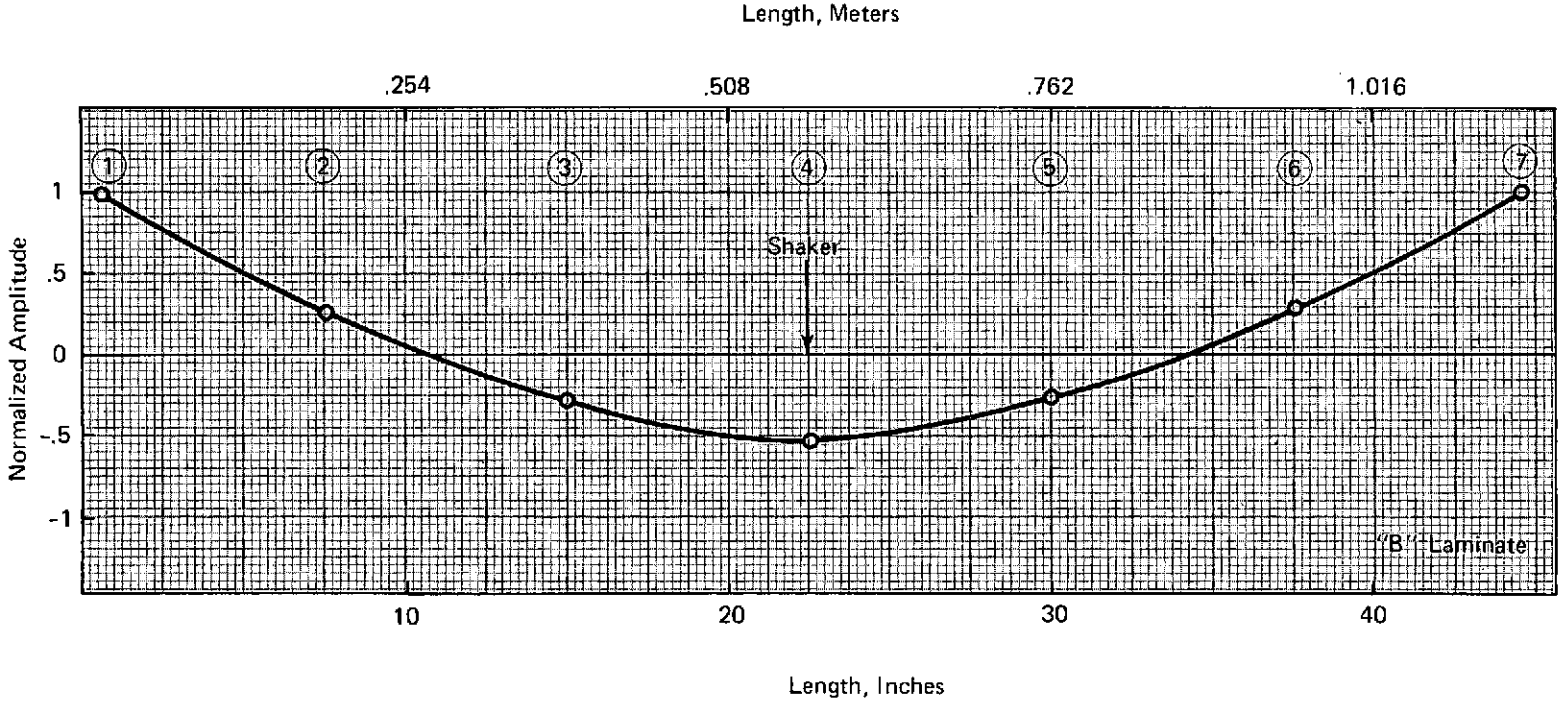

Figure 2-31 Typical Fundamental Mode Shape, Gr/Ep Tube

It was determined from the Co-Quad plots (a typical plot is shown in Figure 2-32) that resonant conditions other than the fundamental mode (578.2 Hz) are indicated. These resonant indications were carefully investigated for possible higher frequency bending modes. However, all resonant points examined produce no characteristic second and third bending mode shapes. The failure to identify the second and third bending mode has been attributed to the problem associated with high frequency modal density and mode couplings. At these high frequencies the shell and ring modes couple with the higher order bending mode and become difficult to separate.

This phenomenon is clearly evident upon examination of Figure 2-33. This plot shows the quadrature response of 2 accelerometers located 3.14 rad. (180°) apart at one end of the tube as the frequency was varied from 350 to 3500 Hz at a constant 1.11 N (.25 lb) vibrating force applied at tube mid-span. For true bending mode indication these accelerometers must show an in-phase condition (out of phase condition on plot indicates an in phase condition since accelerometers are mounted back to back). This condition occurs at 578 Hz (fundamental bending) and 1420 Hz. Further investigation of 1420 Hz failed to produce a pure resonant condition.

During the test, a discrepancy was noted in the measured values of damping. An investigation of this discrepancy revealed that the transducer wires were contributory. All accelerometer and acceleometer wires were removed except accelerometer No. 1. The damping measurements were re-taken on all tubes and the results show excellent agreement, see results on Table 2-14.

Also investigated was the effect of shaker drive rod weight on tube resonant frequency. The resonant frequency of the tube with 4 known drive rod clamp weights was determined and the 0 weight condition extrapolated. These results are presented on Figure 2-34.

Although data for the second and third bending mode was not obtainable, based on the first bending mode data, it can be concluded that the dynamic behavior of the Gr/Ep composite structure appears quite similar to that of standard structural metal. There was no indication of non-linearity in stiffness and/or damping and no appreciable difference between tubes.

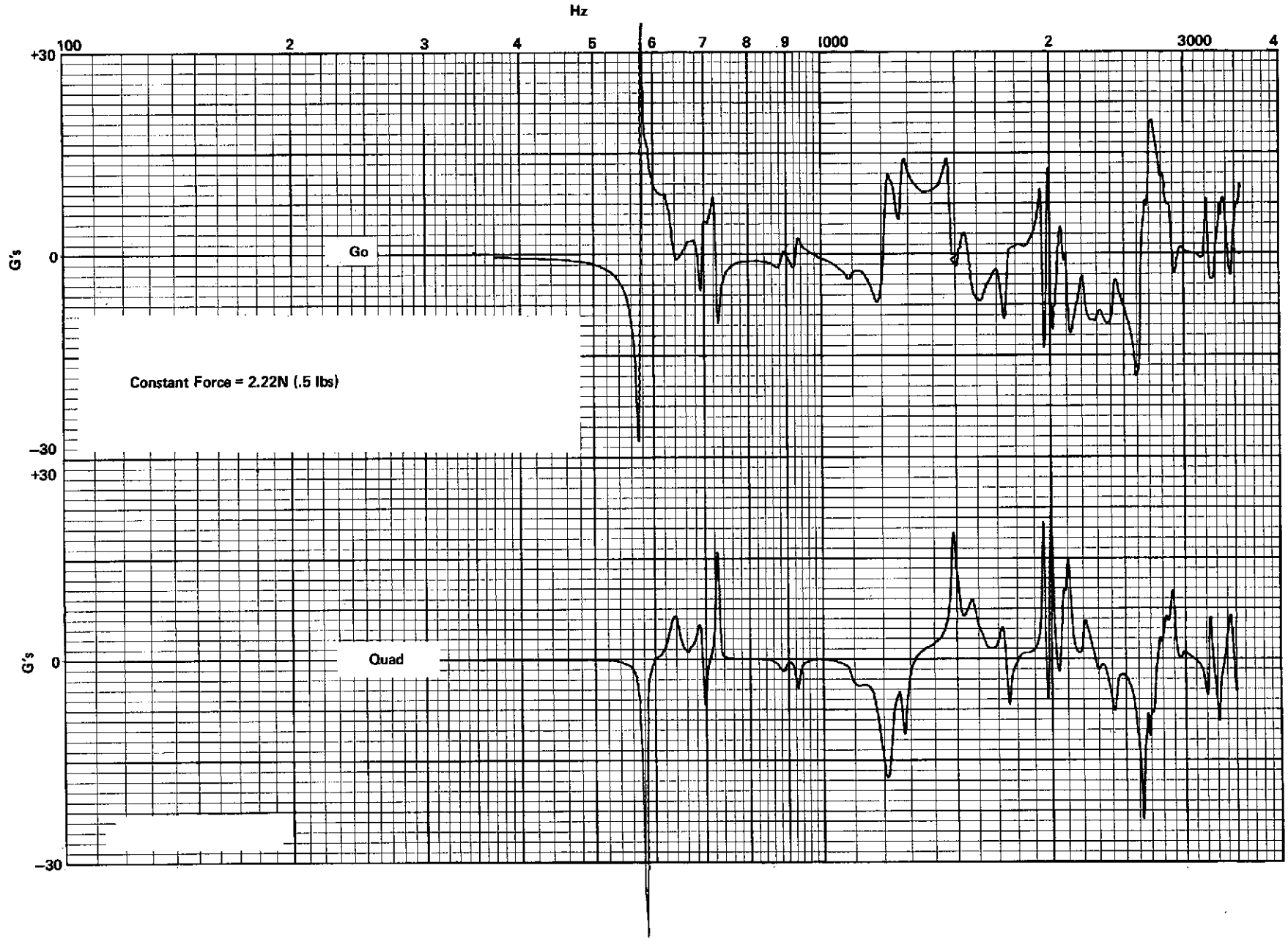

Figure 2-32 Co-Quad Response, Gr/Ep Tube Number 2

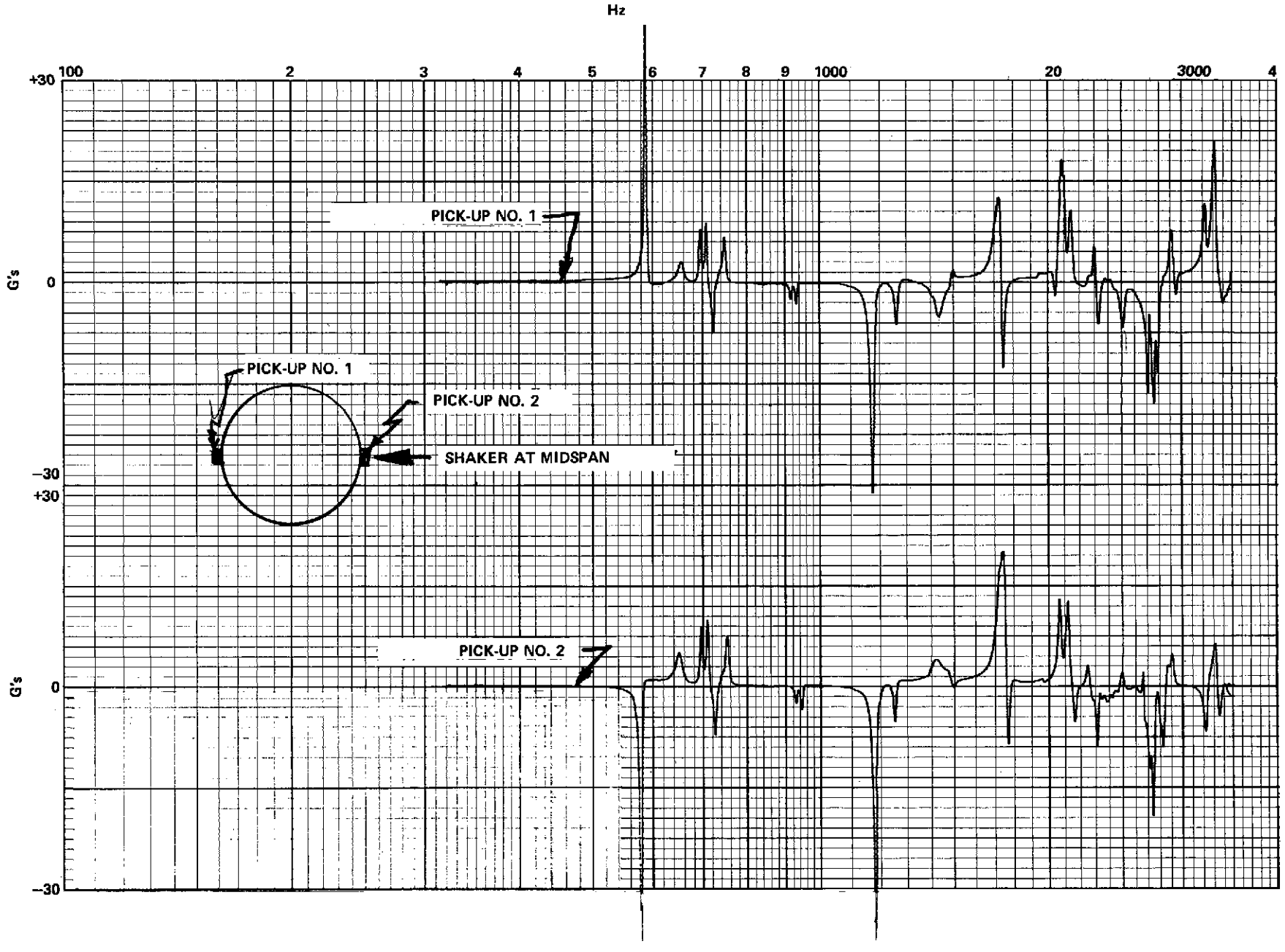

Figure 2-33 Quadrature Response, Gr/Ep Tube Number 2

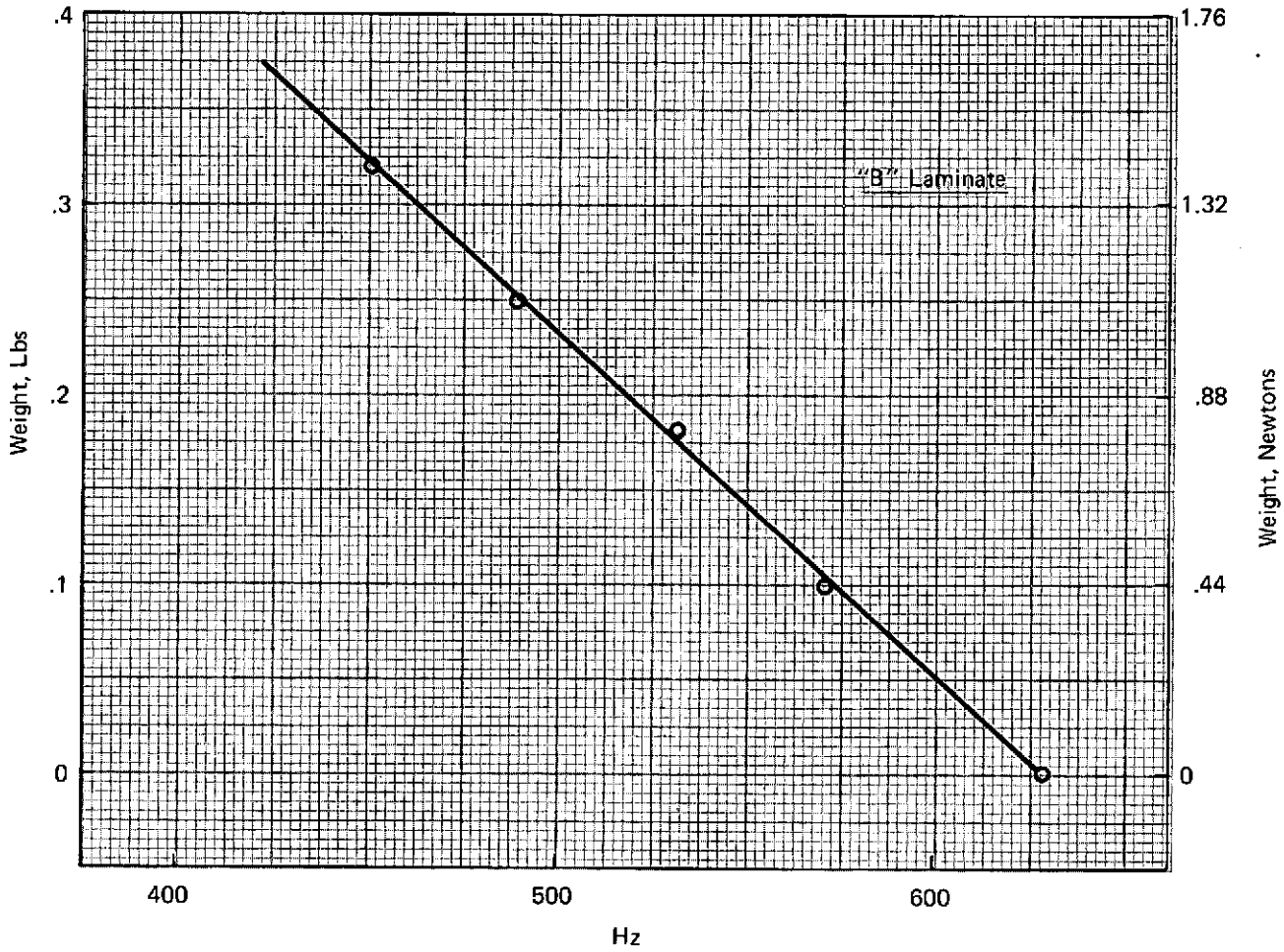

Figure 2-34 Effect of Weight at Drive Point on Resonant Frequency of Tube

Examination of the high frequency response, shows excellent dynamic behavior correlation between tubes.

2.6 Structural Verification

The two member metering truss assembly was tested in compression in a Tinius Olsen Electromatic 60,000 pound capacity universal testing machine. Strain was measured by the use of twelve axial SR4 Model FAP25-35S6G-1 resistance strain gages (BLH Electronics, Inc.). Four gages were located at the center of each tube along the longitudinal axis - 1.57 rad (90°) to each other. Two gages were located on the outside face of each of the two gusset plates. Figure 2-35 shows the strain gage locations. Readout of the strain gages was provided by a BLH Electronics, Inc. Digital Indicator Model 902. Head deflection was also recorded during the test using a Tinius Olsen Model D2 Deflectometer.

The truss assembly was incrementaly loaded in initial steps of 4448 N (1000 lbs) to an applied test load of -17792N (-4000 lbs), in -2224N (-500 lb) increments to -26688N (-6000 lbs) and then to the design ultimate load of -28155N (-6330 lbs). Readings above design ultimate were taken at every -4448N (-1000 lbs) of load. Initially, a preload of 2000 lbs was applied to exercise the strain gages and truss assembly. All testing was conducted in standard laboratory conditions of 23°C (73.5°F) and 50 $\pm$ 2% RH. Load introduction to the structure was accomplished through the use of metal test fittings. At the apex fitting end of the structure, an aluminum bearing plate was provided, into which the gusset plate extensions were potted. At the opposite end of the structure, split aluminum fittings were bonded to each Gr/Ep tube. A tension strap joined the two fittings. Figure 2-36 shows the test set-up.

The structure was tested in axial compression, with the magnitude of applied loads adjusted to yield load levels on the apex fitting representative of those anticipated for the flight vehicle.

Results of the test were satisfactory, with the structure failing at an applied test load of 105,417 N (23,700 lbs) or 374% of design ultimate load. Failure occurred in one of the graphite/epoxy tubes approximately .101 m (4 inches) from the fiberglass overwrap at the test fitting end.

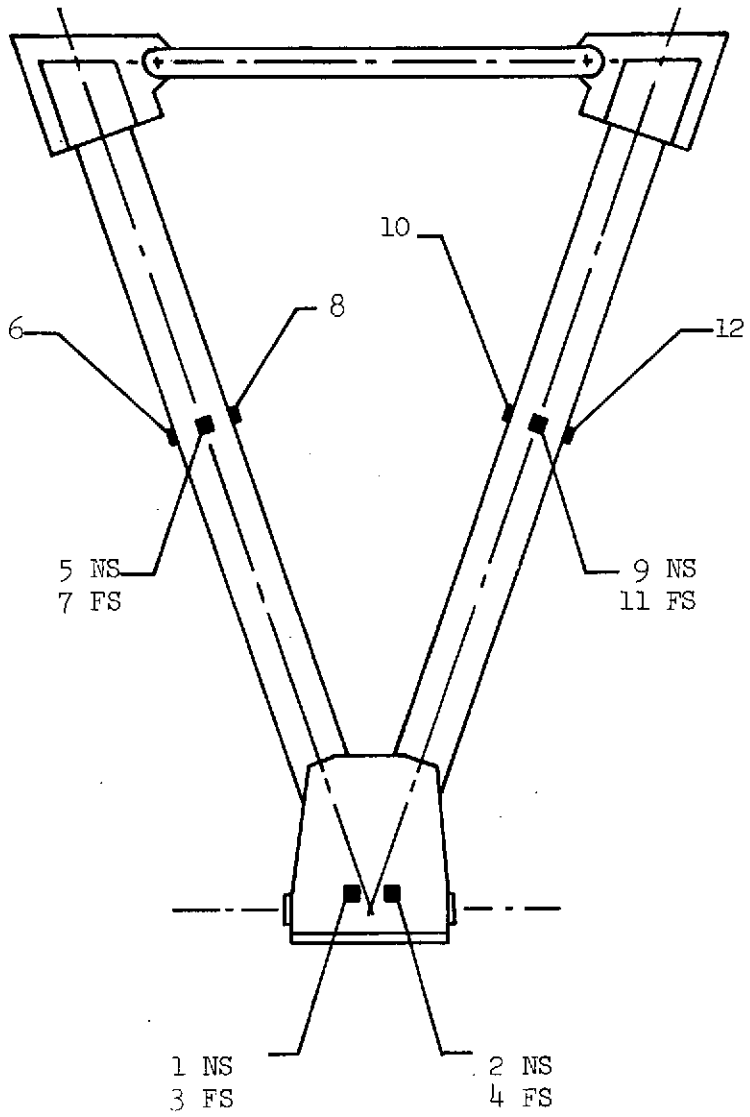

NS = Near Side

FS = Far Side

Figure 2-35 Strain Gage Locations - Two Member Truss

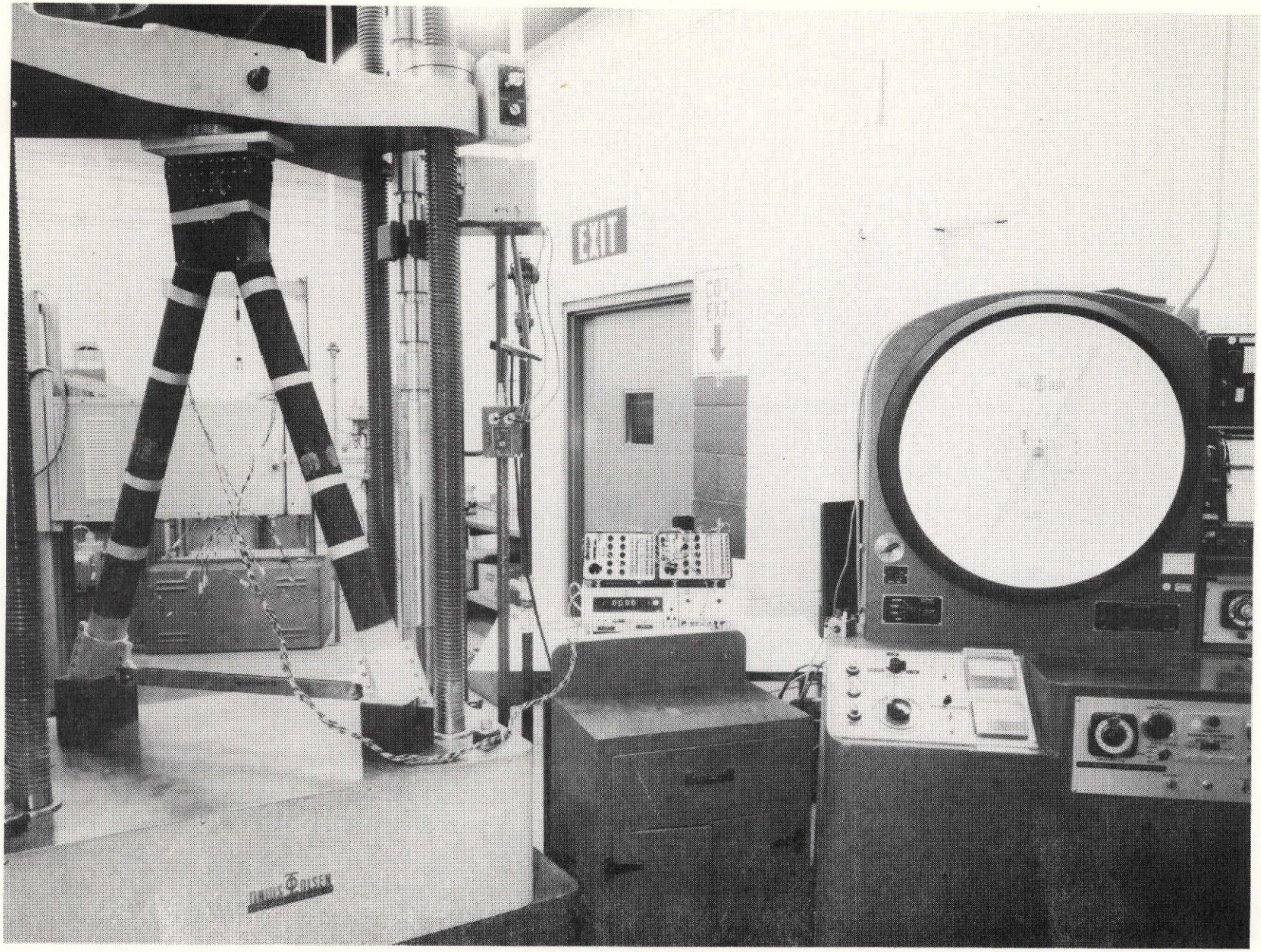

Figure 2-36 Test Set-Up-Two Member Truss Component

The failure is shown in Figures 2-37 through 2-39. At first glance it may appear that the structure is significantly over designed, however, that is not the case. All members of the structure were designed primarily for stiffness and/or maintaining exceptionally low thermal growth; as such operating stress levels were extremely small. This accounts for the detail parts of the structure sustaining such high test loads. The critical area of the structure, as defined by the stress analysis, was the adhesive bonded joint between the tubes and the gusset plates. This joint showed a 98% margin of safety based upon an allowable average adhesive shear stress of 3791 x 10^3 N/m^2 (550 psi). The apparent average adhesive stress was 7073 x 10^3 N/m^2 (1026 psi) at failure. The allowable was arrived at based upon the length of the overlap (the longer the overlap the lower the allowable) and the type of adhesive system. The adhesive system, Aerobond 2143, is a R.T. cure cast epoxy resin, exclusive of any positive bondline thickness control (such as carrier cloth in most film adhesives). As such, allowables for these systems are universally conservative. In addition, minimization of peel (as accomplished by the peel stop fasteners) on any bonded joint will significantly improve joint performance. It is for these reasons that joint failure did not occur.

Strains associated with the test of the two member truss are presented in Table 2-15. Of the twelve gages affixed to the structure only six functioned properly; two on each tube (6, 8, 10 and 12), directly opposed and in the plane of the truss and one on each gusset plate (2 and 4). All gages behaved linearly. As can be seen from Table 2-15, strains were monitored for all functional gages up to 53376 N (12000 lbs), after which a continuous loading was used and only one selected gage (10) was monitored to failure. Strain at failure was -1225 μ mm/mm (-1225 μ in/in) or a compressive stress of -170.59 x 10^6 N/m^2 (-24,745 psi). This is below the design allowable of 237.15 N/m^2 (34,400 psi) as derived from the material characterization program. There was, however, considerable out of plane bending, as implied by gage numbers 2 and 4 located on opposite gusset plates. If strain values of these gages are linearly projected to the failure load a net difference of -605 μ mm/mm (-605 μ in/in) exists which, when added to the tube strain at failure, would indicate a stress level of approximately -255.07 x 10^6 N/m^2 (-37,000 psi) in the tube, which is generally in good agreement with

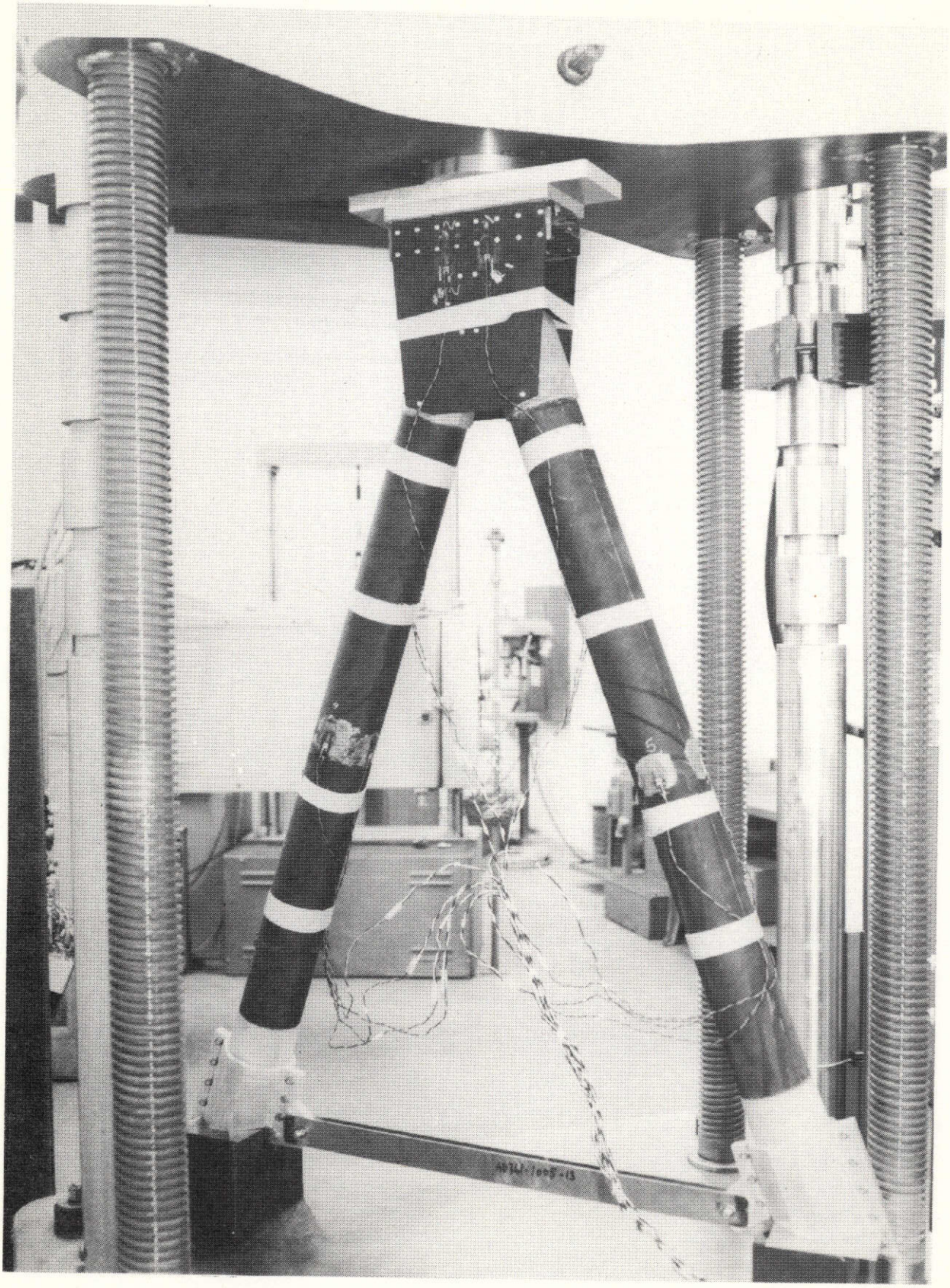

Figure 2-37 Component Failure-Overall View

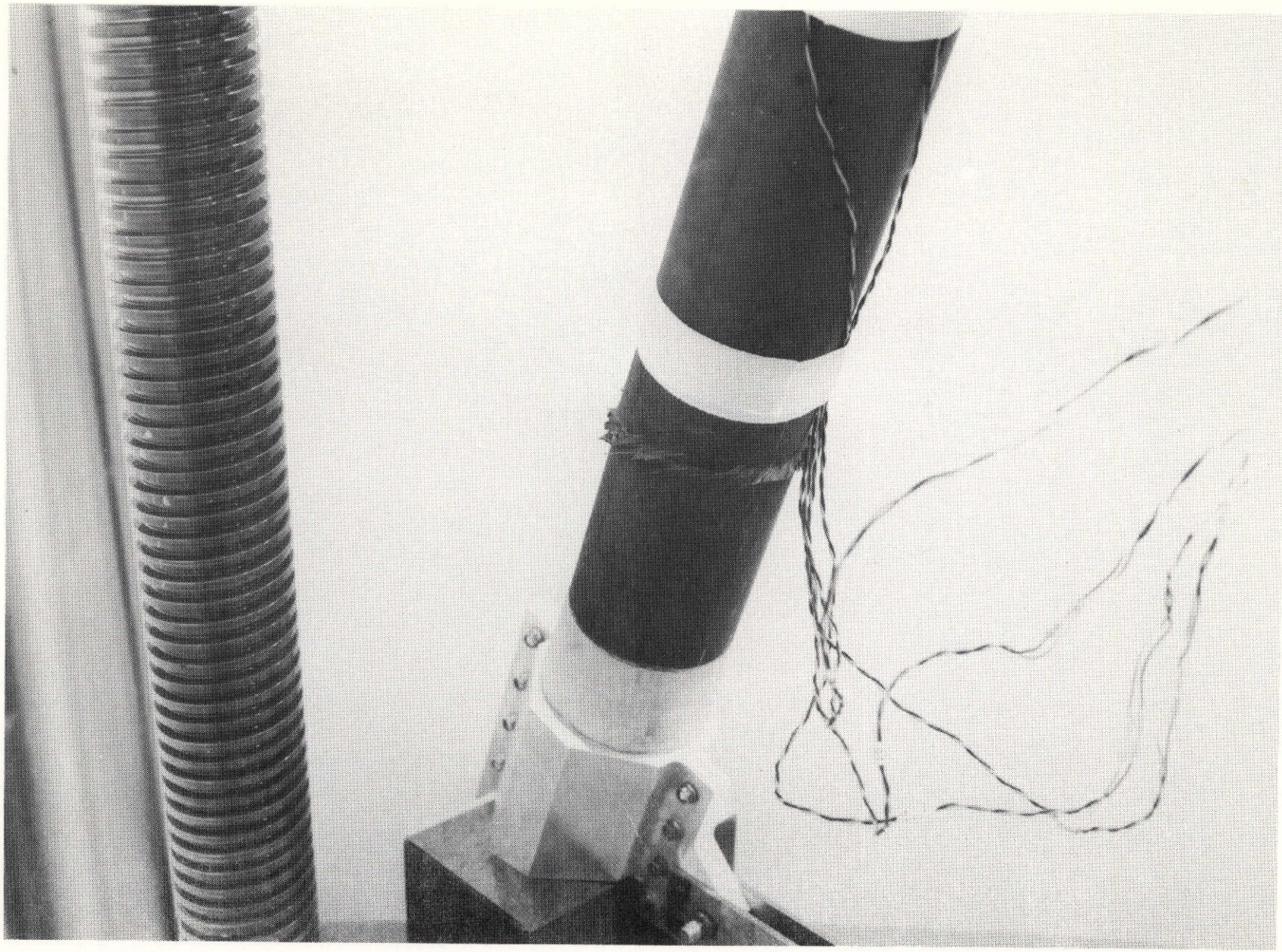

Figure 2-38 Component Failure-Close-Up of Near Side

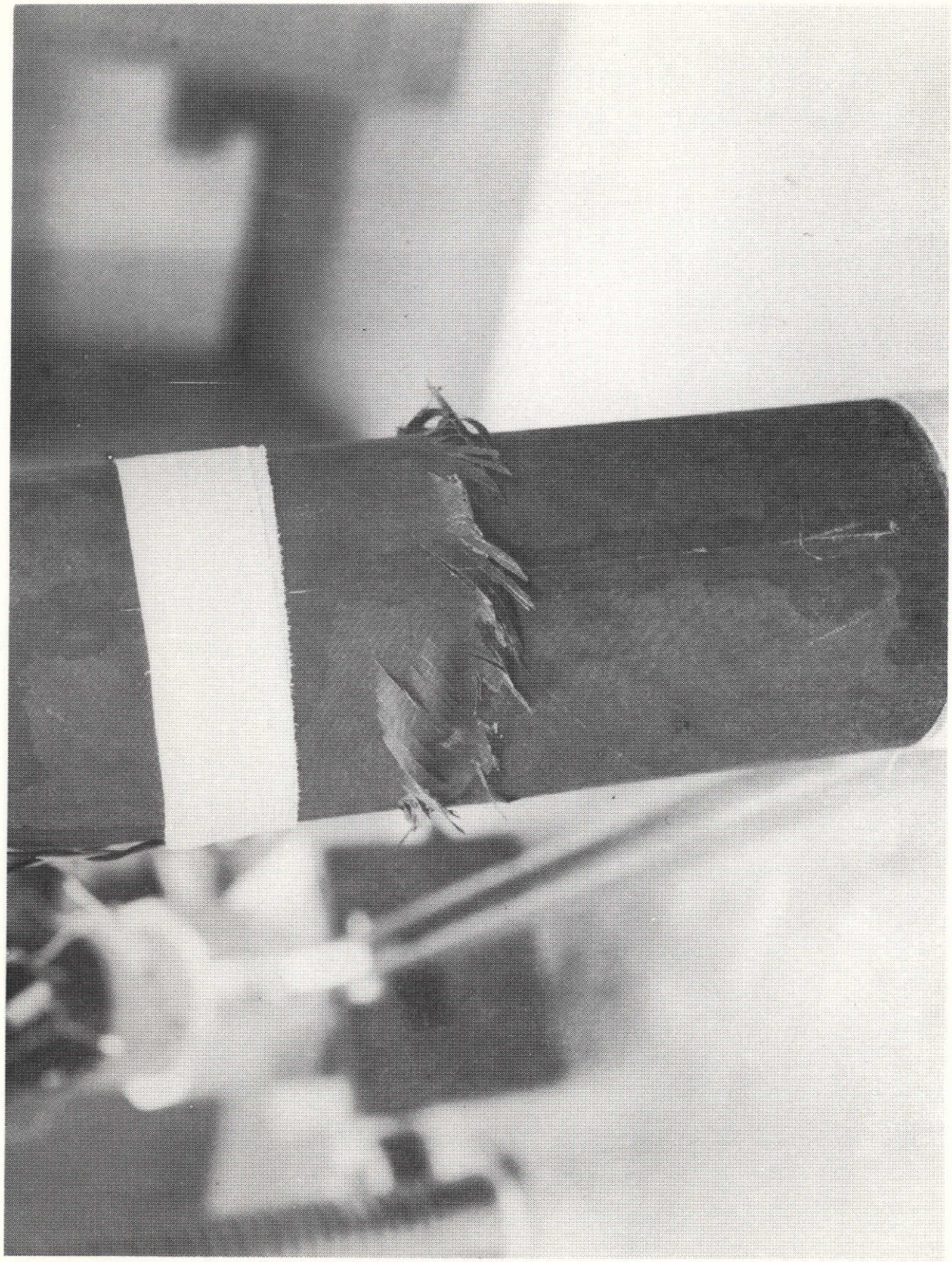

Figure 2-39 Component Failure-Close-Up of Far Side

Table 2-15 Measured Strains - Two Member Truss Component

Load N x 10^3(lbs)	Strain μ mm/mm (μ in/in)					
	Gage No.					
	2	4	6	8	10	12
4.44(1000)	-36	-54	-30	-42	-45	-41
8.89(2000)	-84	-116	-78	-97	-100	-88
13.34(3000)	-130	-182	-124	-150	-150	-138
17.79(4000)	-173	-253	-170	-200	-200	-188
20.01(4500)	-195	-290	-191	-228	-220	-214
22.40(5000)	-224	-329	-216	-250	-248	-242
24.46(5500)	-248	-366	-240	-280	-270	-270
26.68(6000)	-272	-400	-265	-304	-296	-294
28.15(6330)D.U.L.	-288	-427	-278*	-320*	-315*	-315*
31.13(7000)	-312	-480	-310	-360	-344	-345
35.58(8000)	-360	-556	-353	-408	-392	-396
40.03(9000)	-408	-600	-400	-455	-440	-448
44.48(10000)	-455	-700	-454	-500	-482	-500
48.92(11000)	-510	-787	-495	-553	-532	-554
53.37(12000)	-558	-863	-540	-603	-580	-600
57.82(13000)					-632	
62.27(14000)					-678	
66.72(15000)					-725	
71.16(16000)					-775	
75.61(17000)					-820	
80.06(18000)					-868	
84.51(19000)					-920	
88.96(20000)					-972	
93.40(21000)					-1023	
97.85(22000)					-1075	
102.30(23000)					-1128	
105.41(23700)					-1225	

* Predicted strain at D.U.L. = 292 μ mm/mm (292 μ in/in)

anticipated strengths. Other secondary effects most probably exist near the support which would further raise the stress level, but are difficult to account for with the limited instrumentation available.

Total machine head deflection at failure was approximately .203 mm (.008 in) and remained linear throughout the test. A plot of head deflection versus applied load is presented in Figure 2-40.

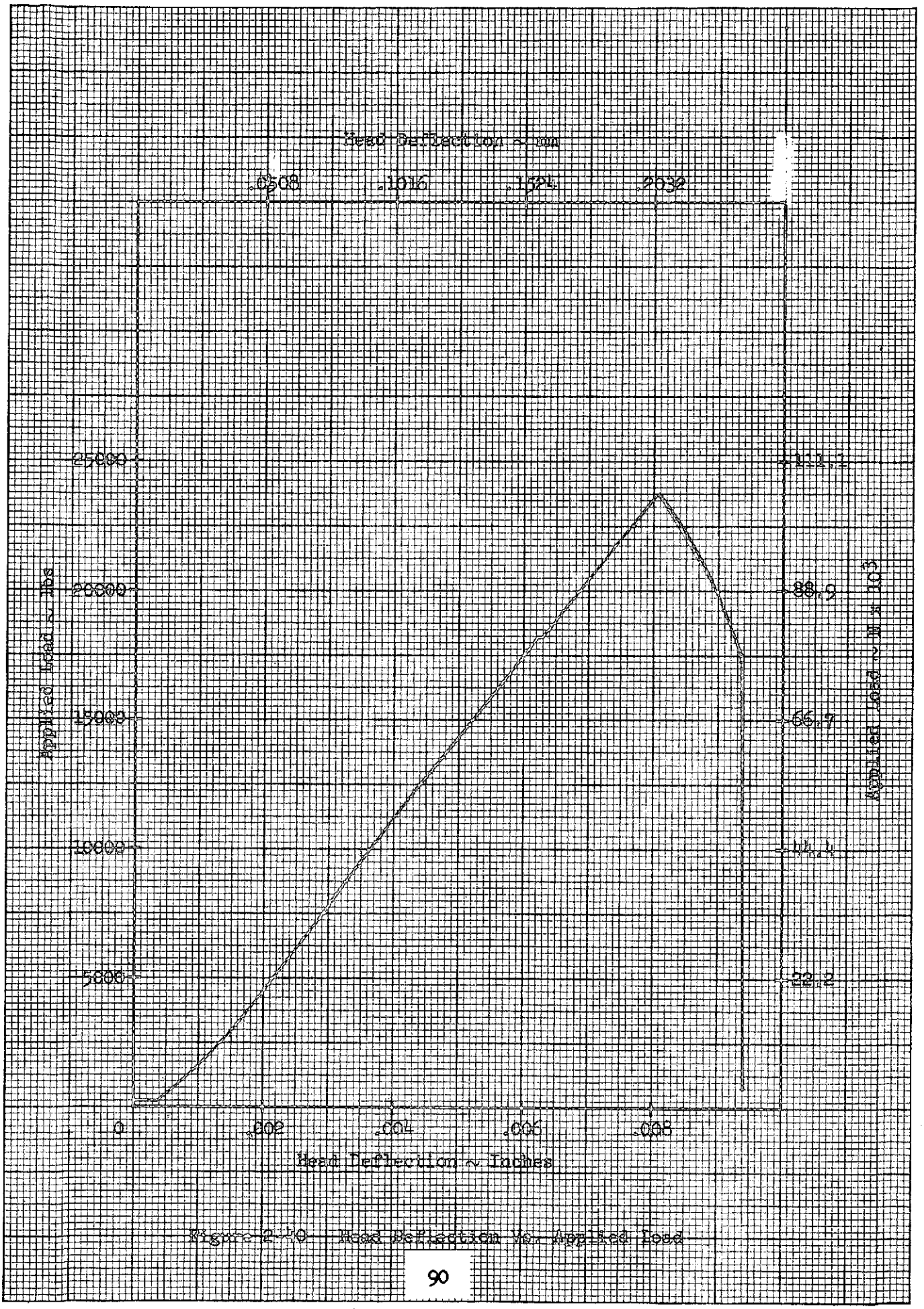

Figure 2-10 Head Deflection Vs. Applied Load

3.1 Material Procurement

The material required for fabrication of the Gr/Ep details and truss assembly were:

- GY-70/E-702 Graphite/Epoxy preimpreguated tape - 66.5mm (2.62 inches) wide.
- Type A/E-702 Graphite/Epoxy preimpregnated tape - 76.2mm (3 inches) wide.
- Metlbond 329 Type IA adhesive
- Aerobond 2143 A/B adhesive
- NAS 1919 blind rivets
- Glass/Epoxy F161/7781/GAC Specification GM 4001, Comp. G-12.

The graphite/epoxy tape procured for this program was the Celanese GY-70 Fiber and the Hercules Type A fiber, both impregnated with the U.S. Polymeric E-702 resin system which is capable of complete cure at 122.2°C (250°F), thermally stable up to 148.8°C (300°F) and exhibits minimal total outgassing.

The initial shipment of GY70/E702 graphite/epoxy was combed to a 76.3mm (3 in.) tape width, to yield a cured per ply thickness of .133mm(.00525 in.) at 60 v/o fiber, was of unacceptable quality and therefore rejected. The material supplier was contacted to determine the cause of the problem and the corrective action to be taken. As a result, it was determined that inherent properties of the GY70 material limits the width to which the material may be combed.

The problem was resolved by allowing the supplier to reduce the tape width to 63.5mm -66.5mm (2.5 - 2.62 inches) at a 60 v/o fiber to provide high quality at an acceptable thickness. The reduced tape width material molded to a nominal per ply thickness of .160mm (.0063 in.) at 60 v/o fiber.

3.2 Tool Design

Tool requirements for the fabrication of the various Gr/Ep detail parts were as follows:

Tube Mold Form (MOF)
Tube Layup Mandrel (TFT)
Tube Layup Template (LT)
Tube Wrapping Machine (MCA)
Truss Assembly Fixture (AF)
Channel Section Mold Forms (MOF)
Shear Clip Mold Forms (MOF)

3.2.1 Mold Forms

The mold form used for fabrication of both the subcomponent and full length Gr/Ep tubes was a re-worked version of that used under the second phase of this program to fabricate boron/epoxy thrust structure members. Rework of the tool was limited to approximately .304m (12 inches) at each end, where a conical taper existed for transition to a larger diameter. The taper was eliminated by first reboring the .304m (12 inch) section to the larger diameter, followed by insertion of steel cylinders with undersize inside diameters. The entire inside diameter was then rebored to the original 81.50mm (3.209 inch) diameter. In basic design, the tools were configured as female molds split along the longitudinal centerline, with the inside surface being the molding surface. The molds were rough machined from steel bar stock with finish grinding of the mating surfaces. Both halves were then assembled with locating pins and cap screws. A flat pattern contour template was made of the molding surface and checked for accuracy. The molding surfaces were then machined to finish dimensions using a tracing lathe. Index holes, vacuum grooves and vacuum fittings were then added.

3.2.2 Layup Mandrel

The layup mandrel, which was of the break-away type in design to facilitate removal, consisted of a solid core with a split tube fastened to the core with holding collars. To remove this mandrel from the layup, the holding collars were unfastened and the solid core removed. The split tube pieces

then collapse into the space vacated by the core and were removed from the layup. The layup madrel was also reworked from Phase II tooling. The rework consisted of adding shim material to the split sections, to compensate for the larger inside diameter.

3.2.3 Tube Wrapping Machine

The tube wrapping machine is a hand operated tool that laid-up and compacted the graphite tape on the tube layup mandrel. This tool consists of a wind-up roller, pressure roller, vacuum table and tube layup mandrel.

The tube fabrication procedure utilized with the wrapping machine was:

- Apply graphite tape to the mylar layup template
- Position the template on the wrapping machine and attach to the wind-up roller
- Apply vacuum to the template
- Wind template 2 turns on the wind-up roller
- Position layup mandrel and adjust pressure roller
- Turn wind-up roller until graphite tape is fed between the layup mandrel and the pressure roller, transferring the tape to the mandrel

3.2.4 Layup Templates

The layup template is a mylar master of each ply and contains all the information needed for laying up that ply.

Information on the template includes ply number, ply trim, ply orientation, ply position, and template feed direction. To minimize handling problems, each template was made to include no more than five plies. Plies of graphite are initially layed up on the template and subsequently transferred to the layup mandrel via the tube wrapping machine.

3.2.5 Assembly Tooling

The assembly fixture for the two member truss consists of a jig board aluminum plate, locating dowels, bank stops and plastic shims used to simulate glue lines. The dowels, which are inserted in the jig bored holes locate the test fittings, position the tubes in the proper angular orientation and locate them in both the longitudinal and lateral directions. The bank stops, which

are also located from jig bored holes are used to set-up the locations of the various apex fitting and ring details, as well as the aluminum test bearing plate. Additional shims (metallic) are also provided for external height adjustment. A sketch of the tool and its component parts is shown in Figure 3-1.

3.3 Parts Fabrication

3.3.1 Test Specimen Fabrication

The Graphite/Epoxy test panels AD361-100, AD361-101, AD361-102 and AD361-103, required for subsequent fabrication of element test specimens, were fabricated using standard processing techniques. Layup was accomplished using nylon peel ply on both surfaces of all panels and a bleeder system consisting of style 120 dry glass cloth (1 layer per 1.8 layers of graphite/epoxy) perforated tedlar, and two plies of style 181 dry glass. Aluminum caul plates .508mm (.020 inches) thick were used to enhance the surface flatness of the test panels. The panels were cured in the Devine (air circulating) autoclave using the following cure cycle:

1. Bag parts and draw .508mm Hg (20 inches Hg) minimum vacuum and place into the autoclave.
2. Apply 586 -621 x 10^3 N/m^2 (85-90psi) pressure, turnoff the vacuum and check the bag for leaks. The vacuum shall fall from 508mm - 254mm (20 inches to 10 inches) in not less than 2 minutes.
3. If the bag passes the test, apply 508mm (20 inches) minimum vacuum and drop the pressure to 0 (zero).
4. Heat from 48.8°C (120°F) to 115.5 - 126.6°C (240-260°F) in 25-45 minutes under vacuum.
5. When all part thermocouples reach 104.4°C (220°F), apply 586 - 621 x 10^3 N/m^2 (85-90 psi) pressure with CO_2 and drop vacuum to 50.8mm (2 in).
6. Hold 115.5 - 126.6°C (240-260°F), 586 x 10^3 - 621 x 10^3 N/m^2 (85-90 psi), and 50.8mm (2 inches) vacuum for 60-70 minutes.
7. Cool under full pressure to 51.6 - 65.5°C (125-150°F) in not less than 45 minutes.

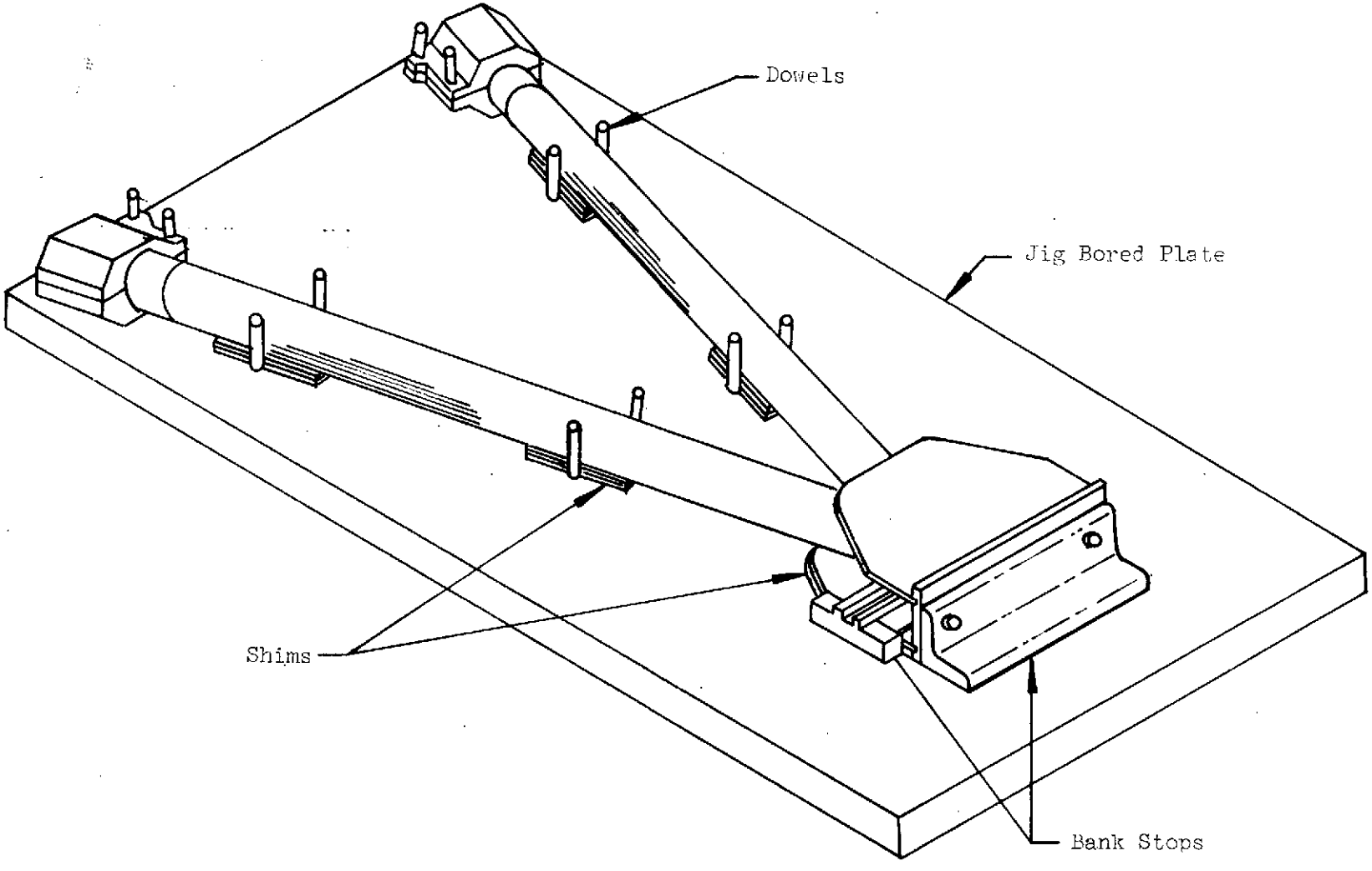

Figure 3-1 Assembly Fixture, Two Member Truss

8. Apply 508mm (20 inches) minimum vacuum and remove the parts from the autoclave.

9. Post cure for 3 hours at 148.8 - 160°C (300-320°F).

The panels were then inspected for voids by ultrasonic NDT, trimmed to net size and the various tension, compression, flex and shear specimens machined from the trimmed panels.

The tension and compression specimens had E-293 fiberglass doublers bonded to them with FM1000 adhesive and cured for one hour at 176.6°C (350°F) and, a pressure of 1.37 -3.10 x 10^5 N/m^2 (20-45 psi).

3.2 Subcomponent/Full Length Tube Fabrication

- Subcomponent Tubes (AD361-104)

Fabrication of the first of the three .305m (12 inch) x 81.28mm (3.20 inch) diameter subcomponent tubes exhibited severe wrinkling on the inside diameter of the tube with resin ridges on the outside diameter. An investigation to determine the cause of the deficiencies revealed two items. The primary cause was due to a failure of the bag during cure, this being caused by a burr on the vacuum pipe. The secondary cause was traced to a slightly oversize mandrel (about .507mm or .020 inches) which made it difficult to place the wrapped part in the mold and remove the mandrel. This contributed to the wrinkling of the bleeder and also pinched the outside diameter of the tube (causing the resin ridges) when the tube was inserted into the split female mold. Corrective action was instituted and the first tube re-made. The corrective action consisted of reworking the mandrel by removing .507mm (.020 inch) from the outside diameter and usage of a felt bleeder system. The tube was then layed up, rolled on the mandrel and the felt bleeder added. The total bleeder system consisted of 1 ply TX1040, 4 plies 116 cloth and 1 ply of felt (inserted in two halves to allow for tube expansion).

This resulted in a good tube except for a slight ridge on the inside diameter caused by the felt overlapping. Subsequent Quality Control NDT inspection did however indicate a sound part. Further corrective action

was taken to completely eliminate any ridge formation on the inside diameter. This was accomplished with the use of a paper bleeder and a modified fabrication sequence which is presented below:

1. Omit the bleeder when rolling the tube.
2. After the tube is rolled, place in the mold form and check for tightness of fit.
3. Re-open mold form and remove layup mandrel
4. With the mold form open, insert new bleeder system consisting of 1 ply TX1040, 2 plies 6910 paper bleeder and 1 ply of slotted mylar - 3.17mm on 5.06mm (1/8" on 2") centers.
5. Install nylon bagging film.
6. Install sheet of expanded mylar to maintain shape.
7. The MOF was then closed and the tube was cured in the Devine air circulating autoclave using a carbon dioxide atmosphere.

The above noted modifications proved to be very successful, yielding tubes with extremely smooth inside and outside diameters and of exceptional quality. All further tubes manufactured for this program used identical procedures.

The cure cycle for the subcomponent tubes was as follows:

1. Bag parts, draw 508mm (20 inches) min. vacuum and place in autoclave.
2. Apply 586-621 x 10^3 N/m^2 (85-90psi) pressure, turn vacuum off and check bag. Vacuum shall fall from 508 to 254mm (20 to 10 inches) in not less than 2 min.
3. If bag passes test, apply 508mm (20 inches) min. vacuum and drop pressure to zero.
4. Heat from 48.8 to 115.5-126.6°C (120 to 240-260°F) in 25 to 45 min under vacuum.
5. When all part thermocouples reach 104.4°C (220°F), apply 586-621 x 10^3 N/m^2 (85-90 psi) pressure with CO_2 and drop vacuum to 50.8mm (2 inch).

6. Hold 115.5-126.6°C (240-260°F), 586-621 x 10^3 N/m^2 (85-90 psi), and 50.8mm (2 inches) vacuum for 60-70 min.

7. Cool under full pressure to 51.6-65.5°C (125-150°F) in not less than 45 min.

8. Apply 508mm (20 inches) min. vacuum and remove parts from autoclave.

9. Post cure 3 hrs at 148.8-160°C (300-320°F).

The completed tubes were ultrasonically inspected for voids and found to be acceptable. The tubes were then ground to finished length as specified on the engineering drawing. A completed subcomponent tube is shown in Figure 3-2.

- Full Length Tube (AD361-1001-1)

Five tube assemblies, see Figure 3-3, AD361-1001 were fabricated following the procedure and cure cycle previously described for fabrication of the subcomponent tubes. NDT(ultrasonic inspection) indicated all tubes to be void free and of good quality.

The tube assemblies were made to an overall length of 1.143m (45 inches) and 81.38-81.63mm (3.204-3.214 inch) diameter. The tubes were ground to an overall length of 1.124m (44.25 inches) to remove the oversize trim allowance. Of the five tubes fabricated, two were slated for incorporation into the two member truss assembly, with the remaining three being sent to the NASA for further testing. The members used as details for the truss assembly required further detail fabrication which consisted of bonding 18 overwrapped plies of F161/7781 glass epoxy prepreg to one end and 23 plies of F161/7781 glass epoxy prepreg on the opposite end. Metlbond 329 IA was used to bond the fiberglass to the tube. After the fiberglass ends were cured the tubes were ground to a finished length of 1.117m (44 inches). The end with the 18 plies of fiberglass was ground to a finished outside diameter of 86.86-87.12mm (3.420-3.430 inches) and slightly bevelled. The end with the 23 ply fiberglass overwrap was ground to an octagonal shape having an across the flats dimension of 82.42-82.67mm (3.245-3.255 inches.) Subsequent to the grinding operation the tube end that mated with the apex fitting was shaped. The completed tube detail is shown in Figure 3-4.

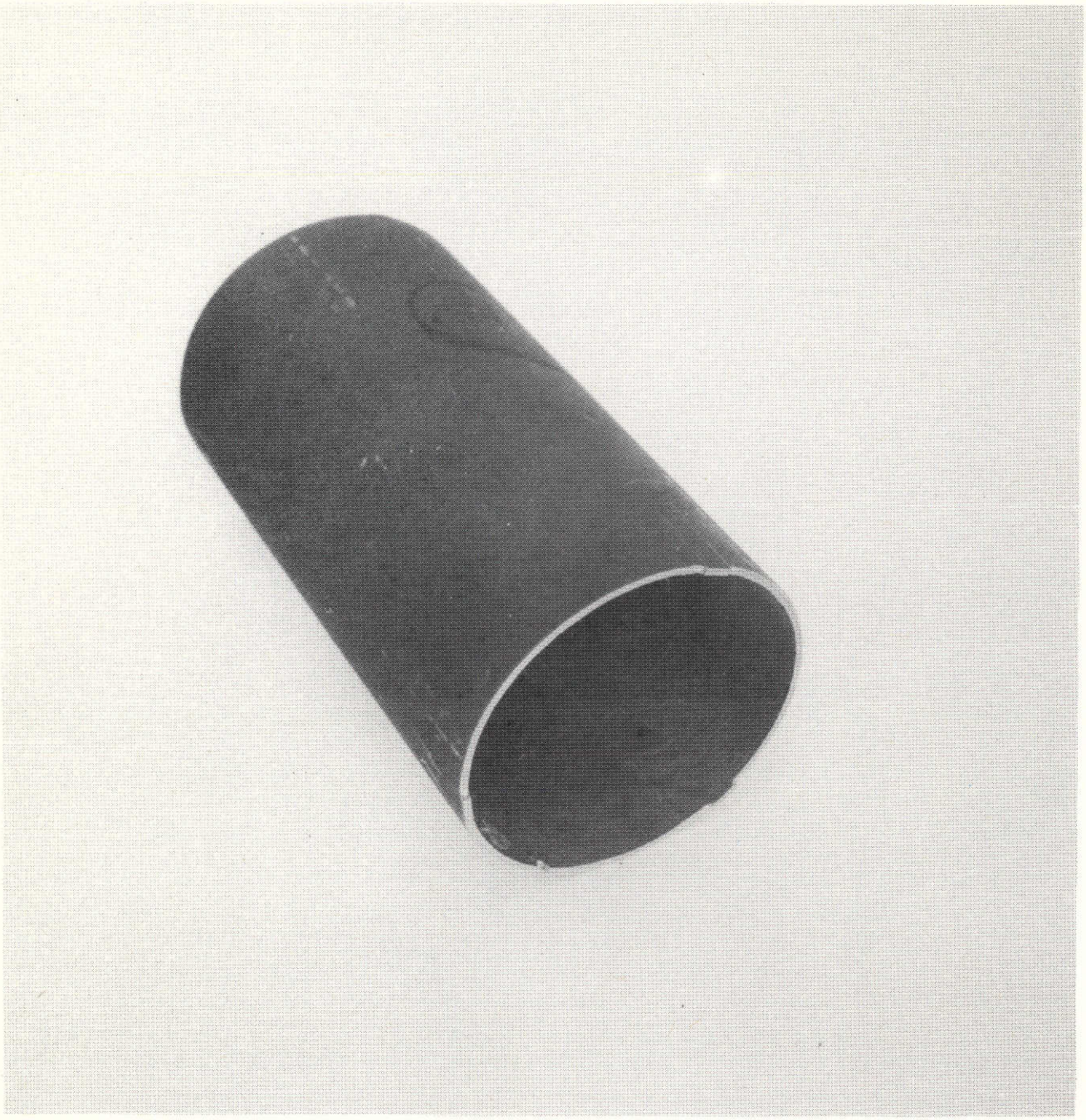

Figure 3-2 Gr/Ep Subcomponent Tube

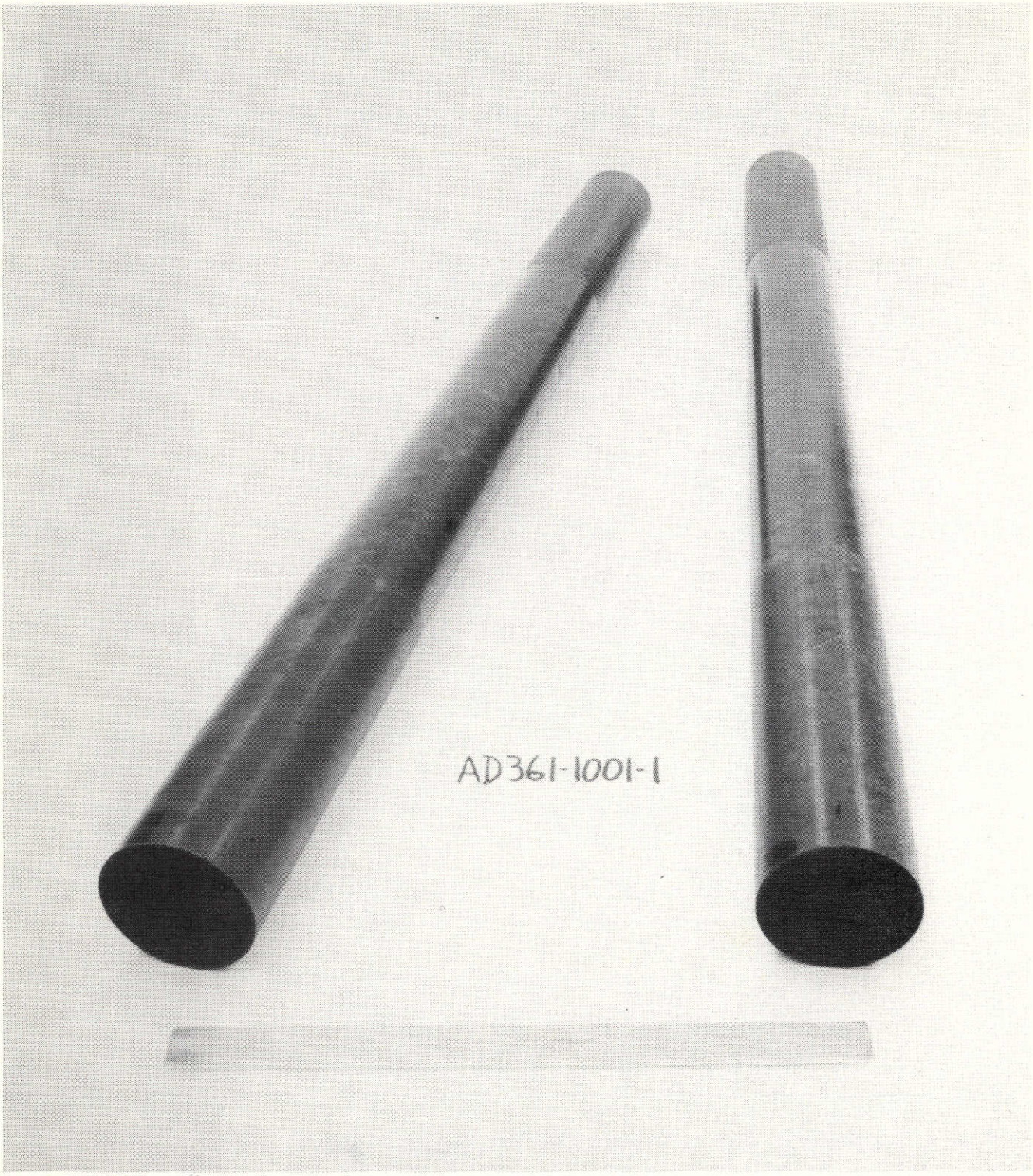

Figure 3-3 Gr/Ep Tube (AD361-1001)

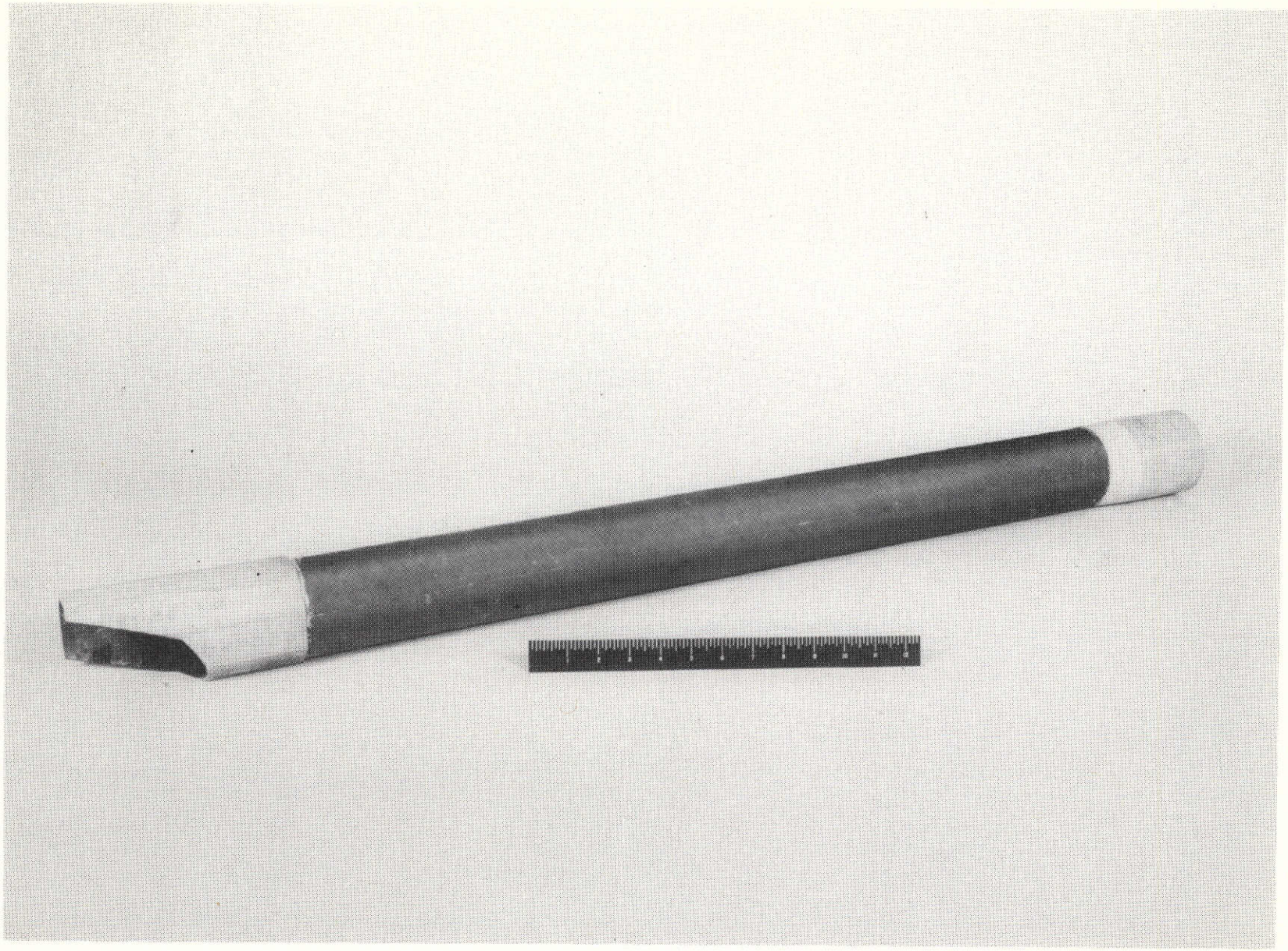

Figure 3-4 Gr/Ep Tube Assembly For Two Member Truss

3.3.3 Graphite/Epoxy Apex Fitting/Ring Detail Fabrication

The graphite/epoxy details required for assembly of the two member metering truss component consisted of apex fitting details (P/N AD361-1002) and simulated ring details (P/N AD361-1003). The apex fitting details included two gusset plates, two channel sections and four clips. The ring details comprised two cap strips and two channel sections. All parts were layed up and cured on steel mold forms, such that the bond surface required for subsequent assembly was layed up on the tool side. The cure cycle used for the various details was the same as that utilized for the tubes. The completed graphite/epoxy details were fabricated without structural defects, except for two channel sections noted in the Q.C. section of this report, as evidenced by the acceptable results of the NDT ultrasonic inspection. Although the channel sections exhibited slight "mark-off" ridges on the inside surface of the flanges (caused by insufficient height of the silicone rubber pressure intensifiers), the functional quality of the parts were determined to be unaffected and rendered acceptable for use. The various detail parts are shown in Figures 3-5 and 3-6.

3.3.4 Two Member Truss Component Assembly

The assembly of the two member truss component was accomplished using the double bonding technique for all structural adhesive bonding. The technique is outlined as follows:

- Double Bonding Technique

  1. Apply two plies of 4 mil mylar tape and one ply of teflon tape to one of the graphite surfaces (over the peel ply) to be bonded. Remove the peel ply from the mating (opposite) graphite surface.

  2. When bonding graphite to fiberglass, tape the surface of the graphite part (peel ply intact) and treat the fiberglass as the mating (opposite) surface. Prepare the fiberglass by:

     a. Solvent wipe with a lint free cloth moistened with MEK.
     b. Lightly abrade cleaned surface with aluminum oxide paper.
     c. Clean off residual dust with filtered air.
     d. Solvent wipe area as in step (a).

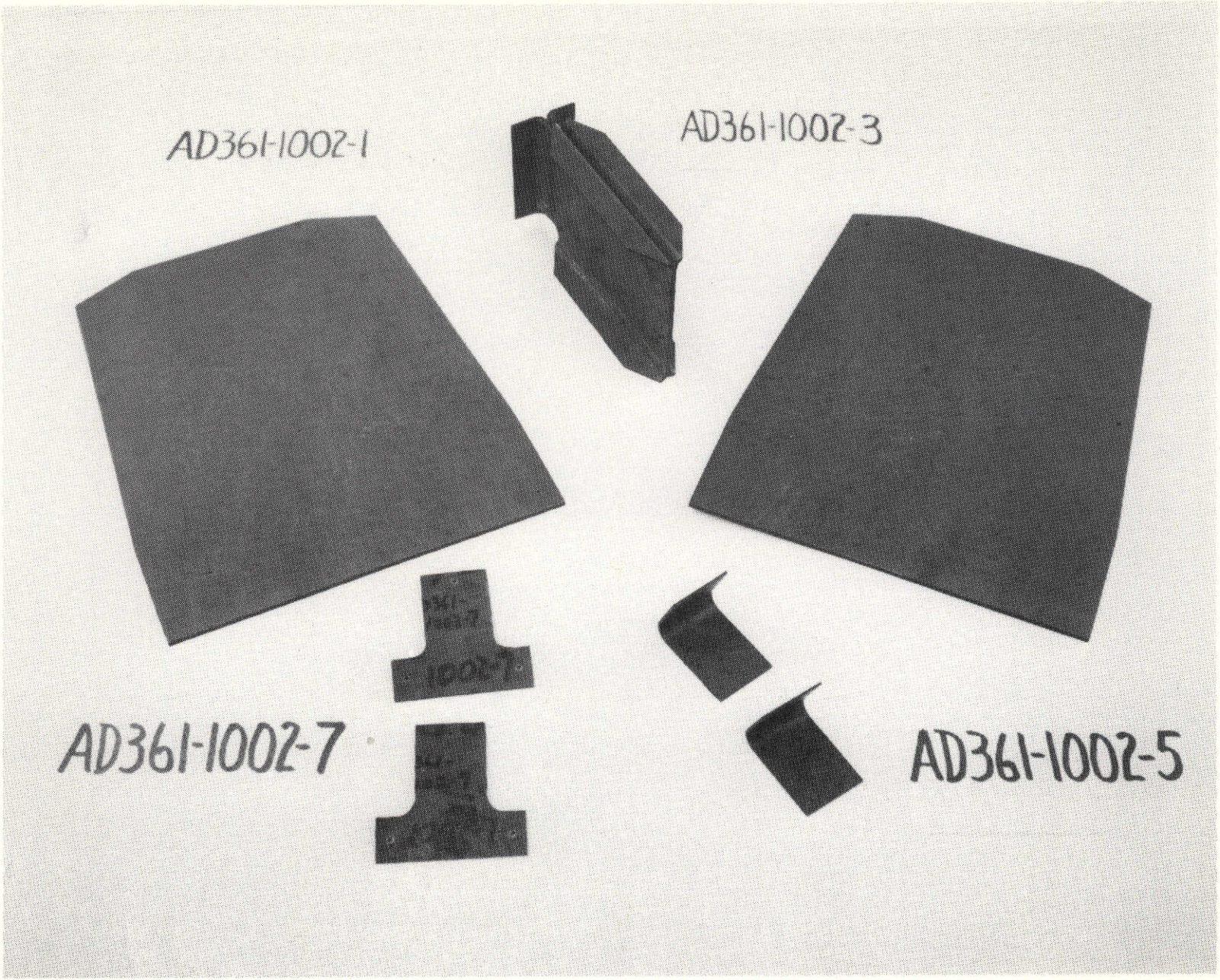

Figure 3-5 Gr/Ep Apex Fitting Details-Two Member Truss Assembly

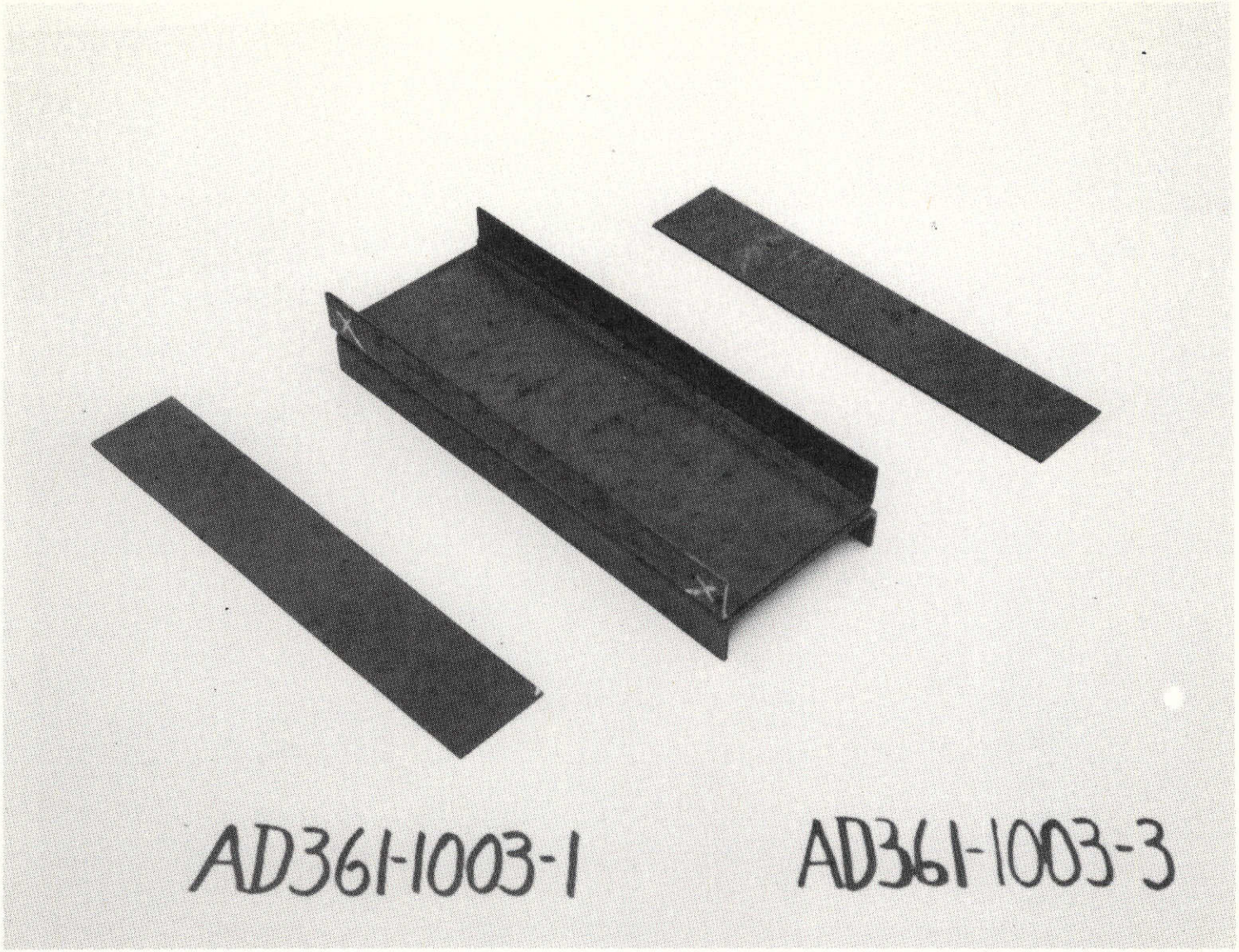

Figure 3-6 Gr/Ep Simulated Ring Details-Two Member Truss Assy

3. Mix Aerobond 2143 adhesive A(base)/B(hardener) in a 100:40 PBW ratio of A:B.

4. Apply the adhesive (approximately 10 mils thick) to the mating (opposite) surface.

5. Clamp or join the assembly together.

6. When the adhesive has partially cured (becomes rubbery), remove the squeezeout.

7. Complete the adhesive cure - 4 hours at 51.66°C (125°F).

8. When the adhesive has cured, break down the assembly and repair any voids in the adhesive by trowelling a light level coating of adhesive over all the void areas. Allow to cure 4 hours at 51.66°C (125°F). When cured, lightly abrade the surface with aluminum oxide paper.

9. Remove the mylar and teflon tape and peel ply from the graphite surfaces taped in steps 1 and 2.

10. Apply a coating of Aerobond 2143 adhesive (approximately 10 mils thick) to the surface from which the tape and peel ply were removed.

11. Repeat steps 5 and 6.

12. Final cure for 4 hours at 51.66°C (125°F.)

The truss assembly technique involved initial pre-fit of the entire structure in the assembly tool to achieve proper alignment and fit. After pre-fit had properly located all parts two subassemblies were made, these being the simulated ring, (comprised of two back to back channel sections and two cap strips) and the central intercostal (comprised of two back to back channels and two shear clips). This was followed by bonding the intercostal assembly to the ring assembly, the subassemblies being located by the tool. With these members in place the tube end test fittings were bonded to the tubes, as well as the two outside shear clips at the apex fitting end. The bonded details were then inspected by Quality Control. The final operations involved bonding the tubes to the central intercostal and ring via the shear clips, followed by bonding the two gusset plates to the tube, intercostal and ring common bond planes. Subsequent to completion of the adhesive bonding operation the structure was drilled and NAS1919 blind anti-peel fasteners were installed. All

drilling was accomplished with standard carbide tools. Figures 3-7 through 3-10 show various prefit configurations of the structure. Figure 3-7 depicts the apex fitting and ring details with one tube in place. Figure 3-8 shows the complete apex fitting pre-fit, sans the nearside gusset plate. Figure 3-9 shows the entire assembly, again without the gusset plate and one test fitting half in place, while Figure 3-10 presents the completed pre-fit assembly. Figures 3-11 thru 3-13 depict three views of the completely assembled structure, both bonded and fastened.

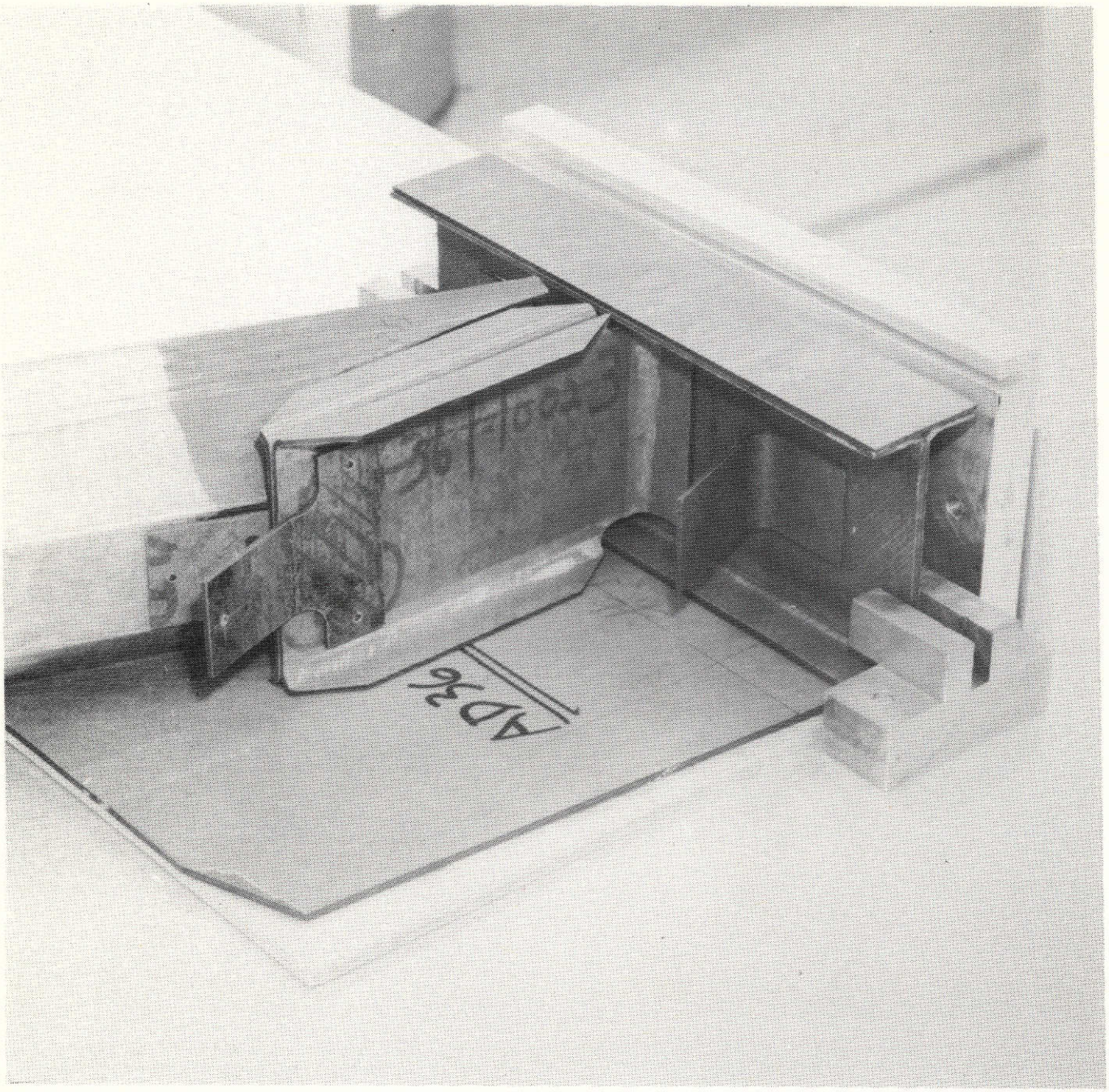

Figure 3-7 Details Pre-Fit-Two Member Truss Assembly

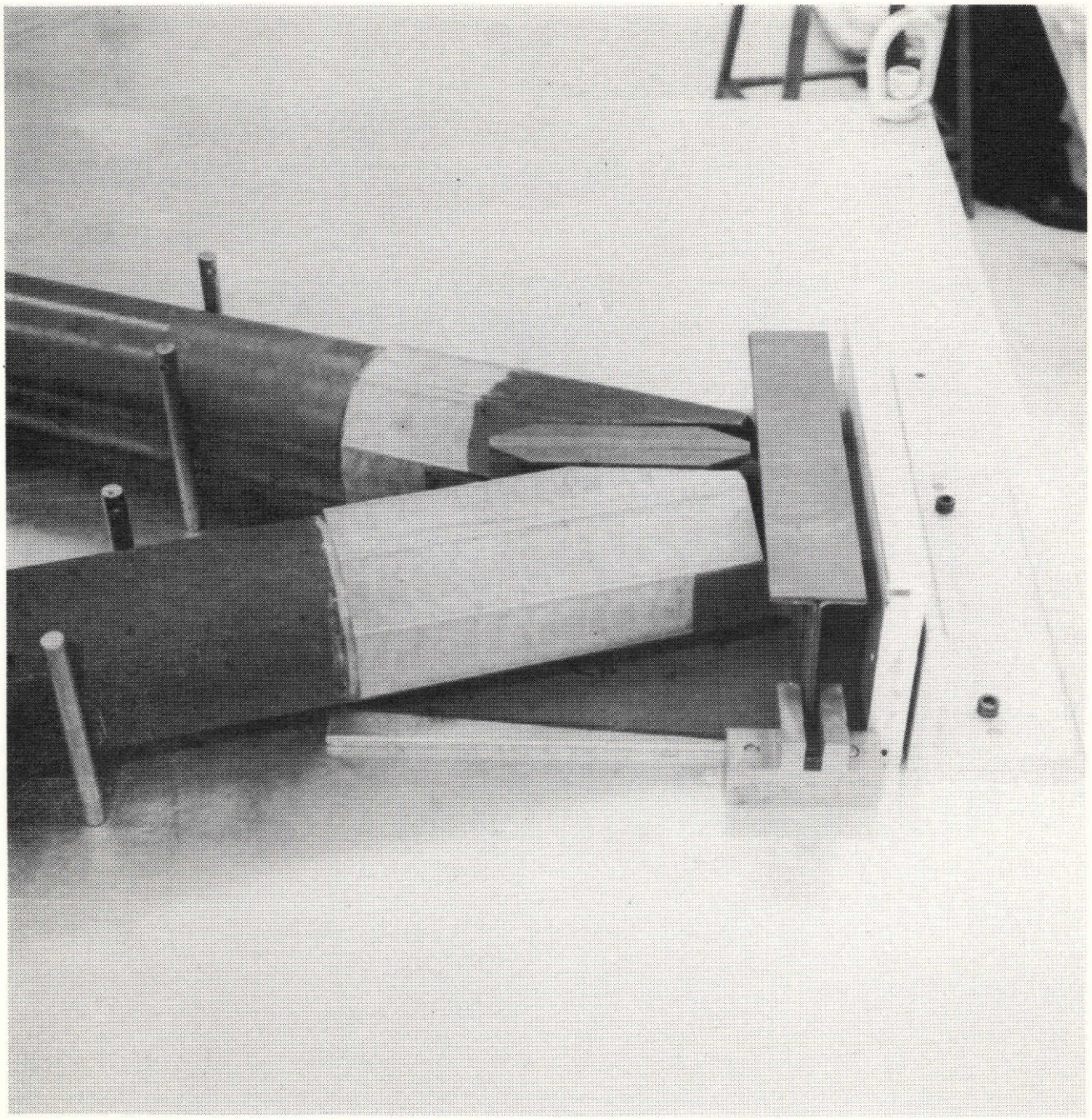

Figure 3-8 Details Pre-Fit-Two Member Truss Assembly

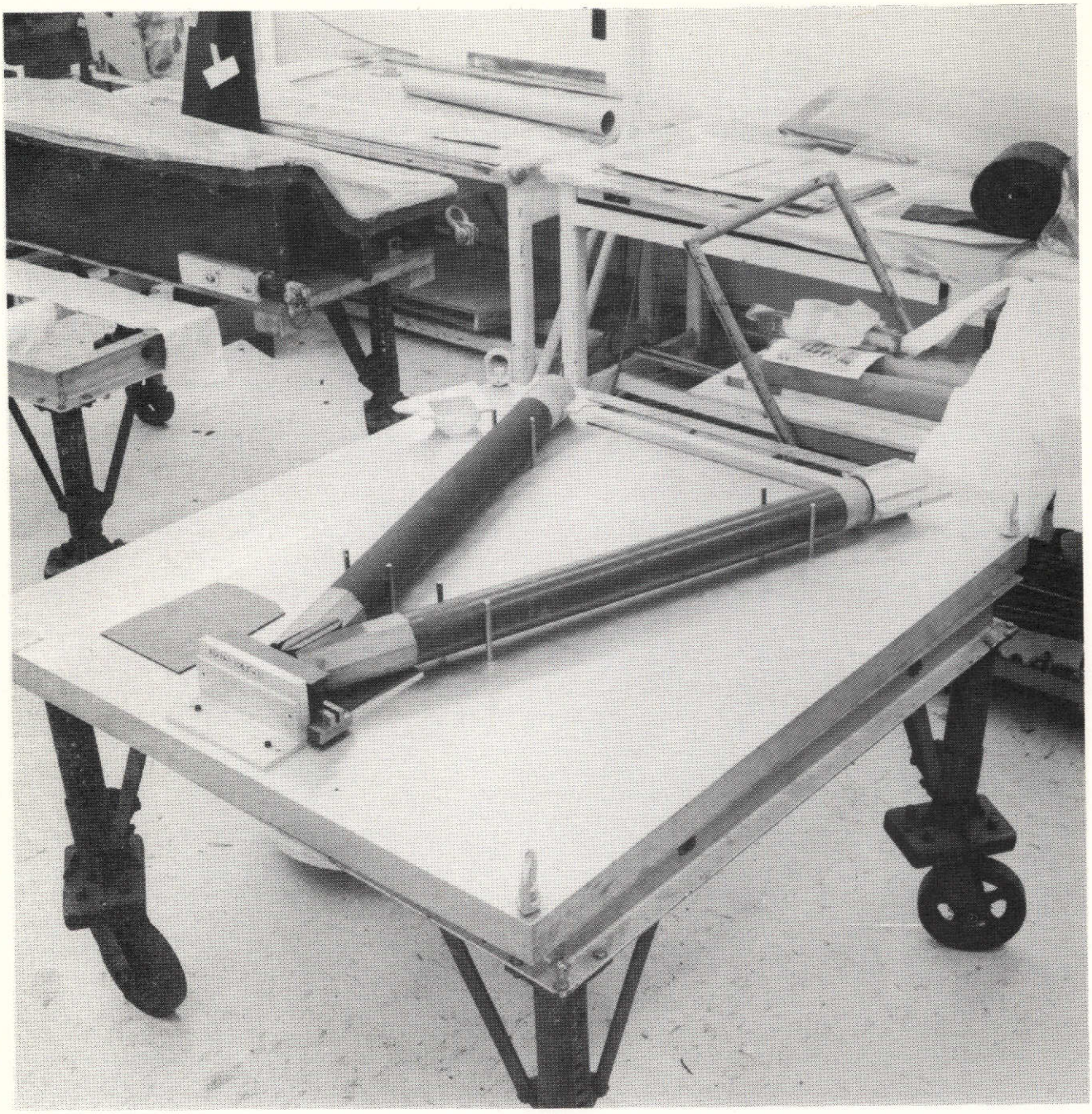

Figure 3-9 Details Pre-Fit—Two Member Truss Assembly

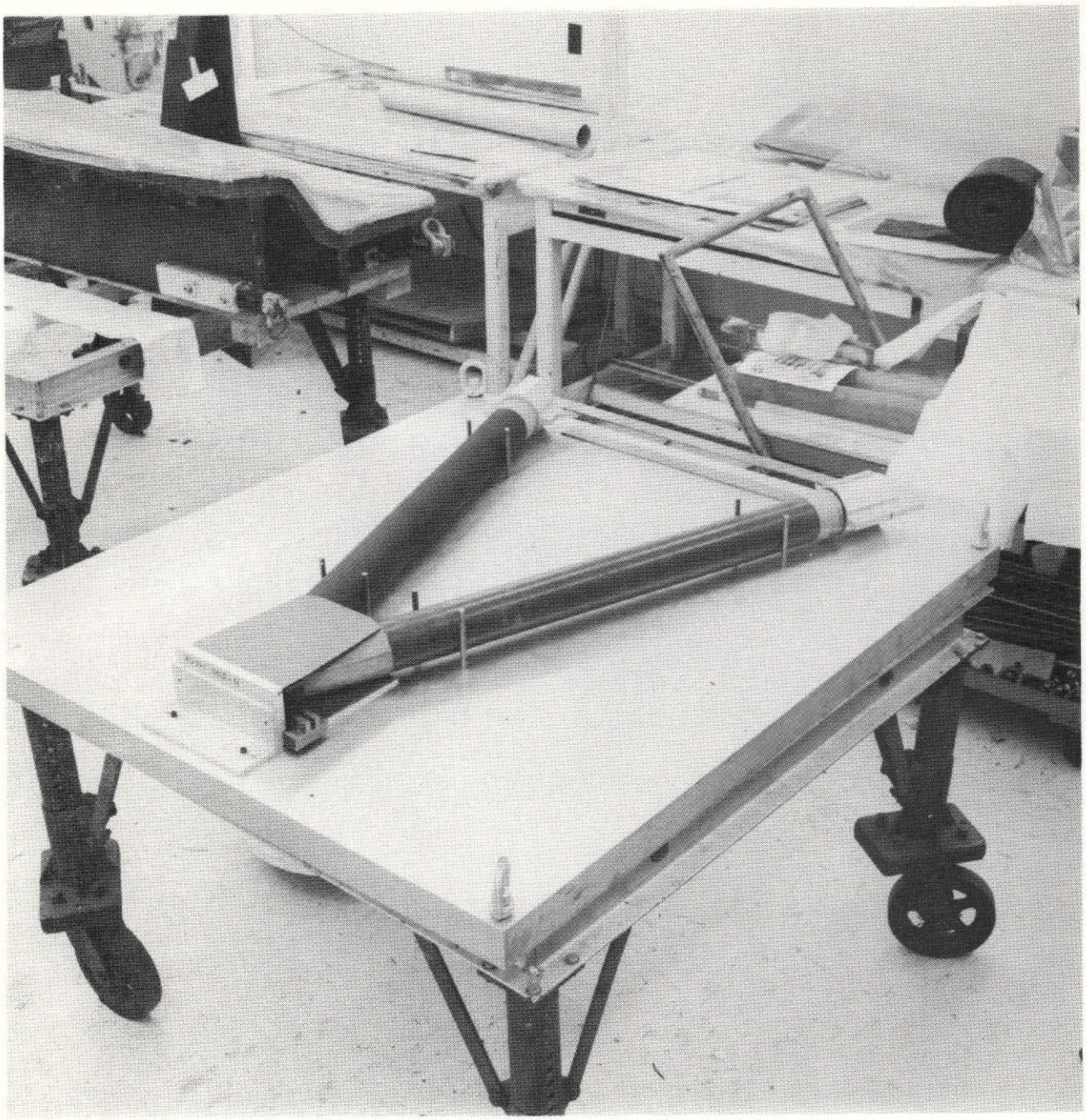

Figure 3-10 Details Pre-Fit-Two Member Truss Assembly

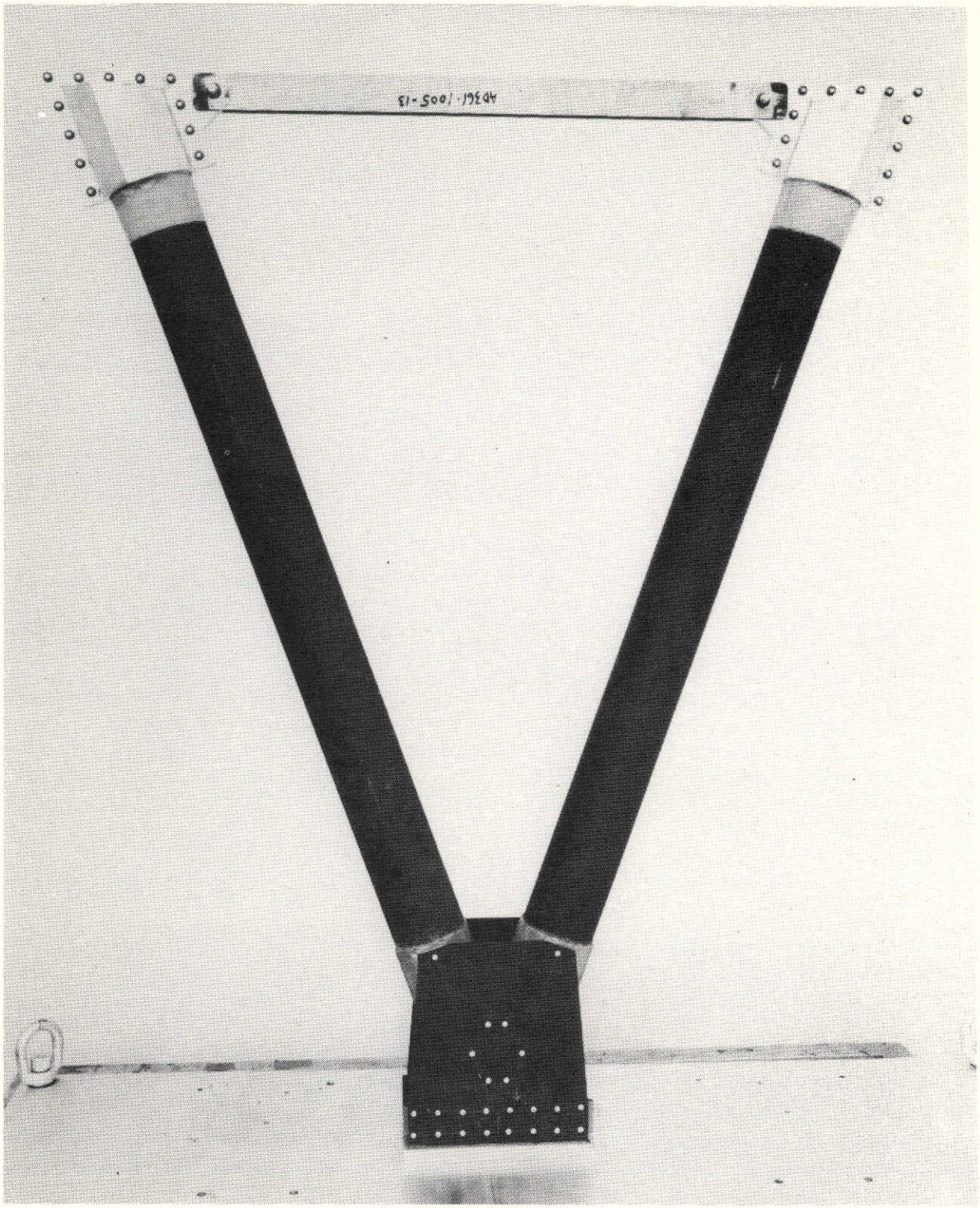

Figure 3-11 Completed Assy-Two Member Truss

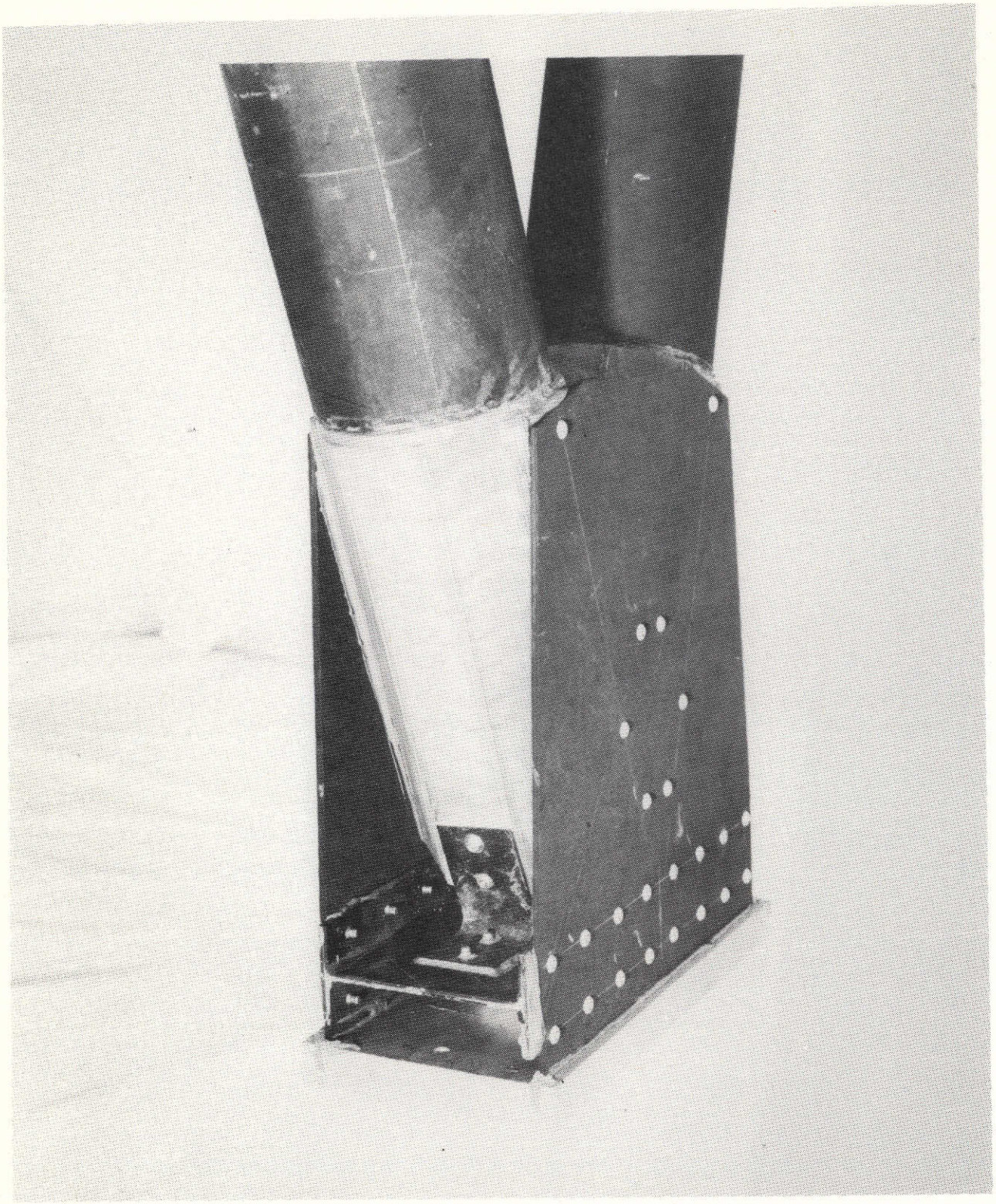

Figure 3-12 Completed Assy-Two Member Truss, Close-up of Apex Fitting

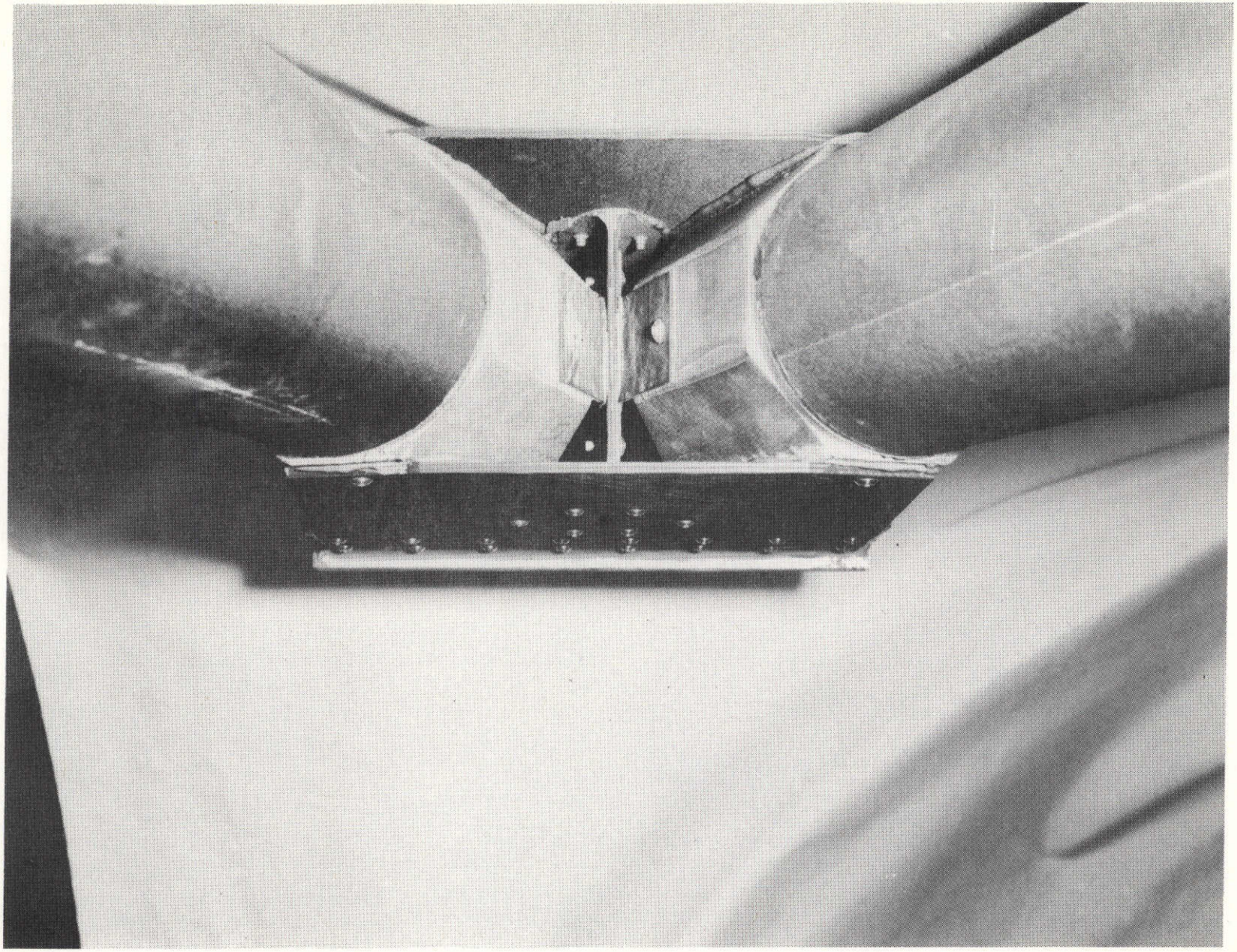

Figure 3-13 Completed Assy-Two Member Truss, Close-Up of Apex Fitting

4.0 QUALITY CONTROL

The Quality Control tasks performed for this program included:

- Receiving Inspection
- In process Inspection
- Non-destructive Inspection
- Dimensional Inspection

4.1 Receiving Inspection

All incoming materials were inspected in accordance with applicable Grumman Material Specifications and/or requirements of Grumman prepared purchase orders. The ultra-high modulus (UHM) graphite/epoxy was inspected in accordance with Gr 102 while the low cost high strength (LHS) graphite/epoxy was inspected in accordance with Gr 101. The UHM material utilized was U.S. Polymeric's E702 epoxy resin on Celanese's GY-70 graphite fiber. The LHS material was U.S. Polymeric's E702 epoxy resin on Hercules' Type A graphite fiber. The mechanical properties checked were longitudinal flexural strength and modulus at 23.8°C (75°F) and horizontal shear strength at 23.8°C (75°F). The properties measured on the material utilized in this program are given in Table 4-1. The UHM and LHS prepreg tape used in this program was in two batches. The physical properties of the various batches were satisfactory as measured by the material supplier.

4.2 In process Inspection

Process verification test tabs were processed with each autoclave cycle to verify that the graphite/epoxy was adequately cured. Testing was conducted at room temperature on coupons from a unidirectional 15 ply test panel fabricated from the same batch of tape and undergoing the same cure cycle as the part. Coupons from this panel were tested for longitudinal flexural strength, modulus and horizontal shear strength.

The process control coupon test results, which are shown in Table 4-2, were satisfactory for Part Nos. -104 and -1002 and -1003 series. The test tabs representing part no. -1001 series was somewhat low in flexural properties (approximately 5%) but not to a level that would indicate improper autoclave

Table 4-1 Graphite/Epoxy, Receiving Inspection Data at 24°C (75°F)

Mat'l Designation	Batch No.	Roll No.	Average Longitudinal Flexural Properties		Average Horizontal Shear Strength
			Strength $N/m^2 x10^6$ (ksi)	Modulus $N/m^2 x10^9$ (msi)	$N/m^2 x10^9$ (ksi)
UHM(GY-70)	2247	1	682.5 (99)	234.3 (34)	57.2 (8.3)
UHM(GY-70)	3040	3	675.6 (98)	235.0 (34.1)	44.1 (6.4)
UHM Specification Value			689.4 (100)	244.4 (35)	39.9 (5.8)
LHS(Type A)	3030	3	1468.4 (213)	103.4 (15)	91.6 (13.3)
LHS Specification Value			1378.8 (200)	110.3 (16)	48.2 (7.0)

Table 4-2 Process Control Data

Panel No.	Part No. (AD361-)	Material Batch/Roll	Longitudinal Flexure				Horizontal Shear Strength	
			Strength		Modulus			
			$N/m^2 x10^6$	($Psix10^3$)	$N/m^2 x10^9$	($Psix10^6$)	$N/m^2 x10^6$	($Psix10^3$)
B1932	-104 No.1	Type A-3030/1	1502.8	(218)	115.8	(16.8)	96.5	(14)
B1997	-104 No.2	Type A-3030/1	1447.7	(210)	115.8	(16.8)	97.2	(14.1)
B2003	-104 No.3	Type A-3030/1	1509.7	(219)	111.6	(16.2)	108.9	(15.8)
S 34	-1002 -1003	GY70 3040/4	641.1	(93)	226.1	(32.8)	58.5	(8.5)
S 35	-1002 -1003	Type A 3030/3	1392.5	(202)	102.7	(14.9)	83.4	(12.1)
S 47	-1001 No.1	GY70 3040/3	682.5	(99)	235.7	(34.2)	51.0	(7.4)
S 48	-1001 No.2	GY70 3040/3	654.9	(95)	241.2	(35)	48.9	(7.1)
S 49	-1001 No.3	GY70 3040/5	641.1	(93)	226.7	(32.9)	29.6	(4.3)
S 61	-1001 No.4	GY70 2247/1	648.0	(94)	212.3	(30.8)	66.1	(9.6)
S 67	-1001 No.5	GY70 3040/5	585.9	(85)	193.0	(28)	48.2	(7.0)

cure. Based on acceptable NDT testing of the parts the tabs represented, the engineering disposition was to accept the parts for program use.

4.3 Nondestructive Inspection

Ultrasonic inspection was performed using two basic techniques: pulse-echo-reflector plate and resonance. The basic underlying principle behind the pulse-echo technique is that by employing a single transducer, ultra-sound is passed through the specimen under test and in turn is reflected off an appropriate reflector surface through the specimen and back to the transducer. If a defect is present, it presents an interface which blocks a proportional amount of the accustic energy from reaching the reflector. This results in a loss of sound energy reflected back to the transducer, (Figure 4-1) which in turn produces an attenuated signal on the cathode ray tube. The equipment used for resonance ultrasonic testing is the Fokker Bond Tester. The non-destructive test method utilized by the Fokker Bond Tester is called the Transducer Resonance Method. The heart of this method is the crystal in the transducer. The crystal is fabricated from a piezoelectric material. Under distortion from pressure, the crystal will generate an electrical current. When an electrical current is induced across the crystal, it can be made to resonate at some natural frequency. With the transducer coupled to a simulated void area, a driving current is induced into the crystal until a resonating frequency is attained. Thus, the simulated void has created a coupling demanding a specific amount of current to drive the crystal at a certain resonant frequency. When the transducer is applied to a bonded joint, the resonant frequency is dampened. If the coupled load is large, a shift in the resonant frequency occurs. If the coupled load is small only a change in impedance occurs. The pulse-echo-reflector plate method provides a rapid means of locating and sizing potential voids and permits 100% coverage. It does not, however, determine defect depth. When and if a void is located using this technique, resonance ultrasonics was employed for depth information.

The criteria employed for N.D.T. inspection of the various details and assemblies were:

- Laminates - The maximum permitted void or delamination shall not exceed 12.70 mm (0.50 in.)

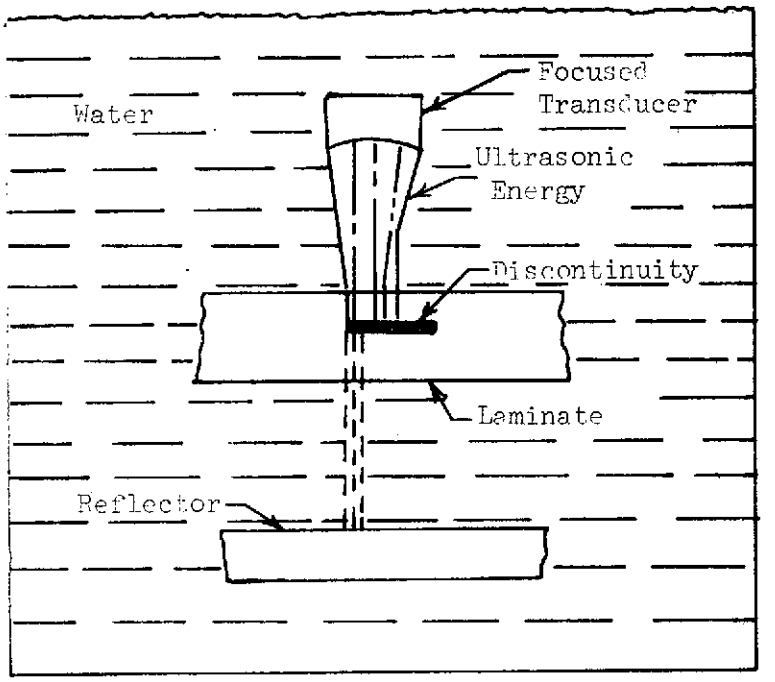

Figure 4-1 Through-Transmission-Reflection Technique, Single Transducer

- Adhesive Bonded Joints - The maximum permitted void or delamination shall not exceed 6.35 mm (0.25 in.)

All tubes (three subcomponent and five full length) fabricated and tested by N.D.T. under this program were found to be satisfactory. All other laminated details were satisfactory except two channels which contained void areas in the radius. Both parts were placed on non-conforming material reports for engineering disposition. Disposition resulted in both channels being scraped and replacement channels fabricated. Corrective action involved using larger pressure intensifiers (of proper contour) with steel backing . The replacement channels were satisfactory.

The two-member truss bond assembly was inspected using the Fokker Bond Tester and found to be satisfactory.

4.4 Dimensional Inspection

All details were dimensionally inspected. Results of the inspection indicated that on average the thicknesses were generally about 10% full, or about 1.62 mm (.064 inches) for the 10 ply "B" laminate. All parts fabricated consistently exhibited this tendency which may be related to a pre-preg tape width (which is related to cured per ply thickness) on the low side of the tolerance - the allowable width was from 63.5 - 66.5 nm (2.5 - 2.62 inches) or a non optimum bleeder to ply ratio. The inspection results were presented to engineering for part disposition, and were accepted based upon a clean N.D.T. ultrasonic inspection report, the relatively minor nature of the discrepancy and confidence the slight thickness increase would not adversely affect part performance.

5.0 CONCLUSIONS AND RECOMMENDATIONS

Based upon the results of this program, the following conclusions and recommendations are presented:

Conclusions

- Effectively zero coefficients of thermal expansion have been achieved
- The zero coefficients were achieved not only in small flat rectangular test specimens, but in parts of the anticipated structural shape
- The consistency of results for thermal coefficient of expansion tests of the chosen laminate was good
- Outgassing of the chosen material system was minimal and well within acceptable limits
- Dynamic behavior of the Gr/Ep composite tubes was totally predictable and consistent
- Potential weight savings of the Gr/Ep tubes over INVAR are on the order of 58%
- The joint design concept has been proven structurally adequate
- The materials and manufacturing process utilized for fabrication of the tubes and apex fitting details are suitable for production.

Recommendations

- Further development work is required in low coefficient of thermal expansion measurement technology
- More extensive coefficient of thermal expansion testing should be planned for laminates covering a broad range of configurations
- Coefficient of thermal expansion tests should be conducted for representative joint specimens.

6.0 REFERENCES

1. "Advanced Composite Wing Structures, Boron/Epoxy Design Data, Volume II, Analytical Data", Grumman Aerospace Corporation, Technical Report AC-SM-ST-8085

2. "Advanced Composites Data for Aircraft Structural Design", AFML-TR-70-58, Volume IV, September 1972

3. "Graphite/Epoxy, Boron-Graphite/Epoxy and Boron/Aluminum Design Allowables", AFML-TR-232 December 1972

APPENDIX A

Conversion of U.S. Customary Units to S.I. Units

Physical Quantity	U.S. Customary Unit	X	Conversion Factor	=	SI Unit
Length	in.		2.54×10^{-2}		Meters - m
Angle	Degrees		1.745×10^{-2}		Radians - rad
Force	lbs		4.448		Newtons - N
Stress	lbs/in^2		6.894×10^{3}		Newtons Per Square Meter - N/m^2
Bending Moment	in. -lbs		1.129848×10^{-1}		Newton Meters - N-m
Temperature	^{o}F		$\frac{5}{9}[t_{o_F}-32]$		Degrees Centigrade - ^{o}C

APPENDIX B

Test Results

Table B1 Test Results - Longitudinal Tension
(unidirectional laminates)

Material	Test No.	Thickness (in.)	Width (in.)	Pre-Load (lbs)	Failure Load (lbs)	F^{ult} (ksi)	E (msi)	Location of Failure
GY70/E-702	1	.041	.500	760	1010	49.3	40.9	Tab
	2	.042	.496	760	1140	54.7	40.5	
	3	.041	.494	760	1080	52.1	38.6	
	4	.043	.499	760	1065	49.6	37.6	
	5	.042	.498	760	1170	55.9	38.7	
	6	.040	.501	760	970	48.4	39.1	
Type A/E-702	1	.036	.498		1770	98.7	16.6	Tab
	2	.036	.502		1220	67.5	15.9	
	3	.033	.500		1365	82.7	17.9	
	4	.036	.500		1220	67.8	17.2	
	5	.030	.503		1330	88.1	16.9	
	6	.034	.500		1320	77.6	17.5	

Table B2 - Test Results - Transverse Tension
(unidirectional laminates)

Material	Test No.	Thickness In.	Width In.	Failure Load Lbs.	F^{ult} ksi	E msi	Location of Failure
GY70/E-702	1	.105	.500	150	2.86	1.08	center
	2	.105	.497	174	3.33	.97	center
	3	.107	.495	170	3.21	—	edge of tab
	4	.110	.498	175	3.19	.98	edge of tab
Type A/E-702	1	.076	.503	288	7.58	1.67	center
	2	.076	.499	264	6.98	1.72	center
	3	.076	.504	290	7.57	1.70	center
	4	.076	.498	268	7.09	1.60	center
	5	.076	.508	280	7.25	2.28	center

Table B3 Test Results - Tension Coupons

Specimen Type	No.	Thickness (in.)	Width (in.)	Preload (lbs)	Failure Load (lbs)	F^{ult} (ksi)	E (msi)	Location of Failure
Laminate 'A'								
Longitudinal (100-11)	1	.037	.502	---	960	51.7	----	Center
	2	.035	.501	750	1004	57.3	24.3	Center
	3	.037	.501	750	1072	57.8	23.6	Center
	4	.037	.502	750	992	53.4	24.5	Tab Edge
	5	.038	.501	750	986	51.8	26.3	Center
Transverse (100-13)	1	.038	.503	260	398	20.8	3.50	Tab Edge
	2	.038	.504	300	350	18.3	2.65	Tab Edge
	3	.039	.503	300	402	20.5	3.26	Tab Edge
	4	.037	.502	300	371	20.0	2.84	Tab Edge
	5	.039	.503	300	477	24.3	3.63	Tab Edge
Laminate 'B'								
Longitudinal (101-11)	1	.059	.500	800	1078	36.5	20.1	Center
	2	.054	.500	800	926	34.3	22.0	Center
	3	.058	.500	800	1300	44.8	20.7	Center
	4	.057	.500	800	1074	37.7	19.1	Center
	5	.054	.500	800	1142	44.3	20.6	Center
Transverse (101-13)	1	.053	.502	630	925	34.8	6.08	Tab
	2	.057	.501	700	780	27.3	5.15	Tab
	3	.060	.501	630	1025	34.1	6.09	Tab
	4	.053	.501	630	980	36.9	6.84	Tab
	5	.058	.502	630	990	34.0	6.20	Tab
Laminate 'C'								
Longitudinal (102-11)	1	.056	.502	---	870	30.9	----	Center
	2	.058	.502	650	1064	36.5	18.5	Center
	3	.064	.500	650	1400	43.8	22.1	Center
	4	.058	.501	800	1090	37.5	19.5	Center
	5	.060	.502	800	850	28.2	18.1	Center
Transverse (102-13)	1	.058	.503	450	592	20.3	11.0	Center
	2	.059	.500	450	660	22.4	10.1	Center
	3	.055	.501	450	598	21.7	9.83	Center
	4	.055	.502	450	562	20.4	11.1	Center
	5	.057	.500	---	450	15.8	----	Center
Laminate 'B'(1) Longitudinal	1	.053	.500	900	1148	43.3	19.86	Center
	2	.053	.498	900	1204	45.6	21.44	Center
	3	.055	.503	900	1206	43.6	20.27	Center
	4	.056	.492	900	1494	54.2	22.68	Center
	5	.055	.492	900	1148	42.4	19.98	Center
Transverse	1	.054	.491	750	980	36.5	5.79	Center
	2	.054	.492	500	950	35.8	5.82	Center
	3	.056	.496	500	1000	36.0	6.39	Center
	4	.055	.498	500	952	34.8	6.08	Center
	5	.055	.499	500	1030	37.5	6.16	Center

(1) Batch No. 2.

Table B4- Test Results - Compression Coupons

Specimen Type	No.	Thickness (in.)	Width (in.)	Failure Load (lbs)	F^{ult} (ksi)	E (msi)	Failure Mode
Laminate 'A'							
Longitudinal (100-15)	1	.044	.748	2530	76.9	20.4	Compression-center
	2	.044	.749	1940	58.9	12.5	Compression-center
	3	.041	.746	2240	73.2	17.2	Compression-center
	4	.042	.747	1970	62.8	17.9	Compression-center
	5	.042	.748	1820	57.9	17.4	Compression-center
Transverse (100-17)	1	.048	.747	822	22.9	7.18	Buckling
	2	.040	.748	1012	33.8	3.85	Buckling
	3	.043	.748	844	26.2	2.66	Buckling
	4	.039	.748	900	30.9	4.37	Buckling
	5	.042	.745	790	25.2	2.76	Buckling
Laminate 'B'							
Longitudinal (101-15)	1	.063	.747	2110	44.8	15.9	Compression-center
	2	.062	.748	1770	38.2	12.8	Delamination
	3	.063	.747	2380	50.6	21.3	Compression-center
	4	.061	.748	2430	53.3	19.4	Compression-center
	5	.064	.748	2150	44.9	15.3	Compression-center
Transverse (101-17)	1	.060	.748	2850	63.5	5.63	Compression-center
	2	.062	.746	2500	54.1	5.21	Compression-center
	3	.057	.746	2880	67.7	6.81	Compression-center
	4	.063	.748	3175	67.4	5.83	Compression-center
	5	.067	.745	2500	50.1	4.94	Compression-center
Laminate 'C'							
Longitudinal (102-15)	1	.065	.747	2460	50.7	14.9	Compression-center
	2	.060	.747	2380	53.1	17.7	Compression-center
	3	.062	.748	2150	46.4	15.9	Compression-center
	4	.061	.748	2320	50.8	19.7	Compression-center
	5	.063	.748	2600	55.2	16.8	Compression-center
Transverse (102-17)	1	.061	.748	1100	24.1	9.56	Compression-center
	2	.057	.745	1384	32.6	9.50	Compression-center
	3	.062	.745	1419	30.7	8.02	Compression-center
	4	.063	.748	1180	25.0	8.35	Compression-center
	5	.061	.748	1344	29.5	9.41	Compression-center
Laminate 'B'(1)							
Longitudinal	1	.057	.743	1948	46.0	17.1	Compression-center
	2	.058	.742	1820	42.3	17.4	Compression-center
	3	.057	.741	1702	40.3	17.6	Compression-center
	4	.059	.743	1704	38.9	15.4	Compression-center
	5	.059	.743	1965	44.8	17.6	Compression-center
Transverse	1	.057	.744	2950	69.6	5.6	Compression-center
	2	.055	.741	2450	60.1	6.4	Compression-center
	3	.056	.743	2040	63.4	5.9	Compression-center
	4	.060	.744	2500	56.0	6.4	Compression-center
	5	.058	.743	2650	61.5	5.8	Compression-center

(1) Batch No. 2

Table B5 - Test Results - Flexure

Specimen Type	No.	Thickness (In.)	Width (In.)	Span (In.)	Secondary Span[1] (In.)	Failure Load (lbs.)	Failure Mode
Laminate 'A'							
Longitudinal	1	.042	.502	1.35		58.0	Flex-Tension & Interlaminar Shear
	2	.048	.500	1.35		62.5	Flex-Tension & Interlaminar Shear
	3	.041	.502	1.35		50.0	Flex-Tension & Interlaminar Shear
	4	.045	.500	1.35		65.0	Flex-Tension & Interlaminar Shear
	5	.043	.502	1.35		56.5	Flex-Tension & Interlaminar Shear
Transverse	1	.044	.503	1.35		9.0	Interlaminar Shear
	2	.040	.503	1.35		9.6	Interlaminar Shear
	3	.041	.503	1.80	.74	16.2	Interlaminar Shear
	4	.042	.503	1.80	.74	7.6	Interlaminar Shear
	5	.040	.503	1.80	.74	9.2	Interlaminar Shear
Laminate 'B'							
Longitudinal	1	.060	.508	1.95		19.0	Interlaminar Shear
	2	.063	.508	1.95		24.5	Interlaminar Shear
	3	.062	.504	1.95		23.8	Interlaminar Shear
	4	.057	.505	1.95		18.0	Interlaminar Shear
	5	.060	.506	1.95		19.6	Interlaminar Shear
Transverse	1	.060	.509	1.95		45.2	Interlaminar Shear
	2	.057	.506	1.95		53.7	Interlaminar Shear
	3	.063	.506	1.95		57.8	Interlaminar Shear
	4	.059	.502	1.95		48.1	Interlaminar Shear
	5	.059	.507	1.95		43.2	Interlaminar Shear
Laminate 'B'[2]							
Longitudinal	1	.055	.500	1.95		22.1	Interlaminar Shear
	2	.058	.500	1.95		26.0	Interlaminar Shear
	3	.056	.500	1.95		23.2	Interlaminar Shear
	4	.057	.501	1.95		24.3	Interlaminar Shear
	5	.055	.499	1.95		21.0	Interlaminar Shear
Transverse	1	.056	.500	1.95		51.0	Interlaminar Shear
	2	.056	.499	1.95		54.0	Interlaminar Shear
	3	.055	.498	1.95		48.7	Interlaminar Shear
	4	.057	.500	1.95		47.2	Interlaminar Shear
	5	.057	.499	1.95		53.2	Interlaminar Shear
Laminate 'C'							
Longitudinal	1	.059	.508	1.95		25.0	Interlaminar Shear
	2	.058	.505	1.95		28.6	Interlaminar Shear
	3	.066	.506	1.95		35.6	Interlaminar Shear
	4	.063	.505	1.95		32.4	Interlaminar Shear
	5	.062	.502	1.95		33.2	Interlaminar Shear
Transverse	1	.059	.503	1.95		25.6	Interlaminar Shear
	2	.058	.506	1.95		26.0	Interlaminar Shear
	3	.063	.507	1.95		28.2	Interlaminar Shear
	4	.061	.502	1.95		28.5	Interlaminar Shear
	5	.063	.505	1.95		29.6	Interlaminar Shear

[1] For 4-Point Bending

[2] Batch No. 2

Table B6 Test Results - Horizontal Shear

Specimen Type	No.	Thickness (in.)	Width (in.)	Span (in.)	Failure Load (lbs)	F^{ult*}_{max} (ksi)	Failure Mode
Laminate 'B'	1	.059	.258	0.33	89.5	4.41	Hor. Shear
	2	.057	.257	0.33	81.0	4.15	Hor. Shear
	3	.059	.258	0.33	77.5	3.82	Hor. Shear
	4	.056	.258	0.33	83.0	4.31	Hor. Shear
	5	.056	.258	0.33	68.0	3.53	Hor. Shear
Laminate 'C'	1	.062	.258	0.33	94.5	4.43	Hor. Shear
	2	.059	.258	0.33	83.0	4.09	Hor. Shear
	3	.060	.258	0.33	79.0	3.83	Hor. Shear
	4	.058	.257	0.33	86.0	4.33	Hor. Shear
	5	.056	.258	0.33	67.5	3.50	Hor. Shear

$*F^{ult}_{max} = 1.5\ (\frac{P}{2bt}) = .75\ P/bt$